Quantitative imaging of tyrosine kinase-drug interactions in cells

By

Eulashini Chuntharpursat
B.Sc., B.Sc. (Hons), M.Sc.

Submitted in fulfillment of the
Academic requirements for the degree of
Doctorate of Philosophy in Biochemistry
University of KwaZulu-Natal
Pietermaritzburg

January 2012

PREFACE

These studies represent original work by the Author and have not been submitted in any other form to another University. Where use was made of the work of others, it has been duly acknowledged in the text.

Eulashini Chuntharpursat
January 2012

Dr E. Elliott
January 2012

Professor P.I.H Bastiaens
January 2012

Declaration – Plagiarism

I, Eulashini Chuntharpursat declare that

(i) The research reported in this dissertation, except where otherwise indicated, is my original work.

(ii) This dissertation has not been submitted for any degree or examination at any other university.

(iii) This dissertation does not contain other persons' data, pictures, graphs or other information, unless specifically acknowledged as being sourced from other researchers.

(iv) This dissertation does not contain other persons' writing, unless specifically acknowledged as being sourced from other researchers. Where other written sources have been quoted, then:

a. their words have been re-written but the general information attributed to them has been referenced;

b. where their exact words have been used, their writing has been placed inside quotation marks, and referenced.

(v) Where I have reproduced a publication of which I am an author, co-author or editor, I have indicated in detail which part of the publication was actually written by myself alone and have fully referenced such publications.

(vi) This dissertation does not contain text, graphics or tables copied and pasted from the Internet, unless specifically acknowledged and the source being detailed in the dissertation and in the references sections.

Candidate signature

January 2012

Abstract

Kinases play a crucial role in regulating cellular signaling cascades, making them therapeutic targets for several human diseases. In human cancers, mis-regulation and mutations of kinases such as EGFR (epidermal growth factor receptor) have been found to drive malignant transformation. Due to the conserved structural elements of protein kinases, the majority of kinase inhibitors available have a tendency to inhibit multiple targets. The biological impact of this promiscuity is insufficiently defined and the prevalence of cellular compensatory mechanisms additionally varies the clinical responses to drug treatment. In order to understand the relationship between selectivity and efficacy, prior to clinical trials, it is essential to characterize how inhibitors interact with the kinome within a cellular context.

Monitoring inhibitor-target interactions generally involves *in vitro* assaying with purified proteins or protein domains, which compromises the native integrity of the kinases. Cell-based assays either gain outcomes from bulk populations that average out cell variance or phenotypic assays that lack molecular resolution. To obtain information on drug interactions on a single cell level, we have developed a method to measure the direct binding of kinase inhibitors to their targets *in situ* and *in vivo*. Kinase inhibitors are chemically tagged with fluorophores that serve as acceptors to genetically tagged donor fluorophores on the enzyme and the interaction is measured using FRET-FLIM. With epidermal growth factor receptor (EGFR) and irreversible EGFR inhibitors as the model system, this approach has been applied to image inhibitor-kinase interactions in live and fixed cells. Using this method, a small panel of tyrosine kinase targets, and labeled inhibitors, we were able to investigate the cross-specificity within the panel. Additionally it was found that the specificity of inhibitors for specific kinase conformations enables the distinction between EGFR in the active and inactive conformation by the inhibitor-probes.

Acknowledgements

I would like to thank the following people for the influential role they have played in the completion of this thesis and my scientific development over the duration of my Ph.D.

Prof. Philippe Bastiaens (Max Plank Institute of Molecular Physiology, Dortmund) for giving me the opportunity to work in his lab. I am deeply grateful to him for allowing me access to all facilities at his disposal, giving me the room to grow as a scientist and to develop my own ideas, and for the kindness he has shown me over the last few years.

Dr. Edith Elliott (University of KwaZulu-Natal, Pietermaritzburg) for her continuous guidance, support and going to extra lengths to ensure I could follow my chosen path. I would also like to thank her for reading and editing to my thesis.

The Reviewers of my thesis for taking the time to read and assess the work I have presented.

Dr. Hernán-'McGyver'-Grecco for the constructive role he has played in the development and execution of this project, for the late-night online help with technical issues and for opening my eyes to the many applications of a piece of foil in an optics lab.

My collaborators, Dr. Daniel Rauh and Dr. Haridas Rode for their major role in the design and synthesis of probes used in this study and their insight into kinase-drug interactions.

Dorothee Vogt, Dina Truxius and Jutta Luig for their assistance in cloning and mutation of constructs used in this study.

Petra Glitz and Anetta Langerak for their assistance with cell culture. Hendrike Schultz and Kirsten Michel for their technical assistance.

Drs. Sven Müller, Michael Schultz, Klaus Schuermann, Jana Harizanova, Hernán Grecco for technical assistance pertaining to the setup and application of the various microscopes used in this project. Dr Michael Schultz for his help with cell sorting.

Drs. Nachiket Vartak, Malte Schmick and Hernán Grecco for their much-appreciated assistance with development and automation of data analysis pipelines.

Sven Fengler, Dina Truxius and Dr. Pedro Roda-Navarro for their advice and assistance on the cellular biological aspects of this project.

Franziska Thorwirth and Dr. Nachiket Vartak, for their continuous input, extensive help with troubleshooting all aspects of my project and the general scientific discussions and for keeping me motivated through their contagious passion for science.

My 'editor-in chief' Dr. Robin Bon for tirelessly editing my thesis and input on the chemical aspects of my work.

Current and past members of the Bastiaens lab for their support, advice, assistance and discussions: Ola Sabet, Jian Hou and Drs. Andreas Girod, Ali Kinkhabwala, Peter Verveer, Eli Zamir, Ivan Yudushkin, Piotr Liguzinski.

The office members: Sven Fengler, Lisa Karajannis, Maja Sinn, Johan Jarzombek, Rahul Ravindran, Thies Kluessendorf and Björn Papke (honorary officemate).

Dr. Astrid Krämer the lab manager for ensuring the lab ran smoothly so I could focus on the science and the occasional, 'subtle' reminders about my deadline.

Finally I would like to thank the NRF and Max Planck Gesellschaft for funding.

Table of Contents

List of Figures

List of Abbreviations

°C	degrees Celsius
Abl1	Abelson tyrosine-protein kinase 1
ABP	activity-based probe
abs	absorption
Ac	acetyl
ADP	adenosine diphosphate
Akt	protein kinase B
APE	alanine-proline-glutamic acid
AR	analytical reagent
ATP	adenosine triphosphate
BCR	breakpoint cluster region
BDP	Bodipy (boron dipyrromethene)
Bodipy	boron dipyrromethene
bp	base pairs
BSA	bovine serum albumin
C	cysteine
Cbl	Casitas B-lineage lymphoma
CFP	cyan fluorescent protein
CIP	calf intestine alkaline phosphatase
CMV	cytomegalovirus
Csk	C-src tyrosine kinase
$\Delta\phi$	phase shift
D	donor
DA	donor in presence of acceptor
DD	doubly distilled
DFG	aspartic acid-phenylalanine-glycine
DMEM	Dulbecco's Modified Eagle Medium
DMSO	dimethylsulfoxide
DNA	deoxyribonucleic acid
DPBS	Dulbecco's Phosphate-Buffered Saline
DPF	Dortmund Protein Facility
ds	double-stranded
DTT	dithiothreitol
E	efficiency
E. coli	*Escherichia coli*
EDTA	sodium ethylenediaminetetraacetate
EGF	epidermal growth factor
EGFR	epidermal growth factor receptor
EGR1	early growth response protein 1
Elk-1	E twenty six (ETS)-like transcription factor 1
em	emission
ErbB	erythroblastic leukemia viral oncogene
Et	ethyl
et al.	et alii (and others)
EtBr	ethidium bromide
EYFP	enhanced yellow fluorescent protein
exc	excitation
F	phenylalanine
FAK	focal adhesion kinase
FCS	foetal calf serum
FP	fluorescent protein
g (in centrifuging)	gravity
G418	neomycin
GFP	green fluorescent protein
GPI	glycosylphosphatidylinositol
h	hour

HB-EGF	heparin-binding EGF-like growth factor
HEPES	4-(2-hydroxyethyl)-1-piperazineethanesulfonic acid
HSP90	heat shock protein 90
I	intensity
IRF	instrumental response function
κ^2	the relative orientation of transition dipole of a fluorophore
kb	kilobase
k_{cat}	rate constant of catalysis
λ	wavelength
L	leucine
LB	lysogeny broth
LRh	lissamine rhodamine
LRIG1	Leucine-rich repeats and immunoglobulin-like domains protein 1
LSCM	laser scanning confocal microscopy
LUT	lookup table
µg	microgram
µl	microlitre
M	modulation depth
M/Met	methionine
mCit	monomeric Citrine
MCF-7	Michigan Cancer Foundation-7 (cell line)
mg	milligram
MHz	megahertz
MIG6/RALT	receptor-associated late transducer
min	minute
ml	millilitre
mm	millimeter
mM	millimolar
NA	numerical aperature
NaN	not-a-number
NBD	nitrobenzoxadiazole
NEB	New England Biolabs
nm	nanometer
nM	nanomolar
NRG	neuregulin
ns	nanosecond
Ω	Ohm
P-value	probability value
PBS	phosphate-buffered saline
PCR	polymerase chain reaction
PDGFB	platelet-derived growth factor B
PDGFR	platelet-derived growth factor receptor
PEG	polyethyleneglycol
PKC	protein kinase C
PKI	protein kinase inhibitor
PLL	poly-L-lysine
PMA	phorbol-myristate acetate
PMT	photomultiplier tube
ps	picoseconds
PTP	phosphor-tyrosine phosphatase
pTyr	phosphor-tyrosine
PTB	phosphotyrosine-binding domain
Q	quantum yield
r	radius
R	arginine
R_0	Förster radius
rpm	rounds per minute
RT	room temperature
RTK	receptor tyrosine kinase

s	second
S/Ser	serine
SH(2/3)	Src homology domain (2/3)
SLO	streptolysin-o
SOB	super optimal broth
SOC	super optimal broth with catabolite repression
SPAD	single photon avalanche diode
SPRY	sprouty
SP1	specificity Protein 1
STDEV	standard deviation
SV40	simian virus 40
T/Thr	threonine
TAE	tris/acetate/EDTA
TBS	tris buffered saline
TGFα	transforming growth factor alpha
TCSPC	time-correlated single photon counting
TIFF	tagged image file format
Tyr	tyrosine
TyrK	tyrosine kinase
U	units
unstim	unstimulated
V	Volt
v-Src	sarcoma (Schmidt-Ruppin A-2) viral oncogene homolog
VEGFR	vascular endothelial growth factor receptor
WT	wild type
YFP	yellow fluorescent protein

Chapter 1

Introduction

1.1. Perspective

The aim of systems biology is to generate a global view of cellular function through an understanding of cellular networks, in the combined context of their components, and their dynamics in space and time. Through the iterative process of acquiring experimental data, mathematical modeling and making predictions, the systems biology approach comes closer to obtaining the causal connectivities leading to the emergent properties displayed as cellular outcomes.

A combination of genomics, proteomics and high throughput technology has enabled extensive identification and characterization of components of biological systems. Biochemical approaches continue to provide essential basic information to deduce the connectivity patterns of biological components in a reductionist manner. However, it is still difficult to gauge the global complexity of the cellular environment by these methods. The move to using the intact cell as the vessel for reactivity and quantification of biochemical events has been facilitated by the advent of genetic manipulation. The availability of genetic tags, such as GFP and its derivatives, together with fluorescence microscopy approaches, has made it possible to view proteins in their native environment. Imaging approaches facilitate progression from the "homogenized freeze frame" models given by "omics" approaches to quantitative, dynamic models of temporal and spatial parameters in individual cells. Spatial distributions of proteins in different cellular compartments are in themselves a highly precise dimension of cellular regulation.

Systems biologists are continuously seeking tools, be they mathematical or experimental, to improve the predictability of a system. On the experimental front, the field of chemical biology has been evolving in parallel to that of systems biology and both fields have now reached a point of regular intersection. Systems biologists are employing small molecule probes developed by chemical biologists as tools for manipulating biological networks in a controlled manner to gain insight about their causal connectivity. The combination of

systems and chemical biology approaches facilitates unraveling of the mechanistic processes of disease leading to better drug targets. The work described in this thesis presents a method designed at the intersection of chemical and systems biology.

The major aim of this Ph.D. project is to develop a method for imaging tyrosine kinase-drug interactions in cells. This method would be directed at the gap between *in vitro* drug target validations, using purified proteins or cell extracts, and studies in whole organism models.

Additionally, acute protein activity perturbation by small molecule inhibitors is a powerful tool for resolving network causalities. Imaging techniques are being employed to quantitatively solve networks spatially and temporally at the single cell level (Simpson et al., 2007; Grecco et al., 2010). The advent of approaches such as those of Simpson et al. (2007) and Grecco et al. (2010) has driven the design of our method as a complementary technique to study inhibitor-target interactions in the context of single cells.

The combination of Förster resonance energy transfer (FRET) with microscopy enables the spatial mapping of interactions occurring on the nanometer scale. Therefore, we propose to measure FRET upon binding of a donor-labeled kinase and an acceptor-labeled inhibitor in cells by fluorescence lifetime imaging microscopy (FLIM). For construction of such a FRET system, we will modify small molecule tyrosine kinase inhibitors to incorporate an acceptor fluorophore and label expressed tyrosine kinases with donor fluorophores. The detection of FRET between the donor-labeled EGFR and acceptor-labeled PD168393 will be used as the model system for the development of the proposed assay. Presented in this thesis is the design of the FRET-based inhibitor probes, optimization of the cellular assays for detecting inhibitor binding, and profiling of multiple probe-target interactions in cells.

The current study focuses on tyrosine kinases because they are key regulators of cell signaling and an intensely pursued class of drug targets. The majority of these are being investigated as anti-cancer therapeutics though deregulation in kinase function has been implicated in several disorders. In the general introduction to this thesis the biology and enzymology of tyrosine kinases (Section 1.2) provides a brief overview of tyrosine kinase classification, signaling and role in cancer. Because tyrosine kinase inhibitors are employed to create imaging tools in this work further information on the regulation of tyrosine

kinases by small molecules is covered in Section 1.3. In Section 1.4 currently available EGFR inhibitor probes, which provide the basis for the imaging probes used in this study are described and the theory behind FRET and FLIM is given in Section 1.5. This is followed, in Section 1.6, by an outline of the work undertaken in this thesis and the order in which the chapters and chapter sections unfold.

1.2. Biology and enzymology of tyrosine kinases

Many activities such as cell proliferation, differentiation, adhesion and motility are regulated by tyrosine phosphorylation. The transfer of a phosphate group from ATP to an amino acid residue is catalyzed by protein kinases. Dephosphorylation is brought about by protein phosphatases.

1.2.1. Classification

Several classification schemes for kinases have been proposed in the literature. Initially, conservation and phylogeny analysis of the catalytic domains of eukaryotic protein kinases was performed by Hanks and Hunter (1995), and has since then been extended by many groups. Approximately 518 protein kinases are encoded in the human genome and included amongst them are the superfamilies, which mediate phosphotransfer to serine, threonine or tyrosine residues on substrate proteins. Serine/threonine kinases are prevalent throughout eukaryotes whereas tyrosine kinases are found only in metazoans and their single-celled relatives (Robinson et al., 2000; Manning et al., 2008). In addition to bearing conserved catalytic domains similar to those of serine/threonine kinases and dual kinases, protein tyrosine kinases possess their own characteristic motifs (Amanchy et al., 2007). Within the protein tyrosine kinase superfamily there are 58 known receptor tyrosine kinases in mammals, which contain extracellular domains in addition to the conserved intracellular kinase catalytic domains (Robinson et al., 2000).

Receptor tyrosine kinases

Receptor tyrosine kinases are transmembrane proteins that relay extracellular signals to bring about intracellular events. The extracellular domains exhibit substantial structural variation, used to partner with various signaling ligands while the cytoplasmic domain has

a highly conserved tyrosine kinase region. Both the extracellular and the intracellular domains remain in an auto-inhibited conformation, which is released upon ligand-induced dimerization (Dawson et al., 2005).

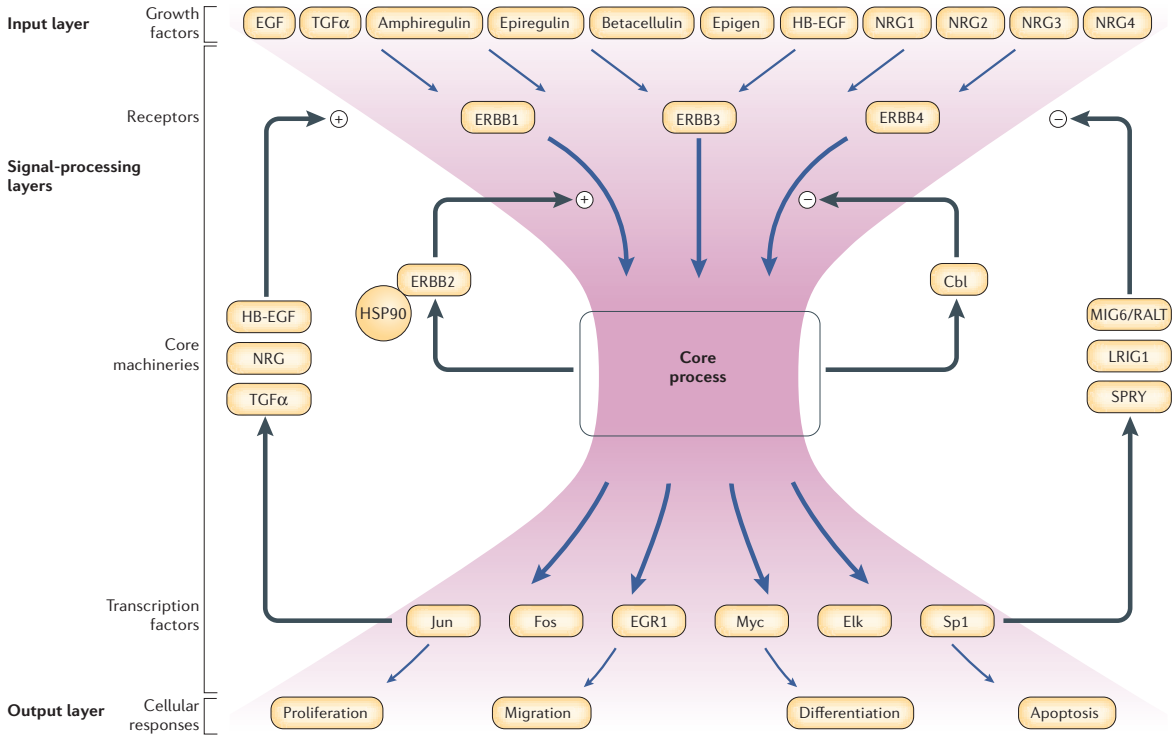

Figure 1.1 Representation of the bow-tie structured signaling network of ErbB family receptor tyrosine kinases.
The core process is a set of biochemical interactions which interface with the input and output modules. The input module refers to activation of ErbB receptor tyrosine kinase in response to their partly redundant ligands. The output of the network is regulated cell behavior arising from gene expression, which is controlled through multiple transcription factors (from Citri and Yarden, 2006).

In terms of their signaling, receptor tyrosine kinases have several features that create a functionally robust system. One representation of such a system is by a bow-tie structure (Figure 1.1). A core process (as shown in the centre of the bow-tie) receives diverse inputs and integrates them to generate multiple outputs. The bow-tie structure comprises of several modules, which are partially redundant. Redundancy allows a compensatory effect in the case of a particular component's failure. Robust networks have plasticity and are able to dynamically switch signals into alternative pathways. They also display tolerance in the

event of transiently accumulated protein aberrations by not significantly altering the network outcomes (Amit et al., 2007).

Non-receptor tyrosine kinases

Non-receptor tyrosine kinases lack a transmembrane domain, are often cytoplasmic and generally function downstream of receptor tyrosine kinases. They comprise the remaining 30% of know tyrosine kinases and in mammals there are 10 families of non-receptor tyrosine kinases (Robinson et al., 2000). Their catalytic domains are closely related to those of receptor tyrosine kinases, and, in addition, have non-catalytic regions linked to kinase activation and substrate specificity (Miller, 2003). Src homology 2 (SH2) and Src homology 3 (SH3) domains originally identified in v-Src are modulators found in a variety of signaling proteins. SH2 domains recognize short polypeptide motifs containing phosphotyrosine and SH3 domains bind to proline-rich motifs (Dawson et al., 2005). SH2 and SH3 domains facilitate protein-protein interactions with substrates and their amino-terminal domains are used in activation. For tyrosine kinases such as Src that lack a trans membrane region, proper sub-cellular localization is aided by the non-catalytic regions.

1.2.2. Catalytic mechanism

The kinase domain is conserved amongst Ser/Thr and Tyr kinases. The ~260 amino acid kinase domain folds into a two-lobe structure (Taylor and Radzio-Andzelm, 1994), which is responsible for catalytic activity and can contribute to substrate specificity. The smaller N-terminal lobe contains the ATP binding pocket and the larger C-terminal lobe is associated with substrate binding (Parang and Cole, 2002).

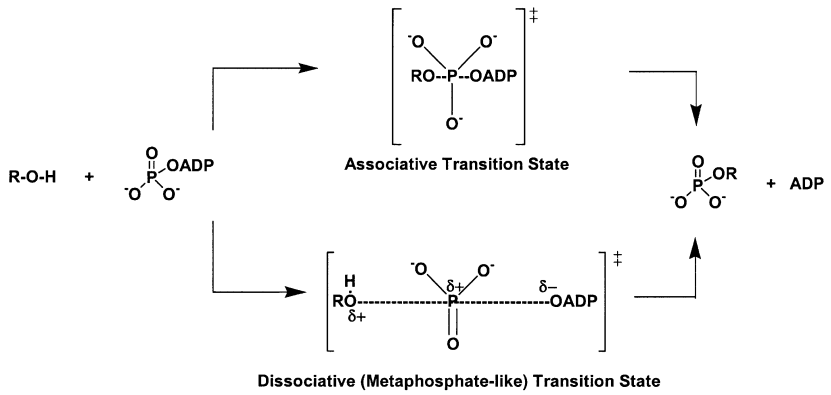

Figure 1.2 Associative versus dissociative transition states for phosphoryl transfer (from Parang and Cole, 2002).

The catalytic mechanism of protein kinases involves the formation of a ternary complex consisting of the kinase, substrate and MgATP (Cole et al., 1994; Ho et al., 1988). In general the transfer of the phosphoryl group from ATP to the substrate may occur by either an associative or dissociative reaction (Åqvist et al., 1999).

Dissociative mechanism

In the dissociative transition state, the bond between the attacked phosphorous and ADP is broken prior to formation of the bond between the attacked phosphorus and the nucleophile (Tyr, Thr or Ser) (Figure 1.2) (Åqvist et al., 1999).

Associative mechanism

In the associative transition state, there is significant amount of bond formation between the nucleophile and attacked phosphorus, with relatively little bond breakage between the phosphorus and ADP (Figure 1.2) (Åqvist et al., 1999).

These mechanisms are distinguished by characteristics such as nucleophile strength, distance between the phosphorous and oxygen atoms of the attacking and leaving groups, as well as pH dependence of the reaction.

Arguments for an associative mechanism propose that enzymes surround the attacked phosphate with positively charged groups. In this way the negative charge on the phosphate is neutralized making it a better electrophile. Justification for this argument is based on a non-enzymatic phosphate triester reaction, which showed associate behavior (Kim and Cole, 1998).

Studies on the catalytic phosphoryl transfer state of Csk, with a series of fluoro-tyrosine containing substrates, indicate that the substrate phenol must be neutral to be phosphorlated. These results support a dissociative transition state for phosphoryl transfer and a potential role for the conserved aspartate residue in the active site. Mutation of the conserved aspartate in Csk and Protein Kinase A (PKA) results in a reduction in the k_{cat} of both kinases by a factor of ~ 10^4 (Kim and Cole, 1998).

The long coordinate distance of 5.2 Å between the nucleophile and attacked phosphate, found for PKA, provides additional evidence for a dissociative mechanism (Kim and Cole, 1998). Consideration of geometric constraints for dissociative or associative reactions

forms the basis for the design of bisubstrate kinase inhibitors. A successful insulin receptor kinase inhibitor has been developed based on a dissociative mechanism, adding strength to the argument in favour of a dissociative mechanism (Parang et al., 2001).

1.2.3. Phosphotyrosine signaling

The evolution of phosphotyrosine signaling provides one model of how multicomponent biological systems are generated. Through the covalent addition of a phosphate group to tyrosines in cellular proteins, a signaling mechanism has emerged that is speculated to be a key event in the transition to multicellularity (Pincus et al., 2008; Lim and Pawson, 2010).

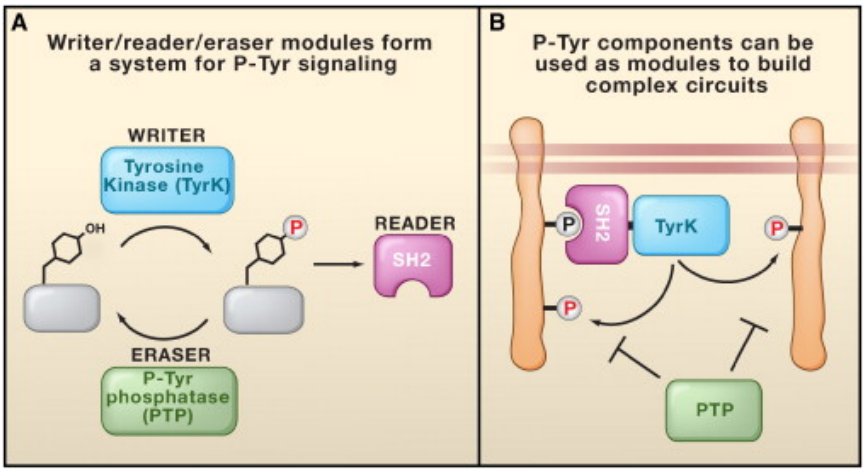

Figure 1.3 The writer, eraser, reader tyrosine phosphorylation toolkit
(A) In pTyr signaling, the tyrosine kinase (TyrK), Src Homology 2 (SH2), and phosphotyrosine phosphatase (PTP) domains form a highly interdependent signaling platform. This platform serves as the writer, reader, and eraser modules, respectively, for processing pTyr marks. (B) Components of pTyr signaling can be used to build complex circuits. For example, recruitment of an SH2-TyrK protein to an initiating pTyr site can lead to amplification of tyrosine phosphorylation through a positive feedback loop (from Lim and Pawson, 2010).

A reductionist overview of tyrosine phosphorylation groups it into three activity modules. These 3 modules have been termed the 'writer', 'eraser' and 'reader' toolkit (Lim and Pawson, 2010) (Figure 1.3(A)). The toolkit modules consist of tyrosine kinases that phosphorylate specific tyrosine residues on substrate proteins ('writer'), phosphotyrosine phosphatases that remove the phosphates ('eraser') and Src homology 2 (SH2) domains that recognize and bind to the phosphorylated site ('reader') (Pawson, 1995).

Each module in the toolkit has its own complex spatio-temporal signaling properties. Together these modules form a cellular information platform through which diverse regulatory schemes can be achieved (Figure 1.3(B)).

1.2.4. Tyrosine kinases in cancer

Tyrosine kinases are normally highly regulated and have low basal activity. Activation is transient and brought about in response to specific stimuli. Despite their tightly regulated activity in normal cells, transforming functions may be acquired by mutation(s), over-expression and autocrine paracrine stimulation, leading to malignancy. Many tyrosine kinases have also been found to be involved in the processes causing tumour cell proliferation and survival.

In cancer cells receptor tyrosine kinase family members are frequently overactive and several receptor tyrosine kinases and their growth factors play a significant role in cancer survival and progression. Examples of receptor tyrosine kinases in cancer include EGFR (ERBB family), PDGFR, VEGFR and RET as reviewed by Zhang et al. (2009) and Noble et al. (2004).

Some well-characterized non-receptor tyrosine kinases include Src, JAK, c-Abl, Csk and FAK. The involvement of non-receptor tyrosine kinases in cancer has been linked to their over-expression, mutation and translocation as reviewed by Zhang et al. (2009) and Noble et al. (2004).

When cellular regulatory mechanisms are overcome by genetic mutations or mis-localization this can result in the transforming capacity of oncogenic kinases. In many cases an ‘oncogene addiction’ arises, which can be related to a single pathway that drives survival and proliferation of cancer cells (Weinstein and Joe, 2008). Once this pathway is disrupted it results in sensitization of the cancer cells to kinase inhibitors responsible for abrogating this pathway, eventually leading to cell death.

1.3. Regulation of protein kinases by small molecules

1.3.1. Protein kinase inhibitors

Strategies for designing small molecule inhibitors targeting kinase activity include: (i) targeting the ATP-binding site; (ii) targeting the substrate-binding site; (iii) bisubstrate inhibitors that simultaneous target both ATP-binding and substrate binding sites; or (iv) targeting an allosteric site on the kinase.

Protein kinase inhibitors that occupy the protein substrate-binding sites are generally comprised of peptide inhibitors. The advantage of targeting the substrate-binding surface is greater drug-target specificity, because there is less conservation of this area amongst different family members. One naturally occurring example is protein kinase inhibitor (PKI), which shows nanomolar affinity and high specificity for PKA (Knighton et al., 1991). Designing synthetic small molecule inhibitors against the substrate-binding site is complicated because of the comparatively shallow pocket used to bind peptides. Peptides themselves typically exhibit poor bioavailability, pharmacokinetic properties and are easily proteolyzed thereby limiting their suitability as therapeutic drugs. Despite these drawbacks, approaches combining unnatural amino acids within a peptide motif have lead to potent inhibitors of PKC, Src and Akt (Lee et al., 2004; Hah et al., 2006; Lee et al., 2008).

Bisubstrate inhibitors contain two conjugated fragments targeting two different binding sites of an enzyme (Lavogina et al., 2010). In the case of protein kinases, one fragment of the bisubstrate inhibitor targets the ATP-binding site and the other fragment targets the substrate binding. The understanding of the transistion state in the catalytic mechanism of protein kinase activity facilitates the design of these inhibitors. An advantage of this approach is that it improves selectivity and affinity to the target by generating more interactions as compared to single site inhibitors. Bisubstrate inhibitors have been generated against various protein kinases including insulin receptor kinase (Parang et al., 2001), PKA (Hines and Cole, 2004), and Csk (Shen and Cole, 2003). This class of inhibitors has been used predominantly as tools for studying kinase conformation. The structure of EGFR in complex with an ATP analogue-peptide conjugate provided a model for the basis of kinase activation through an asymmetric dimer (Zhang et al., 2006).

Allosteric inhibitors comprise a class of compounds that bind outside the ATP binding pocket and regulate kinase activity in an allosteric manner. Such inhibitors have high kinase selectivity because they target unique regulatory binding sites on a particular kinase. One example is CI-1040, which inhibits MEK1 and MEK2 by occupying a pocket adjacent to the ATP binding sites (Adrian et al., 2006). Allosteric activators of kinase activity have also been discovered. One example is RO028165, which activates glucokinase (Grimsby et al., 2003).

In the current study only ATP-binding-site inhibitors were investigated and will, therefore, be the focus of this section.

Protein kinases are defined by their ability to catalyze the transfer of the terminal phosphate of ATP to amino acid residues of substrate proteins. The ATP binding site of protein kinases provides a versatile binding site for relatively hydrophobic molecules (Lawrie et al., 1997). The secondary structural elements of the catalytic pocket are conserved amongst kinases. Most kinase inhibitors are ATP competitive and capable of mimicking the hydrogen bonds formed by the adenine ring of ATP (Traxler and Furet, 1999).

Kinase activity is regulated by the conserved activation loop marked by DFG and APE motifs (one-letter amino acid abbreviations) at the start and end of the loop. The activation loop can assume a large number of conformations; amongst them are the catalytically active conformation (conducive to phosphotransfer, also known as the DFG-in conformation) and the inactive conformer in which the activation loop blocks the substrate-binding site (also known as DFG-out conformation). Inhibitors are available that target the ATP binding site with the activation loop in the active (type 1) or inactive (type 2) conformation (Zhang et al., 2009).

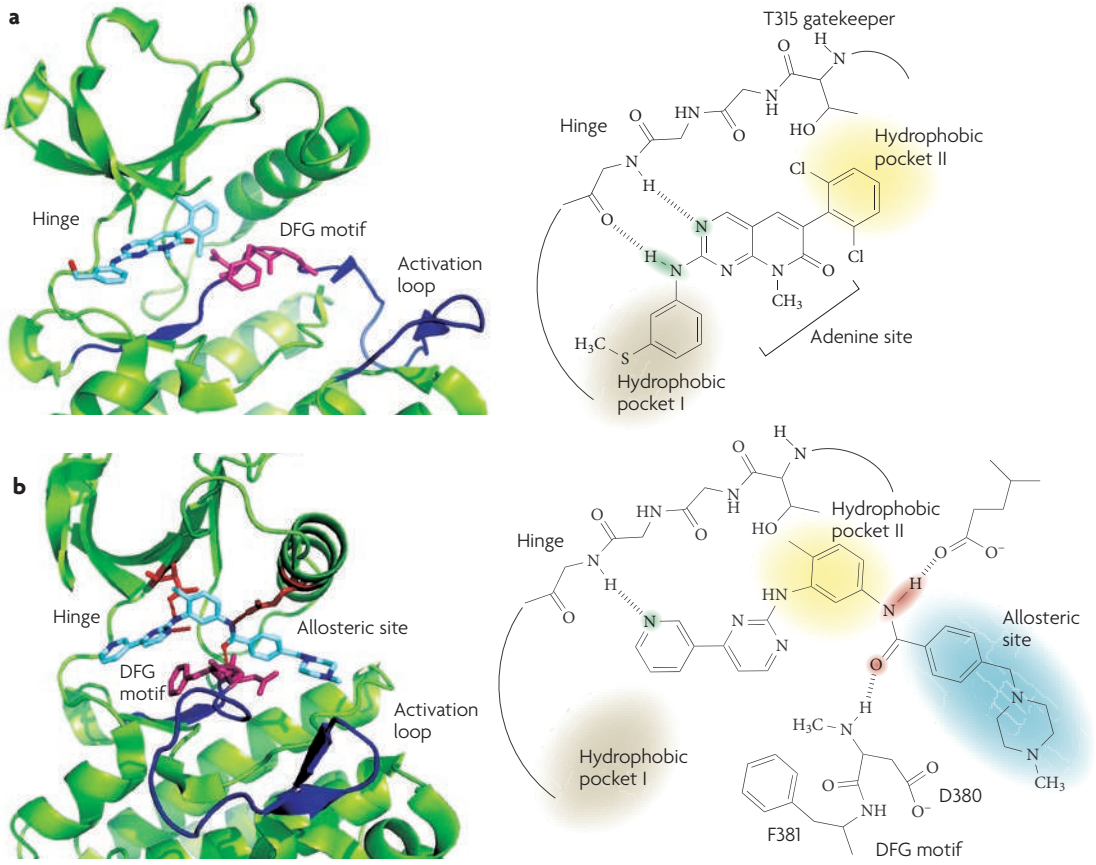

Figure 1.4 The mode of binding of ATP binding site inhibitors targeting the active and inactive kinase conformations.
Kinase inhibitor interactions depicted by ribbon (left) and chemical (right) structures. The chemical structures indicate hydrophobic regions I (beige) and II (yellow). The dashed lines indicate hydrogen bonds between the kinase inhibitor and enzymes at the hinge region (green) or the allosteric site (red). The ribbon representation shows the DFG motif (pink), the kinase inhibitors (light blue) and the activation loop (dark blue). Abl1 is shown in complex with the type 1 ATP competitive inhibitor PD166326 (a) and type 2 inhibitor imatinib (b). The allosteric pocket, exposed in the DFG-out conformation, is indicated by the blue shaded area (left) (from Zhang et al., 2009).

Type 1 ATP-competitive inhibitors recognize the active conformation of the kinase. These inhibitors are believed to have been discovered partially as a result of using enzymatic assays in which kinases were introduced in an active conformation. Typically type 1 inhibitors comprise a heterocyclic ring system that occupy the purine binding site and provides the scaffold for side chains aimed at the adjacent hydrophobic regions I and II (Figure 1.4).

Type 2 inhibitors recognize the inactive conformation of the kinase (Liu and Gray, 2006). When in the DFG-out conformation an additional hydrophobic binding site is exposed directly adjacent to the ATP binding site (Figure 1.4).

Covalent kinase inhibitors form an irreversible, covalent bond, usually to a nucleophilic cysteine residue in the kinase active site (Cohen et al., 2005).

1.3.2. Kinase inhibitor resistance mechanisms

Many kinase inhibitors exert their cytotoxic effects on cancer cells by the down-regulation of a specific kinase/pathway essential to the survival of the cancer cells. In genetically heterogeneous tumour populations this creates a strong selection pressure for cells containing molecular mechanisms that confer drug resistance.

Genetic mutations are one mechanism of drug resistance. Included in these are point mutations such as those at the 'gatekeeper residue', which is known to infer drug resistance of EGFR to the inhibitor erlotinib (Yun et al., 2008). The 'gatekeeper residue' refers to the conserved threonine in the ATP binding pocket of tyrosine kinases and is called as such because the size of the amino acid side chain at this position regulates the accessibility of the hydrophobic pocket located adjacent to the ATP binding site. Hydrophobic interactions within this hydrophobic pocket are crucial for the binding affinities of many kinase inhibitors (Blair et al., 2007). The gatekeeper mutation (T315I) in BCR-ABL1 reduces drug binding by steric hinderance (Quintás-Cardama and Cortes, 2008). The EGFR gatekeeper mutation T790M has been shown to activate wild type (WT) EGFR. The introduction of the T790M mutation, as a secondary mutation to EGFR-L858R, increases the ATP affinity of the oncogenic L858R mutant by more than an order of magnitude (Yun et al., 2008).

Gene amplification is also a major oncogenic activator (Albertson, 2006) and a mechanism for inhibitor resistance. BCR-ABL gene amplification has been found to increase in response to imatinib treatment (Ashworth et al., 2011). In this way the stoichiometry of the drug-target interaction is altered in favor of the target and results in its reduced inhibition.

Non-mutational resistance mechanisms can occur by activation of alternative pathways or changes in drug influx/efflux. EGFR family members have shown inhibitor resistance by activating alternate pathways (Xia et al., 2006). This is achieved by activating the

expression of downstream effectors or the activation of alternate kinases (Desbois-Mouthon et al., 2009). Drug resistance can also result from a decrease of the effective intracellular concentration of the drug. Cellular drug concentrations can be regulated by increased drug influx/efflux and drug plasma sequestration (Gillet and Gottesman, 2010).

1.4. Fluorescence-based probes of EGFR

Fluorescence based imaging tools provide methods for monitoring the spatial and temporal distribution of proteins and biomolecules dynamically. Strategies for monitoring enzyme function in cells have been developed for a range of enzyme families, but there has been an emphasis on proteases and kinases because of the large size of these families, their highly studied function and their potential as drug targets (Baruch et al., 2004).

A photoaffinity probe (AX7593) of EGFR was designed by Shreder et al. (2004). AX7593 has a tetramethylrhodamine fluorophore linked to a 4-anilinoquinazoline based inhibitor. The link was created at the C7 position of the quinazoline via a tetraethyleneglycol linker.

Blair et al. (2007) have also designed a fluorescence based inhibitor probe of EGFR. From the structural analysis of EGFR and Src in complex with PD168393 (also a 4-anilinoquinazoline scaffold inhibitor) and another irreversible C4 derivatized analogue of PD168393, they determined a suitable site for attachment of a fluorophore. The C7 position of the quinazoline was selected because it points outside the ATP binding pocket towards the solvent, and was the point that has previously been shown to accept a modification without affecting drug potency (Smaill et al., 2000). An NBD fluorophore was attached to the C7 position of the 4-anilinoquinazoline inhibitor scaffold of PD168393 via a polyethyleneglycol (PEG) linker. Subsequently fluorescence gel imaging was used to visualize probe binding to EGFR. Minimal background binding to other proteins being observed and probe binding showed a dose-dependence in response to pretreatment of cells with an irreversible ATP binding site inhibitor (Blair et al., 2007).

1.5. Fluorescence-based imaging approaches for studying molecular interactions

Through exploitation of the photophysical properties of emitted fluorescence in combination with advanced microscopy approaches information on intracellular interactions can be obtained.

1.5.1. Fluorescence properties and photophysics

The interaction of a molecule with a photon leads to an electron being promoted from a ground state to an excited state. Fluorescence can occur when an electron in the excited state is paired by opposite spin to the electron in the ground state (singlet state) and relaxes to the ground state upon emission of a photon (Lakowicz, 2006). The energy of the absorption is typically higher than that of the emission photon and in the case of fluorescence this decay takes place on the timescale of nanoseconds.

The Jablonski (or State) diagram (Figure 1.5) depicts the accessible states in the molecule. The singlet ground, first and second states are represented by S_0, S_1 and S_2, respectively. Each electronic state comprises various vibrational states (not shown in Figure 1.5).

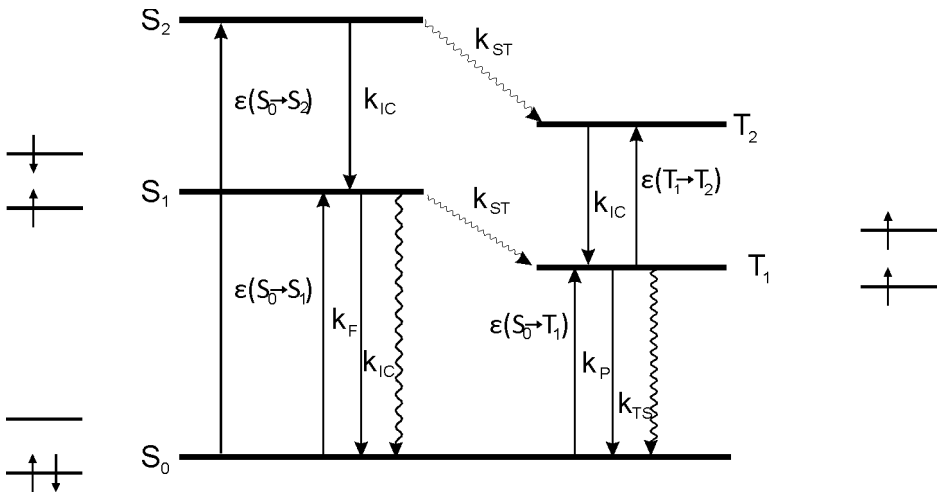

Figure 1.5 Jablonski or State Energy diagram.
Jablonski or State Energy diagram showing the singlet ground state (S0) and the first two excited singlet (S1, S2) and triplet (T1, T2) states and the respective rate constants.

Upon light absorption, an electron is usually excited to either S1 or S2. Thereafter several processes can occur. Two electrons in one orbital are always spin-paired (Singlet), however, after the excitation the electrons can change their spin to create an unpaired electron couple (Triplet, T_1). The excited singlet state can deactivate either radiatively (fluorescence – k_F) or nonradiatively (internal conversion – k_{IC}) to a lower singlet state. Alternatively, the excited singlet state can deactivate non-radiatively to the first triplet state T1 (inter-system crossing – k_{ST}). Deactivation of the triplet state occurs either radiatively (phosphorescence – k_P) or non-radiatively (inter-system crossing – k_{TS}) to the singlet ground state.

The rate of radiative deactivation k_F cannot be measured directly. However, the excited state lifetime τ that is inversely proportional to the sum of all deactivation states (radiative and non-radiative) can be measured:

$$\tau = \frac{1}{k_F + k_{IC} + k_{ST}} \tag{1}$$

1.5.2. Resonance energy transfer between fluorophores

Förster resonance energy transfer (FRET) refers to the non-radiative, nanometer ranged process whereby energy from an excited donor fluorophore is transferred to an acceptor fluorophore (Clegg, 1995). FRET is a photophysical phenomenon used to measure protein interactions. The distance between the donor and acceptor fluorophores r (nm) dictates the efficiency *E* at which Förster-type energy transfer occurs:

$$E = \frac{R_0^6}{R_0^6 + r^6} \tag{2}$$

R_0 (nm) is the Förster radius that represents the distance at which the energy transfer has an efficiency of 50% (Figure 1.6, left). R_0 typically has a value between 2 and 6 nm, which compares to typical globular protein radii:

$$R_0 = \left[\kappa^2 \times J(\lambda) \times Q\right]^{\frac{1}{6}} \times 9.7 \times 10^2 \tag{3}$$

R_0 is affected by the relative orientation of the transition dipoles of the fluorophores (κ^2), the overlap integral ($J(\lambda)$; $cm^6 \cdot mol^{-1}$), the refractive index of the intervening medium (n), and the quantum yield of the donor (Q). The overlap integral depends on the overlap region of the donor emission (em) and acceptor absorption (abs) spectra (Figure 1.6, right).

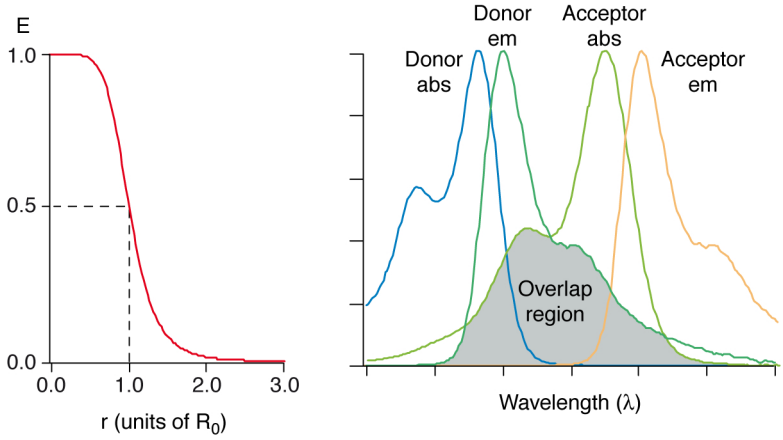

Figure 1.6 Factors affecting FRET efficiency.
(Left) The Förster radius (R_0) is the distance between two molecules at which 50% energy transfer takes place. (Right) The overlap integral depends on the overlap region of the donor emission (em) and acceptor absorbance (abs) spectra (adapted from Bastiaens and Pepperkok, 2000).

FRET reduces the fluorescence lifetime of the donor fluorophore as it provides an additional pathway for depopulation of the excited state:

$$\tau = \frac{1}{k_F + k_{IC} + k_{ST} + k_{FRET}} \qquad (4)$$

FRET efficiency can be experimentally obtained by observing the drop in intensity (I) or lifetime (τ) of the donor (D) upon addition of the acceptor (DA):

$$E = 1 - \frac{I_{DA}}{I_D} = 1 - \frac{\tau_{DA}}{\tau_D} \qquad (5)$$

1.5.3. Principles of fluorescence lifetime imaging microscopy (FLIM)

Combining FRET with microscopy expands the applicability of standard optical microscopy. Spatial mapping of FRET processes within a cell can reveal biological interactions on the nm scale by converting them into a signal detectable on the µm scale.

As shown in Equation 5, the FRET efficiency (*E)* for a donor/acceptor pair can be calculated from excited state lifetime of the donor fluorophore (τ), in the presence and absence of an acceptor fluorophore. The donor fluorescence lifetime (τ) can be measured using either frequency or time domain FLIM.

Frequency-domain FLIM

In frequency-domain FLIM the sample is excited with modulated light. The optimal frequency of the modulated light is in the range of the reciprocal to the fluorescence lifetime of the fluorophore to be measured. The emitted fluorescence has a modulation at the same frequency as the excitation light but with a reduced relative modulation depth (*M*) and a shift in phase $\Delta\phi$ (Figure 1.7). From the shift in phase and relative modulation depth, the phase τ_ϕ and modulation τ_M lifetimes can be calculated:

$$\tau_\phi = \omega^{-1} TAN(\Delta\phi) \quad (6)$$

$$\tau_M = \omega^{-1}\sqrt{(M)^{-2} - 1} \quad (7)$$

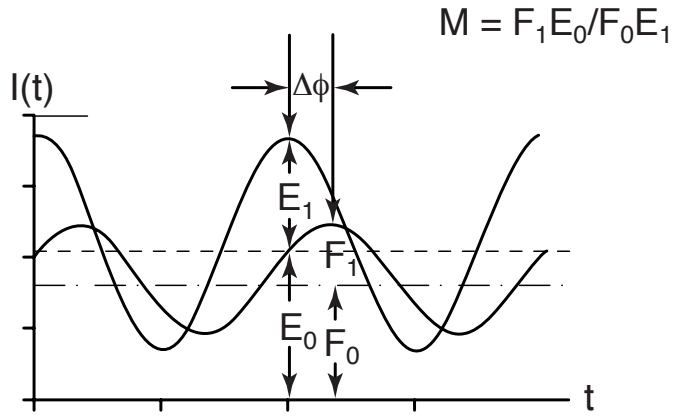

Figure 1.7 Principle of frequency-domain FLIM.
The modulated excitation intensity (I) oscillates around the mean intensity (E_0) with amplitude (E_1). The emitted intensity follows the excitation delayed by the phase ($\Delta\phi$) with a reduced mean intensity F_0 and amplitude F_1 (adapted from Bastiaens and Squire, 1999).

To measure the phase and modulation, the detection photocathode is modulated at the same frequency as the excitation wave. A stack of images is obtained by varying the phase shifts

between excitation and detection at regular intervals; the phase intervals range from 0–2π. From the change in intensity of each pixel through the image stack, the phase and modulation can be obtained. By using a scattering surface as a reference, it is possible to determine the phase and modulation of the excitation beam at the focal plane. No phase shift or demodulation is induced by the scattering sample. The phase shift ($\Delta\phi$) is the difference between the phase of the sample and reference. The demodulation (M) is the quotient of the modulation in the sample and reference (Bastiaens and Squire, 1999).

Time-domain FLIM

In time-domain FLIM the fluorophore is excited with a short pulse of light. The duration of the pulse is much shorter than the fluorescent lifetime τ_f of the fluorophore being measured. This results in an exponential decay of the emission that can be traced and fitted to an (multi) exponential (Figure 1.8).

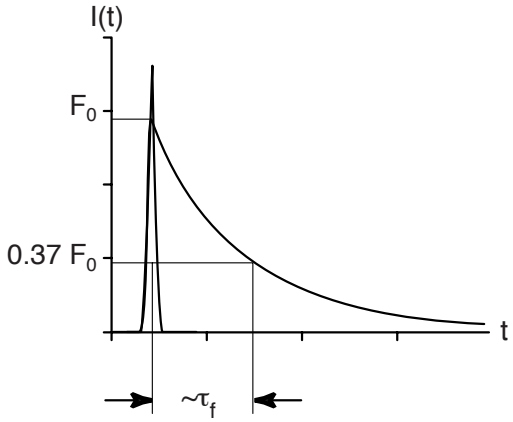

Figure 1.8 Principle of time domain FLIM.
Using a short pulse of light a fraction of fluorophores are excited. Decay from this excited state follows a Poissonian distribution with a maximum of F_0 and a fluorescence lifetime τ_f characterized by $I(\tau_f) = 1/e\ F_0$ (adapted from Bastiaens and Squire, 1999).

For detection of fluorescence lifetimes in the nanosecond (ns) range, time correlated single photon counting (TCSPC) is used. By repeatedly exciting a sample and measuring the photon arrival times a histogram is populated that reflects the decay trace of the sample.

TCSPC requires a detector system that is able to detect very low signals, has an extremely fast electrical response and a low noise margin. The three techniques that meet these requirements are photomultiplier tubes (PMT), micro-channel plate (MCP) detectors and single photon avalanche diodes (SPAD).

The repetition rate of excitation should be selected based on the fluorescence lifetime, to ensure the detection of a full decay curve prior to the subsequent pulse. For fluorophores with the fluorescence lifetime range 2.5–4 ns the pulse rate is 25 MHz. Low intensity excitation light is required so that the probability of two fluorescence photons hitting the detector in the same interval is low.

1.5.4. The advantage of using FLIM to detect molecular interactions in cells.

FRET may be detected in cells using methods other than FLIM. Loss of excited state energy via FRET leads to a decrease of the donor quantum yield. At the same time, there is excitation of the acceptor molecule, which in turn emits part of that energy as photons (sensitized emission). Thus, a decrease of the donor emission together with an increase of the acceptor emission reveals the occurrence of FRET. This FRET is reflected in the donor/acceptor fluorescence ratio, but is highly prone to artifacts if the relative concentrations of donor and acceptor vary within the cell or change over time. Acceptor photobleaching measures the quenching of the donor fluorescence by photobleaching the acceptor to obtain an unquenched reference state of the donor (Bastiaens et al., 1996). Photobleaching of the acceptor may produce fluorescent by-products that interfere with the measurement of the unquenched donor intensity. Otherwise this method is reliable, but can be limited for following dynamic processes in living cells because the acceptor photobleaching step is time-consuming and irreversible. Both sensitized emission and acceptor photobleaching approaches can be applied using standard fluorescence microscopes. FLIM bears distinct advantages over other methods of measuring FRET in cells, despite its technological requirements. The fluorescence lifetime of chromophores is directly dependent on excited state reactions such as FRET. FLIM is independent of chromophore concentration and light path length, parameters difficult to control in cells, providing an advantage for use in cells (Bastiaens and Squire, 1999).

1.6. Outline of the thesis

In this thesis the development, optimization, and application of a method for imaging the interaction of tyrosine kinase inhibitors and their target tyrosine kinases, in cells, is described. The measurement of this interaction is achieved by detecting FRET (using FLIM) when an acceptor fluorophore-labeled drug binds to a donor-fluorophore-labeled target (Figure 1.9).

Chapter 2, materials and methods, contains a description of all standard procedures pertaining to cloning, cell culture, preparation of imaging samples, microscopy and image analysis. All necessary reagents and their sources are listed in this chapter.

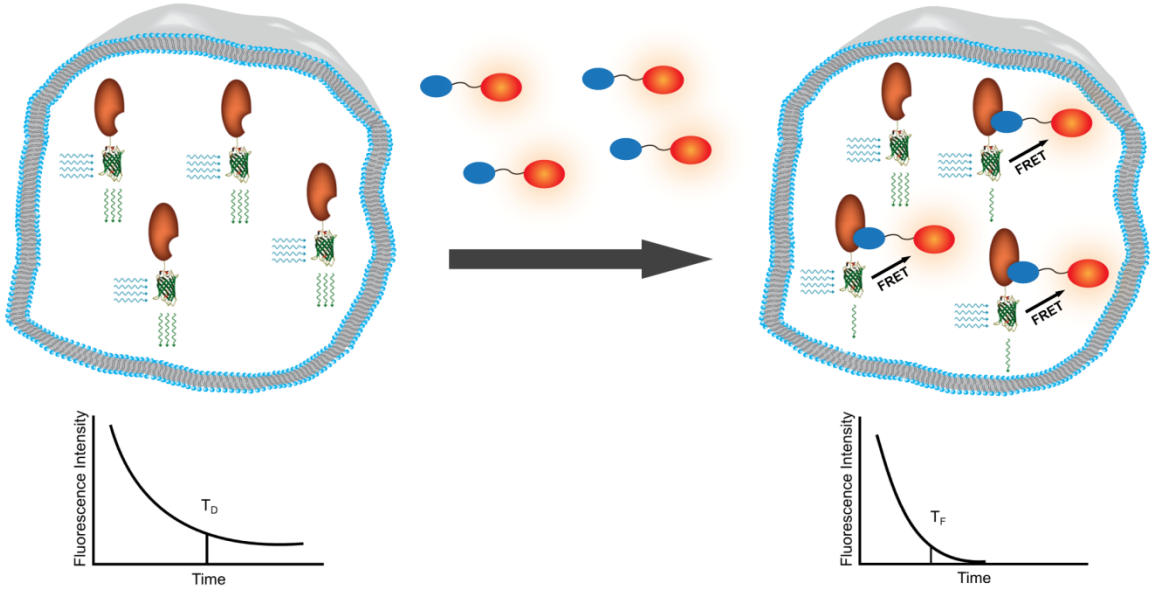

Figure 1.9 Strategy for measuring tyrosine kinase-inhibitor interactions in cells by FRET-FLIM.

Chapter 3 contains the design and development of assay presented in Figure 1.9. In Section 3.1 the design of fluorescently labeled kinase inhibitors as imaging probes is discussed. Dr. H. Rode chemically synthesized these probes under the supervision of Prof. Daniel Rauh. Several probes were developed comprising various reversible and irreversible tyrosine kinase inhibitors, in combination with various dyes, coupled via a linker these aspects are discussed in Section 3.1. The probes were characterized to determine their suitability for use in live cells (Section 3.2) and the compatibility of their fluorescent labels as FRET

partners for various fluorescent proteins (Section 3.1.2). Using EGFR as the model-kinase, binding of irreversible inhibitor probes to EGFR was measured in fixed cells and live cells (Section 3.1). The specificity of the probes for different EGFR activity conformations was explored and is described in Section 3.3. Applicability of the method to determine the specificity of a variety of inhibitor probes for different tyrosine kinases was assessed and is presented in Section 3.4.

Chapter 4 provides a retrospect on the results described in Chapter 3 and some proposals on the future applications of this technique.

Chapter 2

Materials and methods

In this chapter, standard protocols and microscope setups, and image analysis used repeatedly throughout Chapter 3 are describe. All reagents and their sources and listed in this chapter

2.1. Reagents

All chemical and other reagents were of cell culture or Analytical Reagent (AR) grade.

2.1.1 Inhibitors and probes

The probes (unpublished results) and drugs used in this study were synthesized by Dr. Haridas Rode (Chemical Genomics Centre of the Max Planck Society). NMR, LCMS and HRMS confirmed identity and purity of drugs, inhibitors and intermediates of probes. The purity and identity of final probes was confirmed by LCMS and HRMS.

2.1.2 Sundry reagents

Product	**Supplier**
Human Epidermal Growth Factor	Sigma Aldrich
Phorbol - myristate acetate	Sigma Aldrich
Pluronic	Sigma Aldrich
FuGENE ®	Roche
Poly-L-lysine	Sigma Aldrich
Dithiothreitol (DTT)	Fluka® Analytical
Glycerol	GERBU Biotechnik GmbH

2.1.3 Consumables

Product	Supplier
Glass bottom cell culture dishes (35mm)	MatTek Corp
Lab-Tek™ chambered coverglass (8 well)	Nunc/Thermo Scientific
T75 tissue culture flask	BD Falcon™

2.1.4 General buffers and solutions

Name	Constituents	Supplier
DPBS	KCl (200 mg/l), KH_2PO_4 (200 mg/l), NaCl (8000 mg/l), Na_2HPO_4 (1150 mg/l).	PAN™ Biotech GmbH
1× TBS	Tris (0.05 M) buffered saline, NaCl (0.138 M), KCl (0.0027 M), pH 8.0	Sigma Aldrich
Imaging medium	DMEM with glucose (4.5 g/l), $NaHCO_3$ (3.7 g/ l), without phenol red	PAN™ Biotech GmbH

2.1.5 Equipment

Device	Manufacturer
Gene Pulser™	Bio-Rad Laboratories
Thermomixer Comfort	Eppendorf
JASCO FP-6500 fluorescence spectrophotometer	JASCO GmbH.

2.2. Plasmids and DNA manipulation

Outlined in this section are the general DNA manipulation protocols used for the preparation of plasmids (Sections 2.2.1 and 2.2.2). These general protocols were used to encode the chimeric tyrosine kinases used in this study (Sections 2.2.3 and 2.2.4). Application of these plasmids are indicated in the figure legends of the relevant experiments in Chapter 3.

2.2.1 Cloning reagents

Product	**Supplier**
QIAPrep Spin Plasmid Miniprep Kit	Qiagen
NucleoBond® Xtra Maxi EF	Macherey-Nagel
Quickchange-XL Site-Directed-Mutagenesis Kit	Stratagene
QIAquick Gel Extraction Kit	Qiagen
QIAquick PCR Purification Kit	Qiagen
100× BSA	New England Biolabs Inc.
Zero Blunt® TOPO® PCR Cloning Kit	Invitrogen
BigDye® Terminator v3.1 Cycle Sequencing Kit.	Applied Biosystems
DyeEx® 2.0 Spin kit	Qiagen

2.2.2 General molecular biology protocols for the construction of plasmids

2.2.2.1 Bacterial transformations, selection and culture

Bacterial cells used in this study were either chemically competent or electro-competent. Plasmid DNA used for transformations contain an antibiotic resistance marker enabling selection of only bacteria containing the relevant DNA.

Reagents:

Reagent	Constituents
Bacteria	Ca^{2+}-competent *E. coli* XL10 Gold or Electro-competent *E. coli* XL10 Gold
DTT	Dithiothreitol (2.25 mM) in dd.H_2O
LB medium	Bacto-Trypton (10 g/l), bacto-yeast extract (5 g/l), NaCl (10 g/l), autoclave
SOC medium	Bacto-Trypton (20 g/l), bacto-yeast extract (5 g/l), NaCl (0.5 g/l), KCl (2.5 mM), $MgCl_2$ (10 mM), reconstitute in 1 litre of dd.H_2O, autoclave. (SOB medium). Before use glucose (20 mM) was added to obtain SOC medium

Transformation of chemically-competent E. coli

Chemical transformation of bacteria has a transformation efficiency of 1×10^6–1×10^8 colonies/µg DNA.

Procedure:

Chemically competent *E. coli* (100 µl, XL10 Gold) containing DTT (3.5 µl, 2.25 mM, added before use) was incubated with plasmid DNA (0.1 µl) or ligation product (2.5–7.5 µl) on ice for 20 min. SOC medium (250 µl) was added and bacteria were allowed to recover (45–60 min at 37 °C, 225 rpm). Cell suspension (100 µl) was plated on LB agar plates containing the required antibiotics and incubated at 37 °C overnight.

Transformation of electro-competent E. coli

Transformation efficiencies using electro-competent cells is up to 1×10^{10} colonies/µg DNA. For cases of low plasmid yield or poor chemical transformation efficiency, electro-transformation was employed.

Procedure:

Electro-competent *E. coli* (XL10 Gold, 100 µl) was combined with ice-cold 10% glycerol (50 µl in dd.H_2O) and recombinant DNA (10 µl) on ice. The transformation mix was transferred to a sterile, pre-cooled electroporation cuvette and exposed to an electric field

(1.3 V, 25 F, 800Ω) using the Gene Pulser™ electroporation chamber. Time constants shown according to the device were between 4 and 6 ms. Cells were transferred to a sterile 15 ml Falcon tube containing SOC medium (950 µl). Bacteria were allowed to recover (45–60 min at 37 °C, 225 rpm). Cell suspensions (100 µl) were plated on LB agar plates containing the required antibiotics and placed at 37 °C overnight.

Bacterial cultures

Transformed *E. coli* cells were grown in solution (LB medium + appropriate antibiotic, 37 °C and 225 rpm). Cultures of 4 ml LB medium were inoculated with a single colony from the agar plates. After 6–10 h, the pre-culture was used to inoculate the desired volume of main culture. Steady state cultures obtained after overnight growth at 37 °C were used for plasmid preparation.

2.2.2.2 Plasmid preparation

Bacterial cultures grown in LB medium supplemented with the appropriate antibiotics were centrifuged to form a bacterial pellet. Plasmid DNA was prepared from the bacterial pellet using either QIAprep® Spin Miniprep Kit (for DNA manipulation) or NucleoBond® Xtra Maxi EF Kit (for transfection). Bacterial culture volumes and densities were dependent on the kit used and according to the manufacturers' recommendation.

The QIAprep® Spin Miniprep Kit provides a rapid small-scale plasmid preparation method for routine molecular biology applications and yields up to 20 µg high-copy plasmid DNA, of sequencing quality. Using alkaline lysis of bacterial cells and subsequent absorption of the plasmid DNA onto a patented silica membrane in the presence of high salt concentrations. Plasmid DNA was eluted from the membrane with a low-salt buffer or dd.H_2O as per manufacturer's instructions.

For transfection of mammalian cells, endotoxin-free plasmid DNA was prepared on a large scale. The outer membrane of Gram-negative bacteria consists of amphiphilic lipopolysaccharides, also called endotoxins. Bacterial cells release endotoxins in large amounts upon cell death and lysis. In mammalian cell culture, endotoxins can affect transfection rates and cell viability. Due to their amphiphilic nature and negative charge,

endotoxins can be co-purified with many common plasmid purification systems. The NucleoBond® Xtra Maxi EF Kit provides a fast and highly efficient method for the preparation of endotoxin-free plasmid DNA. It is designed for purification of up to 1000 µg high-copy plasmid DNA. Endotoxin-free plasmid DNA was prepared according to the NucleoBond® Xtra Maxi EF Kit user manual.

2.2.2.3 Agarose gel electrophoresis

Agarose gel electrophoresis is used to separate nucleic acid fragments by size. It was used for the analysis of DNA and to separate restriction digestion products. Ethidium bromide (EtBr) is added to agarose gels to visualize dsDNA.

Reagents:

Reagents	**Constituents**
TAE buffer	Tris/Acetate (40 mM) , NaOAc (20 mM), EDTA (1 mM, (pH 7.5)
Ethidium bromide (10 mg/ml)	Fisher Scientific
Agarose	Ultrapure™ Invitrogen
6× DNA gel loading buffer	Novagen
2-log DNA ladder	New England Biolabs Inc.

Procedure:

Agarose gels were prepared with TAE buffer supplemented with 2 µl ethidium bromide (EtBr)/50 ml gel. TAE buffer was used as running buffer and electrophoresis carried out at constant voltage of 120 V for 20 min. Samples were prepared by mixing DNA with the appropriate amount of loading buffer and dd.H_2O to a final volume as small as possible. For size estimation of dsDNA fragments, a DNA-marker with different bands of known sizes was added to one lane of the gel. The concentration of the agarose gel was chosen according to the size of the DNA molecules in question:

Agarose concentration in % (w/v)	Size of dsDNA molecules
2.5	< 100 bp
2.0	0.1 – 1.0 kb
1.8	0.2 – 2.0 kb
1.5	0.3 – 3.0 kb
1.2	0.5 – 5.0 kb
1.0	0.5 – 7.0 kb
0.8	0.8 – 12.0 kb
0.5	1.0 – 30.0 kb

2.2.2.4 Isolation of DNA from agarose gels

The QIAquick® Gel Extraction Kit was used to purify DNA fragments in a range of 70 bp to 10 kb from agarose gels. This method of purification of PCR products is based on DNA binding to a silica membrane in the presence of high salt concentrations, while contaminants are washed through the column. DNA fragments to be isolated were cut out from the agarose gel under UV illumination and transferred to a 2 ml Eppendorf tube. Purification was carried out as per manufacturer's instructions.

2.2.2.5 Purification of DNA using the QIAquick® PCR purification kit

The QIAquick® PCR Purification Kit is designed for the purification of DNA fragments in a range of 100 bp to 10 kb from PCR or enzymatic reactions. This method of purification of PCR products is based on DNA binding to a silica membrane in the presence of high salt concentrations, while contaminants are washed through the column. Purification was carried out as per manufacturer's instructions.

2.2.2.6 Restriction digest

Restriction endonucleases cleave DNA sequences at specific sites. Restriction digests were used to linearize vector DNA and to create DNA fragments with sticky ends complimentary to those on the linearized vector. Restriction enzymes (New England Biolabs) were

supplied with optimized buffers. As per manufacturer's instructions reaction mixtures were supplemented with bovine serum albumin (BSA).

Procedure:

Plasmid DNA and restriction enzymes were mixed in a ratio of 1 unit/mg of plasmid DNA in the appropriate buffer and incubated at 2 h at 37 °C followed by heat inactivation of the restriction enzyme at 65 °C for 20 min. For the restriction digestion of multiple sites on a single DNA, the enzymes were added simultaneously to the reaction provided optimal buffers were available; otherwise restrictions digestions were carried out sequentially. Linearized plasmids or restriction digestion fragments were analyzed using agarose gel electrophoresis and purified using QIAquick Gel Extraction Kit (Section 2.2.2.5).

2.2.2.7 Dephosphorylation of 5'-phosphorylated DNA fragments

To avoid self-ligation of linearized vector DNA, the 5'-phosphorylated ends were dephosphorylated with calf-intestinal alkaline phosphatase (CIP).

Procedure:

Digested vector DNA and CIP were mixed in a ratio of 0.5 U CIP/µg DNA in NEB reaction buffer 3 at the appropriate dilution and incubated for 1 h at 37 °C. The DNA was subsequently purified using the QIAquick PCR Purfication Kit.

2.2.2.8 DNA ligation

DNA recombination was brought about using a DNA ligase, which catalyzes the formation of a phosphodiester bond between the free 3'-hydroxyl- and the 5'-phosphate group of linear DNA fragments with the consumption of ATP.

Procedure:

Linearized, dephosphorlyated vector backbone was incubated with a three-fold molar excess of insert DNA. The mixture was supplemented with Quick Ligation Reaction Buffer and 1 U Quick T4 DNA Ligase and distilled water to achieve the relevant dilutions. The reaction was incubated at RT for 5–15 min followed by transformation in competent *E. coli* XL 10 Gold.

2.2.2.9 TOPO®-blunt cloning

The Zero Blunt® TOPO® PCR cloning kit was used as a vector system for amplification and storage of PCR products. The linearized pCR® Blunt II TOPO® cloning vector has Vaccinia virus DNA topoisomerase I covalently bound to the 3'-end of each DNA strand. Topoisomerase I binds to specific sites in dsDNA and cleaves its phosphodiester backbone while conserving the energy by formation of a covalent bond between the 3'-phosphate of the cleaved strand and a tyrosyl residue of topoisomerase I. The stored energy of the phosphodiester backbone cleavage can be used to form a new covalent bond between the 5'-hydroxyl of a blunt-end PCR product and the 3'-phosphate of the vector DNA, thereby releasing the enzyme.

Procedure:

Blunt-end PCR product (4 µl) was mixed with the supplied salt solution (1 µl) and pCR® - Blunt II-TOPO R cloning vector (1 µl), gently mixed, incubated 5, RT, and then placed on ice. Finally, TOPO® cloning reaction (2 µl) was transformed into chemically competent *E. coli* (One Shot R TOP10) as per manufacturer's instruction.

2.2.2.10 Polymerase chain reaction (PCR)

PCR exponentially amplifies specific DNA sequences. It is achieved by repeated cycles of *in vitro* DNA synthesis of a target sequence by DNA polymerase. Two oligonucleotide primers flank the DNA sequence of interest and can hybridize to their complementary sequence on opposite DNA single strands. Double stranded DNA molecules are separated into single strands by heat denaturation, enabling hybridization of the primers to the single-stranded DNA molecules at temperatures of 45–60 °C. Excess primer concentrations ensure that formation of primer template complexes are favoured over re-naturation of the single-stranded DNA. Heat-stable DNA polymerases elongate primers at an intermediary temperature as an exact copy of the original template. Cycle repetition leads to the exponential amplification of the target sequence, as every dsDNA molecule synthesized can serve as a template in subsequent cycles (Saiki et al., 1988).

Procedure:

PCR was performed using AccuPrime™ *Pfx* DNA polymerase as per manufacturers' guidelines.

Reaction mix

Component	Volume per reaction (µl)	Final concentration
10X AccuPrime™ *Pfx* reaction mix	5	1X
Primer mix	Variable	50 pM each
DNA Template	Variable	~ 50 ng
AccuPrime™ Pfx polymerase	1	2.5 units
Autoclaved, distilled water	To 50	

PCR thermocycler protocol

Template was denatured for 2 min at 95 °C, followed 30 cycles of PCR amplification as indicated:

Description	Temperature (°C)	Time (min)
Denaturation	95	1
Anneal	55–60	1
Extend	68	1 min per 1000 bp

2.2.2.11 Site-directed mutagenesis

Site-directed mutagenesis was used to introduce point mutations on EGFR to create the relevant mutants (Section 2.2.3). The procedure requires plasmid DNA and either one or two complementary oligonucleotide primers, which contain the desired point mutation. The primers bind to their complementary sequence on the plasmid and are amplified by PCR to generate a mutated plasmid containing nicked single strands. Thereafter the template DNA

within the PCR product is digested by endonuclease DpnI. Template DNA purified from dam$^+$ *E. coli* ensures that all GATC sites are methylated, making digestion specific to only the template DNA.

Procedure:

Mutagenesis PCRs were performed using the Stratagene Quickchange® site-directed mutagenesis kit.

Reaction mix:

Component	**Volume per reaction (µl)**	**Final concentration**
Reaction buffer (10X)	4	1X
Primer	Variable	125 ng
DNA Template	Variable	5-50 ng
dNTP mix	1	
PfuTurbo DNA polymerase (2.5 U/µl)	1	
Autoclaved, distilled water	To 50	

PCR thermocycler protocol:

Template was denatured for 30 s at 95 °C, followed by 18 cycles of PCR amplification as indicated:

Description	**Temperature (°C)**	**Time**
Denaturation	95	30 s
Anneal	55	1 min
Extend	60	1 min per 1000 bp

Dpn I digestion of the amplification products

Dpn I restriction enzyme (10 U/µl, 1 µl) was added directly to the amplification reaction. Mixing was done by pipetting the solution up and down several times and mixture was incubated (37 °C, 1 h).

The Dpn I-treated reaction mixture (1 µl) was transformed in chemically competent *E. coli* (XL1-Blue Supercompetent cells) as per manufacturer's instruction.

2.2.2.12 DNA sequencing

Sequencing of dsDNA was performed using the chain-terminating method (Sanger et al., 1977) to confirm the sequence of the final cloning product. A fluorescently labeled chain terminator ddNTP permits sequencing by capillary gel electrophoresis. Sequencing was carried out at the Zentrale Einrichtung Biotechnologie, Max Planck Institute of Molecular Physiology, Dortmund.

Procedure:

Sequencing PCRs were performed using the BigDye® Terminator v3.1 cycle sequencing kit.

Reaction mix:

Component	**Volume per reaction (µl)**	**Final concentration**
Ready Reaction Premix (2.5X)	4	1X
Primer	Variable	3.2 pM
DNA Template	Variable	150-300 ng
BigDye Sequencing Buffer 5X	2	1X
Autoclaved, distilled water	To 20	

PCR thermocycler protocol:

Template was denatured for 1 min at 96 °C, followed by 25 cycles of PCR amplification as indicated:

Description	**Temperature (°C)**	**Time**
Denaturation	96	10 s
Anneal	50	5 s
Extend	60	4 min
Hold	4	Until ready for purification
Description	Temperature (°C)	Time

Excess ddNTPs were removed from finished sequencing reactions with the DyeEx® 2.0 Spin kit as per manufacturers' instruction. Purified products were dried by vacuum centrifugation.

2.2.3 Recombinant DNA constructs

Table 2.1: Table of mutagenesis products

Insert (Human)	**Oligo Sequence (5′-3′)**
EGFR T790M	T790M-F-ccgtgcagctcatcatgcagctcatgccc T790M-R-gggcatgagctgcatgatgagctgcacgg
EGFR T790M/ C797S	C797S-F-cagctcatgcccttcggctccctcctggactatgtccgg
EGFR L858R	L858R-F- cacagattttgggcgggccaaactgctggg L858R-R- cccagcagtttggcccgcccaaaatctgtg

Table 2.2: Table of subcloning products

Insert (Human)	Oligo Sequence (5′-3′)
EGFR	
PDGFRb	PDGFRb-HindIII-F-cccaagcttgccaccatgcggcttccgggtgcgatg PDGFRb-EcoRI-R-ggaattcgcaggaagct
c-Src	cSrc-XhoI-F-cggctcgaggccaccatgggttagcaacaagagcaagcccaag cSrc-EcoRI-R-cggaattcggaggttctccccgggctggtac
Csk	Csk-XhoI-F-cggctcgaggccaccatgtcagcaatacaggccgcctggcc Csk- BamHI-R-cgggatccgcaggtgcagctcgtgggtttt

2.2.4 Construction of tyrosine kinase-FP expression vectors

The mammalian expression vectors used in the current study (based on Clontech pEGFP-C1) contain a human cytomegalovirus (CMV) promoter, a Simian Virus 40 (SV40) polyadenylation signal downstream of the coding sequence and encodes a (F64L, S65T) monomeric variant of wild type Green Fluorescent protein from Aequorea Victoria. EYFP and mCitrine are yellow-green variants of EGFP fluorescent proteins (Shaner et al., 2005). mCitrine is the monomeric, pH-stable version of EYFP. Antibiotic selection is mediated by a kanamycin resistance in *E. coli* and neomycin (G418) resistance in mammalian cells. The vector containing mTurquoise was a gift from Dr. Mark Hink (University of Amsterdam) and has the same backbone as the GFP derivative vectors (Goedhart et al., 2010). Subcloning carried out by the Dortmund Protein Facility (DPF) uses the pOPIN vector. These vectors are based on the pOPIN plasmid suite, developed by the Oxford Protein Production Facility and utilize multiple promoter systems (for *E. coli*, mammalian or insect hosts) and cloning is ligation free.

Construction of EGFR-FP expression vectors

The EGFR-EYFP plasmid was constructed by former group member Dr. Martin Offterdinger. EYFP was replaced with mCitrine and mTurquoise by restriction digestion to remove EYFP with AgeI/NotI and PvuI/NotI (general protocol outlined in Section 2.2.2.6)

and ligation (Section 2.2.2.8) with the corresponding DNA fragment obtained by digestion of the Clontech vector containing mCitrine and mTurquoise. Site-directed mutants (T790M, L858R and T790M-C797S) of all three EGFR-FP constructs were generated using site-directed mutagenesis (Section 2.2.2.11) using the primers specified in Table 2.1.

Construction of PDGFRb-FP, Csk-FP and c-Src-FP expression vectors

The PDGFRb-mCitrine was constructed by a former group member Dr. Virginie Georget. The coding sequence was amplified by PCR (Section 2.2.2.10) using the primers given in Table 2.2 and subcloned into the mTurquoise vector using HindIII and EcoRI. Expression constructs for cSrc and Csk were obtained from Ms Jutta Luig (current group member) and Bio Cat (BC106073) and the coding sequence was subcloned into mCitrine-pOPIN vector by the Dortmund Protein Facility. The coding sequences for cSrc and Csk were subsequently amplified by PCR (Section 2.2.2.10) using the primers in Table 2.2 and subcloned into the mTurquoise expression vector using sequential restriction digestion (with XhoI/EcoRI and XhoI/BamHI respectively) and ligation.

2.3. MCF-7 Cells

MCF-7 (ATCC: HTB 22) is an epithelial cancer cell line, derived from breast adenocarcinoma. This cell line was selected for this study on the basis of its low EGFR expression levels (deFazio et al., 2000). For the experiments described in Chapter 3, EGFR genetically tagged with a fluorescent protein is over-expressed in these cells. The low endogenous levels of receptor reduce the effect of inhibitor and probe binding to 'dark' receptor. Section 2.3.1 is a list of general cell culture reagents. Passage, seeding and cryo-storage details are given in Section 2.3.2. The creation of transient and stably transfected cell lines is described in Sections 2.3.3 and 2.3.4.

2.3.1 Cell culture reagents

Reagent	Supplier
Dulbecco's Modified Eagle's Medium (DMEM)	Sigma Aldrich
Fetal calf serum (FCS)	PAN™ Biotech GmbH
Fugene® 6 transfection reagent	Roche Applied Science
L-Glutamine	GIBCO® /Invitrogen™ Life Technologies
Penicillin Streptomycin	GIBCO® /Invitrogen™ Life Technologies
Trypsin/EDTA	PAN™ Biotech GmbH
Neomycin (G418)	Sigma Aldrich

2.3.2 MCF-7 cell culture

MCF-7 cell line was maintained in DMEM, supplemented with 10% FCS, 2 mM L-glutamine, 100 U/ml penicillin, 100 µg/ml streptomycin in 5% CO_2, 95% air atmosphere. Cells were starved in DMEM supplemented with 2 mM L-glutamine, 100 U/ml penicillin, 100 µg/ml streptomycin in 5% CO_2, 95% air atmosphere.

MCF-7 sub-culture

Cells were sub-cultured upon reaching a surface area density of 80–90%. Cell growth above this density can lead to contact inhibition of the growth rate. For sub-culture the existing medium was aspirated and cells washed with DPBS. Trypsin/EDTA (2 ml) was added and incubated for ~5min at RT. Trypsinization was terminated by the addition of maintenance medium. Cells were maintained by sub-culture for a maximum of 40 passages to avoid artifacts of genetic drift.

Depending on the application and culture vessel cells were then diluted in the following manner:

Cell culture dishes (maintenance)	**Depending on usage cells were split in ratios of 1:4 to 1:6 into sterile cell culture flasks.**
6 mm Petridishes (stable cell lines)	7×10^5
35 mm glass bottom dishes (Imaging)	3×10^5
8 well Labtek chambers (Imaging)	3×10^4 per well
cell culture dishes (maintenance)	Depending on usage cells were split in ratios of 1:4 to 1:6 into sterile cell culture flasks.

Cryo-preservation of MCF-7 cells for long term storage

Cooling to subzero temperatures preserves cells; at these low temperatures the biochemical activity of the cell is effectively stopped. DMSO is used as a cryo-protectant to prevent mechanical damage to cells by ice crystals.

Procedure:

A 60% confluent T75 flask was washed with DPBS and trypsin (2 ml) was added. Once the cells were detached culture medium (3 ml) was added, cells were transferred to a falcon tube (15 ml) and centrifuged (200 × g, RT, 5 min). The supernatant was removed, leaving behind just the cell pellet to which cryo-medium (10% DMSO in culture medium, 5 ml) was added. Cells were mixed and aliquots (1 ml) were made in cryo-vials and transferred to a room temperature NALGENE® Cryo 1 °C freezing container. The cryo freezing container is regulated by isopropanol which has a freezing rate of 1 °C per minute. The freezing container was placed at -80 °C overnight and vials were subsequently transferred to liquid nitrogen for long-term storage.

Cells should be thawed rapidly to reduce cytotoxic effects of the cryo-medium. Cells were removed from liquid nitrogen and diluted with culture medium pre-warmed to 37 °C, centrifuged (200 × g, 5 min), re-suspended in growth medium (14 ml) and seeded into a new T75 flask.

2.3.3 Transient DNA transfection protocols

Transfection is the delivery of nucleic acids, in our case plasmid DNA, into eukaryotic cells. MCF-7 cells were transiently transfected with endotoxin-free plasmid DNA using FuGENE® 6 Transfection Reagent. This reagent contains a patented blend of lipids and other components in 80% ethanol. Delivery is non-viral and achieved through the formation of DNA loaded micelles, which are able to fuse to the plasma membrane. Uptake is non-liposomal and can be carried out with or without serum with very low cytotoxicity. This protocol was used to obtain transient expression of the fluorescently labeled tyrosine kinases in MCF-7 cells

Procedure:

Cells were plated 24 hours prior to transfection (50–80% confluent on day of transfection) into 60 mm Easy Grip™, 35 mm Matek or 8 well Labtek™ dishes (Section 2.3.2). Transfection was carried out with a FuGENE®: DNA ratio of 1:3. Indicated amounts of FuGENE® and DNA were added to serum-free DMEM (100 µl), gently mixed and incubated for 15 min at room temperature. The mixture was added directly to cells at the indicated volumes:

Dish	**Serum-free medium (µl)**	**FuGENE® (µl)**	**DNA (µg)**	**Volume added to cells**
60 mm	100	6	2	Total volume for 1 dish
35 mm	100	3	1	Total volume for 1 dish
8 well	100	3	1	25 µl per well

Note: All volumes were increased proportionately depending on the number of wells or dished transfected. After addition of transfection mixture, cells were returned to culturing conditions for ~18 h prior to application.

2.3.4 Preparation of stable MCF-7 cells transfected with EGFR-EYFP

Stable integration of foreign DNA, into the genome of a cell type, occurs in a subpopulation of transfected cells. Establishing a stable cell line is dependent on efficient

gene transfer into the cell line and survival of successfully transfected cells during the selection process. Drug selection with a dominant selection marker encoded in the exogenous plasmid enables the subpopulation containing the foreign DNA to persist and kills the non-transfected cells.

Procedure:

MCF-7 cells were sub-cultured into 60 mm dishes as per Section 2.3.2 and transfected with EGFR-EYFP after 24 hours (Section 2.3.3). Cells were allowed to express the gene for 24 hours and transferred to a 75 cm^2 flask with 15 ml culture medium containing 700 µg/ml G418. Medium was replaced every 3 days for 2 weeks. Colonies of resistant cells were observed from the intensity of EYFP detected by fluorescence microscopy. For our experimental setup it was preferable to have cells with an expression level suitable for detection by fluorescence microscopy. Stably transfected cells were trypsinized with 2 ml trypsin until detached. Culture medium (3 ml) was added, the cells transferred to a 15 ml centrifuge tube and pelleted by centrifugation 200 × g, 5 min. Supernatant was aspirated, cells re-suspended in 1–2 ml culture medium and filtered (BD Falcon tube, 35 µm nylon mesh). Sorting was carried out using the BD FACSAria™ cell sorter. Living, single cells were gated using forward scatter (photodiode detector and a 488/10 bandpass filter) and side scatter (photomultiplier with a 488/10 bandpass). Fluorophores were excited using the 488 nm, Coherent® Sapphire™ solids state laser. EYFP fluorescence was detected using standard 515–545 nm filter. Gating for autofluorescence was obtained by plotting the EYFP signal against signal detected by a 564–606 nm filter. Collected cells made up ~6% of the total population. Once sorted, cells were added to 35 mm cell culture dishes. Upon attachment medium was exchanged with culture medium containing 400 µg/ml G418.

2.4. Protein kinase stimulation

Before protein kinase stimulation, MCF-7 cells expressing the kinase of interest were starved for 4 hours in culture medium without FCS. EGFR-expressing cells were stimulated with EGF (100 ng/ml, 5 min), PDGFRb transfected cells were stimulated with PDGFB (100 ng/ml, 10 min) and cells expressing Src or Csk fusion proteins were stimulated using

PMA (10 nM, 20 min). MCF-7 cells contain low endogenous EGFR levels to achieve activation of Src and Csk was brought about via activation of the PKC pathway using PMA. Stimulations were stopped after the indicated time by fixation with methanol.

2.5. Methanol fixation of cells

Methanol (100% methanol, −20 °C), a precipitating fixative, was added to cells after stimulation, and aspiration of stimulation medium. Cells were incubated for 5 min at −20 °C and washed 3× with sterile PBS. Fixed cells were stored in PBS at 4 °C until further use.

2.6. Staining of cells with probes prior to imaging

Probes described in Section 3.1.3 were stored at 200 µM–10 mM concentrations in DMSO at −20 °C. Before use they were diluted to the working concentrations in PBS. Concentrations of diluted probes were periodically confirmed by spectrophotometry using the relevant excitation and emission wavelengths and extinction coefficients of the dyes. All probes with the exception of PD168393-LRh were completely soluble in PBS. PD168393-LRh at high concentrations formed aggregates in PBS; to reduce this effect PBS was supplemented with 0.5% pluronic (a poloxamer used to increase the solubility of hydrophobic substances and as a drug transporter).

2.7. Reversible permeabilization of membranes by streptolysin-o

Reversible permeabilization of membranes is one method of delivering impermeable compounds to the cytoplasm of cells. SLO is a cholesterol-binding bacterial toxin that reversibly forms pores in adherent and non-adherent cells. Toxin monomers bind to the membrane cholesterol, diffuse laterally in the membrane bilayer and oligomerize to arc- or ring-shaped structures that represent very large trans-membrane pores with diameters of up to 30 nm (Palmer et al., 1998b; Palmer et al., 1998a; Shatursky et al., 1999). SLO pore formation can be reversed by adding medium containing foetal calf serum (Palmer et al.,

1998a; Giles et al., 1998). Membrane resealing is a complex structural modification that uses endomembranes as the primary building blocks. A Ca^{2+}-triggered response to disruption delivers the endomembrane to the damaged plasma membrane by ectocytosis (McNeil and Steinhardt, 2003). Cell survival after exposure to low doses of SLO has been linked to a Ca^{2+}-dependent mechanism (Walev et al., 2001; Babiychuk et al., 2009). Proposals for what this mechanism is include endocytosis (Idone et al., 2008) or ectocytosis (Keyel et al., 2011).

Reagents:

Activation buffer: PBS containing 5 mM DTT and 0.05% BSA

Procedure:

SLO was diluted to 1 mg/ml as per manufacturer's instructions and indicated to have (25000-50000 U/mg). Oxidation in solution reduces the activity of SLO, so prior to addition to cells SLO was activated in PBS containing 5 mM DTT and 0.05% BSA for 2 hours at 37 °C. After incubation PD168393-LRh was added to the activated SLO to give a final probe concentration of 1 µM. MCF-7 cells grown in an 8-well Labtek chamber were washed 3× with PBS and incubated with the SLO/probe mix at 37 °C for 10 min.

SLO pore formation can be reversed by adding medium containing foetal calf serum. Probe/SLO solution was aspirated and cells were overlayed with 500 µl culture medium (DMEM with 10% FCS) for 20 min. This procedure was also used for 1, 5 and 10 µg amounts of SLO.

2.8. Native membrane sheet preparation

Native membrane sheets were used to compare the binding of PD16393-LRh to EGFR that has not been subject to fixation. A more detailed description of this technique can be found in Section 3.3.1.

Reagents:

Buffer: HEPES (30 mM), $MgCl_2$ (72 mM) and Trolox (2 mM), pH 7.4.

Procedure:

Poly-L-lysine coating of Matek dishes and coverslip: Matek dishes and glass slides were treated with cell culture-suitable poly-L-lysine (0.01%, Sigma). Coating was carried out under sterile conditions. Sufficient poly-L-lysine solution was added to cover the surface of the Matek or slide-containing dishes. Gentle rocking was used to ensure an even coating of the surface. After 5 min the poly-L-lysine solution was discarded and coated surfaces were washed repeatedly with sterile dd.H_2O. Coated surfaces were allowed to dry for 2 hours prior to use. Coating was always applied on the day of experiment.

MCF-7 cells stably transfected with EGFR-YFP (Section 2.3.4) were allowed to attach for 24–48 h after plating on 35 mm Matek dishes pre-coated with poly-L-lysine. During this period cells were kept under maintenance culturing conditions Section 2.3.2.

For membrane sheet preparation cells were rinsed with PBS and incubated for 1 min with dd.H_2O to induce osmotic swelling. A poly-L-lysine, pre-coated 7 mm coverslip was placed over the glass diameter of the Matek dish containing cells and pressure was applied for 3–4 min. The glass coverslip was removed, with special care being taken to avoid lateral movement. Membranes were rinsed with PBS and then placed in the appropriate buffer for imaging. It was noted in initial experiments that when imaged in PBS, photobleaching of the fluorescent protein occurred. The imaging buffer was then changed to HEPES buffer containing $MgCl_2$ and Trolox. Trolox is a water-soluble analogue of vitamin E and is used to reduce photobleaching (Rasnik et al., 2006; Cordes et al., 2009).

2.9. Measurement of excitation and emission spectra

Dyes were diluted (1 μM in 1.5 ml of the solution indicated in Figure 3.13, Chapter 3). Dyes were excited at 470 nm and emission spectra were acquired from 490–620 nm with emission slits set to 1 nm. Measurements were carried out in cuvettes using a JASCO FP-6500 fluorescence spectrophotometer (JASCO GmbH, Gross-Umstadt, Germany).

2.10. Microscopy

2.10.1 Confocal laser scanning microscopy (CLSM)

Confocal images of live and fixed cells were obtained using an Olympus FluoView FV1000 laser scanning microscope. EYFP, mCitrine and fluorescein were excited using the 488 nm line (Argon laser); LRh and Bodipy 576/589 were excited at 561 nm (DPSS laser). Excitation light was focused onto the sample using 60×/1.2 NA water (fixed cells) or 60×/1.35 NA oil (live cells) objective and DM405/488/561/633 dichroic mirror. Fluorophore emission was detected using the photomultiplier in the following range: EYFP/mCitrine/fluorescein 498–560 nm and LRh/Bodipy 576/589 570–670 nm. mTurquoise was excited at 458 nm and Bodipy-FL at 515 nm with light passing through the DM458/515 dichroic mirror. Fluorescence emission was detected at 475–485 nm for mTurquoise and 530–630 nm for Bodipy-FL. Live cell experiments were carried out in an environmental control chamber at 37 °C and 5% CO_2. Scanning was performed in line-by-line sequential mode with 4× line averaging.

2.10.2 Fluorescence lifetime imaging microscopy (FLIM)

Time-domain FLIM

Fluorescence lifetime images were acquired using a confocal laser scanning microscope (FV1000, Olympus, Germany) equipped with a time-correlated single photon counting module (LSM Upgrade Kit, Picoquant, Germany). For detection of EYFP/mCitrine or mTurquoise, the samples were excited using a 470 nm or 458 nm diode laser (Picoquant), respectively, at 40 MHz repetitions. Emitted light was spectrally filtered using a narrow band emission filter HQ 514/10 (EYFP/mCitrine) or HQ 480/20 (mTurquoise), Chroma, USA). Photons were detected using a single photon counting avalanche photodiode (PDM Series, MPD, Italy) and timed using a single photon counting module (PicoHarp 300, Picoquant).

Frequency-domain FLIM

Fluorescence lifetime imaging microscopy (FLIM) measurements were performed on an in-house-developed FLIM system. An Olympus IX81 provides the basis for the setup. The

FLIM system developed in house comprises of an Argon laser (Coherent Innova 300C) excitation line with a multiline mirror running in light-track mode, an AOTF (AA opto-electronic AOTF.nC) to control wavelength and laser intensity, and an AOM (Intra Action SWM-804AE1-1) for modulating the laser at 80 MHz. The detection is formed by a high rate image intensifier (LaVision PicoStar HR) and a CCD camera (LaVision Imager QE). Both AOM and image intensifier are modulated by a pair of frequency generators (Aeroflex 2023A). The setup is controlled by DaVis software.

A 476 nm argon laser line was used to excite EYFP and mCitrine. Fluorescence emission of EYFP and mCitrine were detected with a dichroic beamsplitter (Q495 LP; Chroma Technology, Brattleboro, VT) and a narrow-band emission filter (HQ514/10; Chroma). LRh/Bodipy 576/589 emission images were obtained using a 100 W mercury arc lamp and an RFP filter set U-MRFPHQ (excitation BP535-555HQ, dichroic BA570-625HQ, emission BA570-625HQ). A 60×/1.35 NA oil objective was used.

2.11. Data analysis and image processing

2.11.1 Software

Software	**Supplier**
ImageJ	National Institutes of Health
OriginPro 8.0	OriginLab
Matlab R2010b	MathWorks
Symphotime v5.12	PicoQuant

2.11.2 Standard confocal image processing

512×512 or 256×256 pixel images were acquired at 8 or 16 bit depth TIFF files. Import of images into ImageJ was with the Bio-Formats plugin. Background subtraction was performed by obtaining the low level intensities using an image histogram and subtracting peak values plus two standard deviations, a Gaussian background distribution was assumed.

For image processing operations images were converted to 32 bit floating point TIFF in ImageJ.

2.11.3 Masking

32 bit TIFF images were thresholded interactively and background values were converted to, the mathematical operation neutral, Not-a-Number (NaN). A mask consisting of the value one was created, by dividing the thresholded images by themselves, using ImageJ (process > image calculator).

2.11.4 Time lapse imaging

Time lapse images were stacked 16 bit TIFFs. Background subtraction was carried out using a rolling-ball radius of 20 pixels, with a sliding parabola. A 'rolling ball' algorithm is used to correct for uneven background illumination (ImageJ-plugin: BackgroundSubstracter). A local background value is calculated for every pixel by averaging over a very large ball around the pixel. This value is then subtracted from the original image. The rolling ball can be replaced by a sliding paraboloid with the same curvature at its apex. The relevant plugin can be found in the Process > background subtract menu in ImageJ.

2.11.5 Time-domain FLIM analysis

Time-domain FLIM images were acquired and analyzed using Symphotime v 5.12 software. Time-correlated single photon counting (TCSPC) was used to record at high time resolution the arrival time of a photon after pulsed excitation. Fitting a sum of exponential model to the acquired decay curve can derive fluorescent lifetimes and relative concentrations of fluorescing populations. For the current data, the initial part of the curve, including the peak, was excluded from the fit to omit the influence of the instrumental response function (IRF). The IRF requires separate calibration and complicates data fitting. A limitation of the tail fit is that the amplitude obtained for the various fluorescence lifetime populations have a slight bias towards the longer fluorescence lifetimes. FLIM analysis using a single exponential tail fit was used to determine the lifetime of a sample containing only donor (τ_1) fluorophores. A bi-exponential tail fit was used in the case of a

donor/acceptor sample with τ_1 being fixed to the fluorescence lifetime obtained for the corresponding donor sample without acceptor.

Intensity and fluorescence lifetime images were exported to ImageJ. Masks were created from the intensity image using the procedure outlined in Section 2.11.3. A pseudo colour was applied to the intensity image and a customized lookup table (LUT) applied to the FLIM images with the upper and lower limits set as indicated in the LUT shown on the relevant figures. Pixels containing NaN were represented by the colour black using Matlab.

2.11.6 Frequency-domain FLIM analysis

All analysis was performed in Matlab. For each FLIM stack, the foreground and background were obtained by Otsu thresholding (Otsu, 1979) the mean projection image. Additionally saturated pixels in the maximum projection image were rejected. The average background was subtracted from the foreground image.

Phase shift ($\Delta\phi$) and demodulation (ΔM) at each pixel were obtained relative to a measured scattering reference by fitting the data using singular value decomposition (Verveer and Bastiaens, 2003). Using these values and the angular frequency of the modulated light (ω), modulation and phase fluorescence lifetimes were determined from Equations 6 and 7 (Section 1.5.3).

Histograms of a field of view were determined using bins of 50 ps size from 50–6000 ps. Several histograms of a particular condition were averaged using OriginPro 8.0. Figure

2.11.7 Statistics

Standard deviation

Error bars on bar graphs represent the standard deviation of the mean. The standard deviation shows the variation in the mean.

$$STDEV = \sqrt{\frac{\sum (x - \bar{x})^2}{(n-1)}} \qquad (8)$$

Where $\bar{x}$ is the sample mean and n is the sample size.

Two-sample Kolmogorov-Smirnov test

The two-sample Kolmogorov-Smirnov test (Massey, 1951) was calculated using the kstest2 algorithm in matlab. The Kolmogorov-Smirnov test is nonparametric. The kstest2 algorithm performs a two-sample Kolmogorov-Smirnov test to compare the distributions of the values in the two data vectors, in our case the control and sample. The null hypothesis is that the control and the sample are from the same continuous distribution. The alternative hypothesis is that they are from different continuous distributions. The *P*-values report if the numbers differ significantly. The null hypothesis is rejected if *P* is less than 0.05.

Chapter 3

Results: development of the FRET-FLIM assay for measuring tyrosine kinase-inhibitor interactions in cells

The general strategy applied in this thesis for the characterization of inhibitor-tyrosine kinase interactions in cells involves the measurement of the change in fluorescence lifetime of a fluorophore due to Förster resonance energy transfer between fluorescent protein-labeled tyrosine kinases (the FRET donors) and fluorophore-labeled inhibitors (the FRET acceptors) using fluorescence lifetime imaging microscopy (Figure 1.9), this approach is referred to as the FRET-FLIM assay. The efficiency at which FRET occurs is steeply dependent on the distance between donor and acceptor fluorophores (Figure 1.6). 50% energy transfer takes place with fluorophores at a distance of 2–6 nm apart this is on the scale of biological interactions.

3.1. Components for the FRET-FLIM assay to measure kinase-inhibitor interactions

The necessary steps for the development of the FRET-FLIM-based assay system (Figure 1.9) include: the selection of appropriate kinase/inhibitor combinations (Section 3.1.1), the selection of appropriate FRET pairs to observe their interactions (Section 3.1.2) and the design of genetically tagged kinases/chemically tagged inhibitors (Section 3.1.3).

3.1.1 Selection of enzyme-inhibitor combinations.

The EGFR signaling pathways have been linked to the regulation of various processes leading to the abnormal proliferation of cells. EGFR was the first growth factor receptor targeted for drug cancer therapy. The design of our assay is based on the interaction of EGFR with a covalent inhibitor.

Most EGFR inhibitors are based on a 4-anilinoquinazoline core and include clinical therapeutics such as gefitinib and erlotinib (Zhou et al., 2009). The inhibitors occupying the

ATP binding site of EGFR are termed ATP competitive inhibitors and can be reversible or irreversible.

Table 3.1: Description of kinase inhibitors on which imaging probes were based

Inhibitor Name	Structure	Mode of binding	Description	References
PD168393	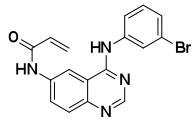	Binding to ATP binding pocket of EGFR	Irreversible inhibition of EGFR	(Blair et al., 2007; Fry et al., 1998)
Lapatinib	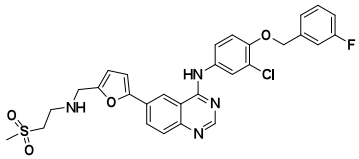	Type II inhibitor	Reversible inhibition of EGFR	(Wood et al., 2004)
Sorafenib	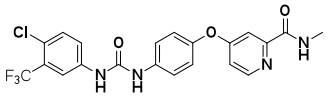	Type II inhibitor	VEGFR and PDGFR reversible inhibition. Blocks RAF/MEK/ERK pathway	(Wilhelm et al., 2004)
BIBW2992	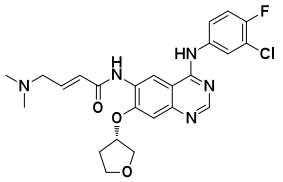	Binding to ATP binding pocket of EGFR	Irreversible inhibitor	(Bean et al., 2008)
RL10	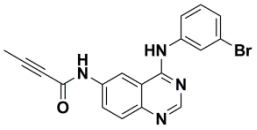	Binding to ATP binding pocket of EGFR	Irreversible inhibitor	(Sos et al., 2010)
RL2	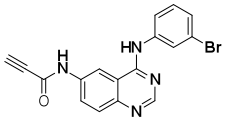	Binding to ATP binding pocket of EGFR	Irreversible inhibitor	(Sos et al., 2010)

A variety of inhibitor units were selected, for design of the inhibitor-probes (Table 3.1). PD168393, BIBW2992, RL10 and RL2 are ATP competitive irreversible inhibitors of EGFR based on a 4-anilinoquinazoline core. Lapatinib, is a reversible ATP competitive

inhibitor of EGFR. The inclusion of sorafenib in the list of inhibitor units was to justify the probe selectivity as sorafenib is an inhibitor of PDGFR with very little activity towards EGFR (Karaman et al., 2008).

3.1.2 Selection of suitable FRET pairs

The use of genetically encoded fluorescent proteins enables the labeling of a wide variety of proteins including membrane bound proteins. With the use of a sufficiently long linker between the fluorophore and protein it is possible to reduce the interference of the fusion on the target protein. Fluorescent proteins have favourable spectroscopic properties for efficient detection and fluorescence lifetime measurements. The donor fluorescent proteins used in this study (EYFP, mCitrine and mTurquoise) emit visible fluorescence and are relatively photostable. Additionally these FP's have a monoexponential fluorescence decay, which reduces the complexity of fluorescence lifetime determination thereby making it possible to quantify the effect of FRET.

Table 3.2: Description of dyes used for synthesis of probes

Dye name	Structure	Exc/Em
Lissamine rhodamine (LRh) (Invitrogen)	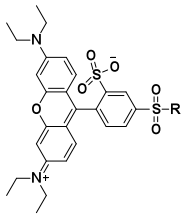	570/590
Bodipy-FL (Invitrogen)	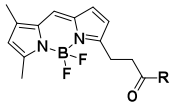	503/512
Bodipy 576/589 (Invitrogen)	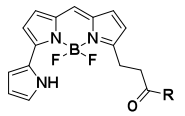	576/590

'R' indicates the point of attachment to the linker. The linker then is attached to an inhibitor at the other side.

The acceptor dyes (Table 3.2) were selected based on their suitability as FRET partners for donor fluorescent proteins. In addition, the lipophilic nature of these dyes renders them

cell-permeable, however, the dyes should also be soluble in aqueous solution in order to access the ATP binding pocket of the EGFR.

LRh was used as an effective FRET acceptor for GFP in live cell experiments when chemically conjugated to a synthetic peptide (Yudushkin et al., 2007). The spectral overlap indicated that it was an equally suitable FRET partner for mCitrine and EYFP (Figure 3.1), which are superior to GFP because of their increased brightness and mono-exponential fluorescence lifetimes (Shaner et al., 2005).

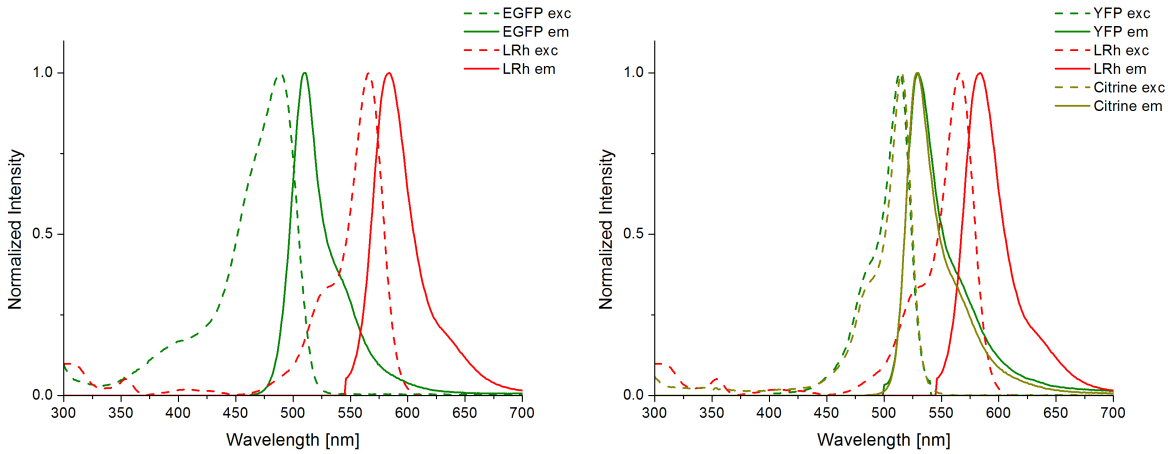

FRET Pair	Förster radius (nm)
EGFP-LRh	4.79
YFP-LRh	5.79
mCit-LRh	6.00

Figure 3.1 Peak normalized excitation (exc) and emission (em) spectra of fluorescent protein donors and LRh acceptor molecules

Left: FRET pair used by Yudushkin et al., 2007. Right: FRET pairs used in current study. The forster radius is partially defined by the overlap the emission spectra of the donor fluorophores (EGFP, Citrine and YFP) and the excitation spectra of the acceptor fluorophore (LRh). Bottom: the. Förster radii, calculated using Equation 3 (Section 1.5.2). The data pertaining to excitation and emission spectra were obtained from the following databases: EGFP/ Citrine (http://www.tsienlab.ucsd.edu), YFP (http://www.fluorophores.tugraz.at/substances/745), lissamine rhodamine (http://www.fluorophores.tugraz.at/substance/10). These data were re-plotted and used for the calculation of the Förster radii (R_0) for each FRET pair.

According to the spectra supplied by the manufacturer Bodipy 576/589 also appeared to be an acceptable FRET acceptor for EYFP/mCitrine (Figure 3.2).

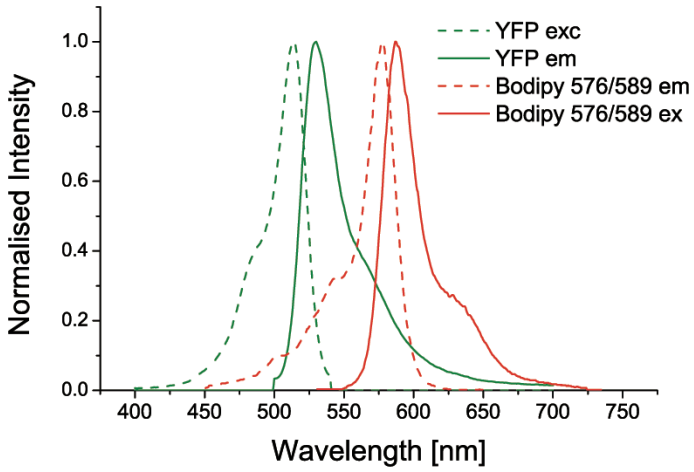

Figure 3.2 Excitation and emission spectra of YFP and Bodipy 576/589

The overlap between the emission spectra of YFP and excitation spectrum of Bodipy 576/589 indicates suitable candidates for FRET. Spectra were re-plotted using data from the following sources: YFP (http://www.fluorophores.tugraz.at/substance/745) and Bodipy 576/589 (from Invitrogen, upon request).

Goedhart et al. published a variant mTurquoise, which is 1.5-fold brighter than mCerulean in mammalian cells, has a long fluorescence lifetime (> 3.7 ns) and decays mono-exponentially. mTurquoise is favoured as a FRET donor because of an increased FRET efficiency and higher fluorescence lifetime contrast when compared to its peer mCerulean (Goedhart et al., 2010).

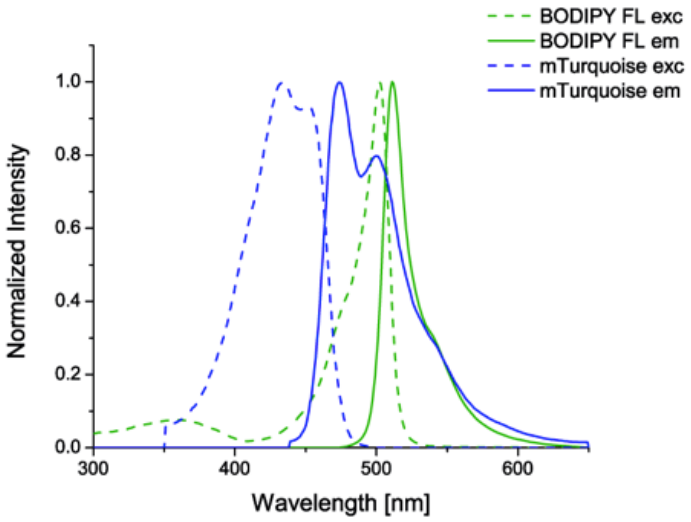

Figure 3.3 Excitation and emission spectra of mTurquoise and Bodipy-FL

The overlap between the emission spectra of mTurquoise (Goedhart et al., 2010) and excitation spectrum of Bodipy-FL (http://www.fluorophores.tugraz.at/substance/636) indicates suitable candidates for FRET.

From the overlay of mTurquoise emission spectra and Bodipy-FL excitation spectra (Figure 3.3) there appears to be a complementary donor/acceptor pair with a Förster radius of 5.28 nm calculated using Equation 3 (Section 1.5.2). mTurquoise has a very broad emission spectrum which overlaps with the emission spectrum of the acceptor. This point is inconsequential for FRET-FLIM measurement, but such a pair would be unsuitable for methods such as acceptor photo-bleaching and sensitized emission.

3.1.3 Construction of labeled EGFR and labeled kinase inhibitors

Acceptor-labeled kinase inhibitors

To construct FRET acceptor probes for the FRET-FLIM assay, the selected acceptor dyes (Table 3.2) had to be chemically attached to the selected kinase inhibitors (Table 3.1). An essential aspect of the probe design involved the choice of the linkers and their points of attachment to inhibitors. The synthesis of the inhibitor probes used in this thesis (unpublished data), was carried out by Dr. Haridas Rode in the laboratory of Prof. Daniel Rauh (currently at Technische Universität, Dortmund), according to adapted literature

procedures (Blair et al., 2007). The general structure for inhibitor-probe design is exemplified by the design of probe PD168393-LRh.

In order to select an appropriate point of attachment of linkers to inhibitors we visited different co-crystal structures of inhibitors. In the case of inhibitor PD168393 in complex with EGFR kinase domain (PDB 2J5F; Blair et al., 2007), the C7 position of the quinazoline was selected for attachment of the fluorophore. This position is solvent-exposed and any modification at this position will most likely not jeopardize the binding of an inhibitor-probe to EGFR (Figure 3.4).

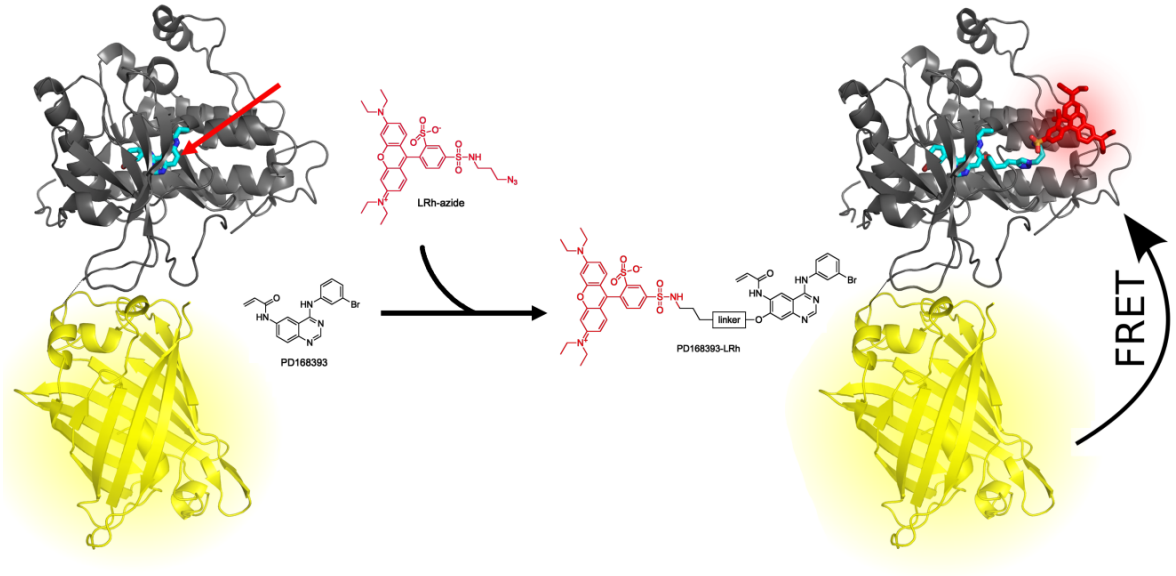

Figure 3.4 Strategy for kinase-inhibitor probe assay development

The design of fluorescent protein-tagged EGFR and fluorescent probes for monitoring kinase-inhibitor interactions was facilitated by analyzing the structures of different quinazoline-based inhibitors in complex with kinases, which revealed that the C7 position of the quinazoline scaffold (red arrow) is likely to be solvent exposed and could, therefore, be derivatized to accommodate different solubilizing groups or fluorophores. The C-terminus of EGFR would be most suitable for attachment of a fluorescent protein because on the N-terminus of EGFR is extracellular. Upon probe binding, FRET between the donor fluorescent protein on the kinase and the acceptor on the inhibitor can be measured using FLIM. This strategy was for example adopted for modifying PD168393 to yield kinase probe PD168393-LRh.

For the construction of inhibitor-probes, we have used linker systems based on polyethylene glycol (PEG), polyproline, and on triazoles. As the physicochemical properties of the probe molecules play a significant role, we have used PEG linkers in order to render the inhibitor-probe molecules more hydrophilic, and therefore more soluble in

aqueous media. The additional advantage of using the hydrophilic PEG linker is that it is attached at a point that is water-exposed and remains in the hydrophilic environment to reduce impairment of binding to the ATP pocket.

For the rapid linking of inhibitor/fluorophore combinations, the copper-catalyzed Huisgen 1,3-dipolar cycloaddition (an example of a 'Click reaction') was also explored (Huisgen, 1984; Rostovtsev et al., 2002). Therefore, inhibitor-probe PD168393-LRh, which is based on the irreversible EGFR inhibitor PD168393 and the fluorophore lissamine rhodamine (LRh), contains a triazole-based linker (Figure 3.5).

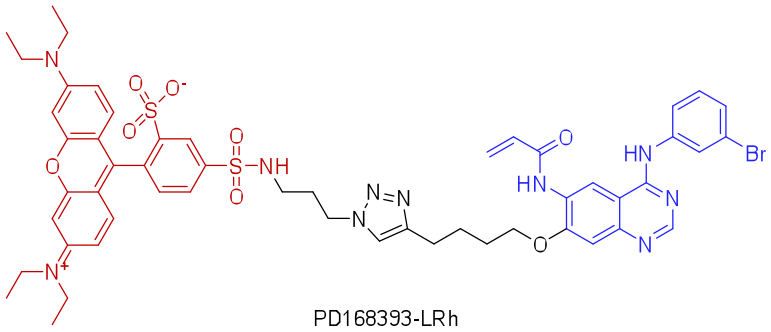

Figure 3.5 Structure of PD168393-LRh.

The EGFR probe consists of a lissamine rhodamine dye (red), connected to the solvent-exposed C7 position of the irreversible EGFR inhibitor PD168393 (blue) via a triazole-based linker system (black).

Other probes used in this study, which were named after their particular inhibitor/fluorophore combinations, were designed according to a similar strategy, but do not necessarily incorporate the triazole linker system. Detailed structures of the probes and their synthesis will be published together with the assay development at a later stage.

Donor-labeled EGFR constructs

In the case of the transmembrane tyrosine kinases (EGFR and PDGFRb) the fluorescent protein was attached on the C-terminus of the protein, as the C-terminus is located on the intracellular domain of the protein together with the ATP-binding pocket. In the case of the cytoplasmic (Csk) and membrane anchored (Src) tyrosine kinases, attachment of the fluorophore on the C-terminus maintained the expected intracellular localization of these proteins.

The fusion of cDNA of interest to the coding sequence of the fluorescent protein is described in Section 2.2. Plasmid DNA encoding the fusion protein is transfected into cells as described in Section 2.3 and ectopically expressed.

3.2. Uptake of kinase probes in live cells

All inhibitors incorporated in the probes are known to be cell-permeable. However, dye attachment and choice of linkers, may modify the permeability of the probe. In dynamic live cell systems, it is preferable to have a probe that is taken up rapidly. With a gradual uptake of a probe, events happening on shorter timescales would be lost.

To assess the rate of uptake of probes, probes were added to MCF-7 cells and probe fluorescence was detected over time (min) using confocal laser scanning microscopy (CLSM).

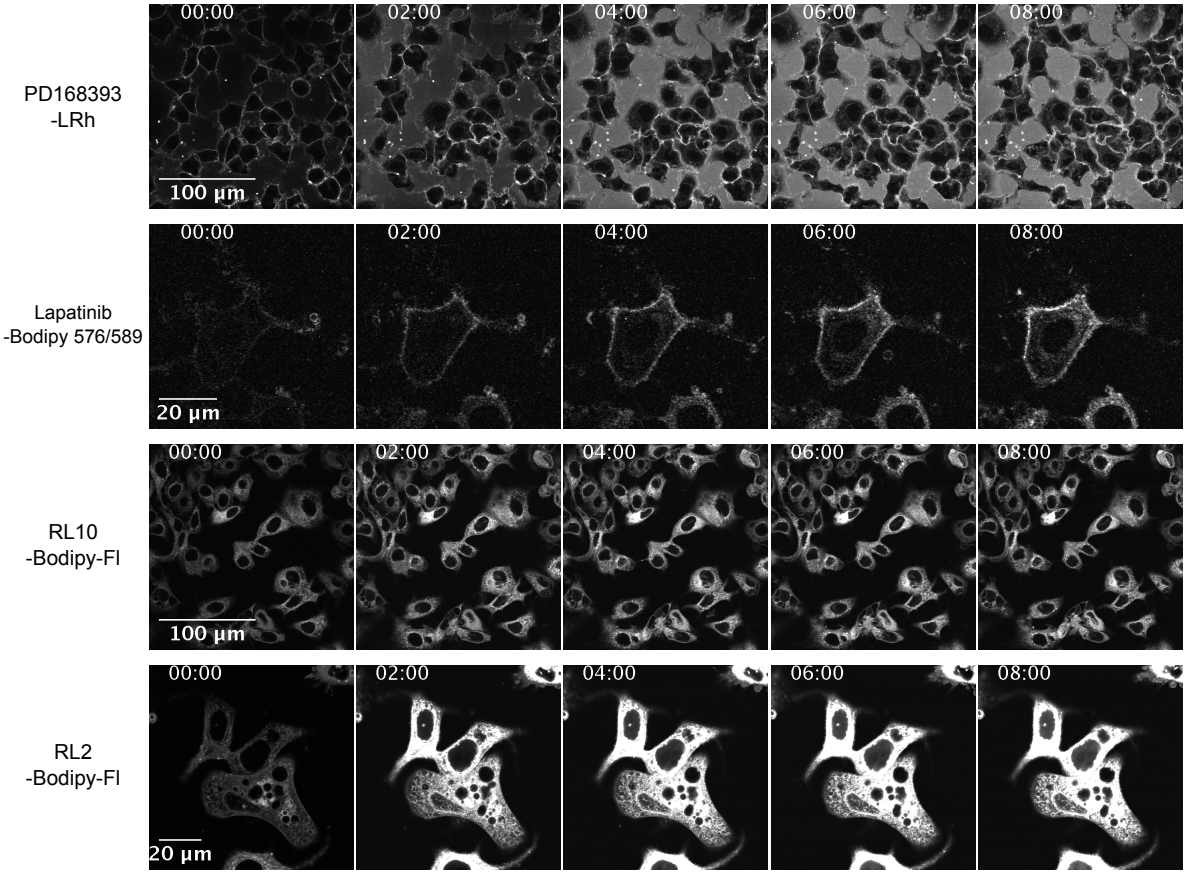

Figure 3.6 Uptake of probes in MCF-7 cells

The grayscale image sequences are time-lapse fluorescence images of probe uptake at 1 µM concentration in live MCF-7 cells. The indicated probes were added to cells in focus and uptake was imaged every 2 min for an hour. Shown are the image sequences for the first 8 min after probe addition.

Cellular uptake of the lissamine rhodamine-probe was slower in comparison to Bodipy 576/589 and Bodipy-FL probes (Figure 3.6). All probes showed an affinity for endomembranes as indicated by the heterogeneous/structured distribution of fluorescence inside the cell.

To enable rapid and efficient delivery of LRh-based probes into cells we explored additional approaches. Methods available for delivering molecules to the cytosol (other than passive uptake), while maintaining cell viability, include microinjection, electroporation and reversible permeabilization of the cell membrane. Microinjection is technically demanding and impractical for large numbers of cells. Electroporation is limited by the long recovery times post addition of compound. We, therefore, used streptolysin-o (SLO)-mediated reversible permeabilization for the delivery of the LRh-labeled compound (Section 2.7).

PD168393-LRh was added to the activated SLO and MCF-7 cells were incubated with the SLO/probe mix. The uptake of PD168393-LRh was monitored in the presence of different amounts of SLO by detection of PD168393 fluorescence using (CLSM).

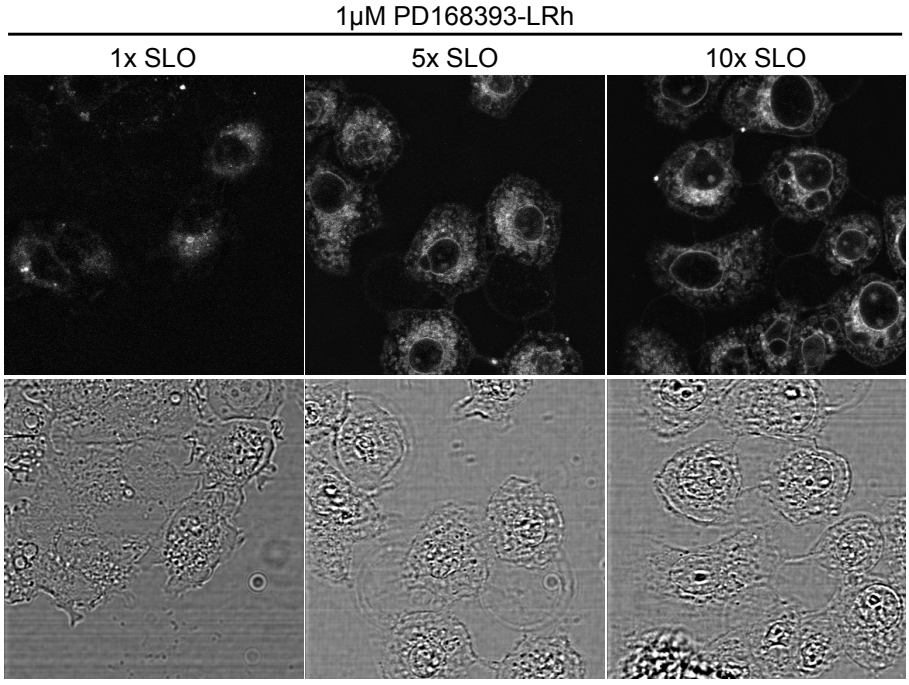

Figure 3.7 Uptake of PD168393-LRh in MCF-7 cells after reversible permeabilization by SLO.

MCF-7 cells were incubated (37 °C for 10 min) with PD168393-LRh (1 μM) in the presence of activated SLO (column1, 1 μg; column 2; 5 μg; column 3, 10 μg). Thereafter, cells were washed and incubated (20 min, 5% CO_2, 37 °C) with DMEM (containing 10% FCS), to enable resealing of the plasma membrane. Confocal fluorescence (upper row) and transmission (lower row) images were acquired after membrane resealing with the cells in imaging medium. The fluorescence shown in the upper row (grey scale) is from PD168393-LRh.

At 1× SLO, uptake of PD168393 was poor; different levels of fluorescence in each cell indicate varying levels of permeabilization (Figure 3.7, column 1). At 5× SLO and 10× SLO (Figure 3.7, column 2 and 3) SLO uptake was prevalent to the same extent in all cells. The heterogeneous distribution of fluorescence in the cells is attributed to staining predominantly on endo-membranes. From the transmission images for 1×, 5× and 10× SLO (Figure 3.7, lower row), it appears as though the higher concentrations of SLO (5× and 10×) led to morphology changes. It was also observed that a high number of cells, in the 5× and 10× SLO samples, began to detach from the surface of the dish. Selecting the correct toxin dose is crucial; toxin concentration will vary depending on cell target and density (Walev et al., 2001). SLO permeabilization could prove to be a promising method for delivery of impermeable probes into cells with further optimization.

From both uptake approaches employed in this section it is evident that the probes have a high affinity for endo-membranes. An advantage of using FLIM measurement is that it relies on the fluorescence signal of the donor fluorophore, which, in our case, is attached to the kinase. The probe binding to the kinase is the only effect that will be detected by FLIM and the nonspecific membrane affinity should not affect our results. One effect the membrane accumulation of probe may have is that it could lower the local concentration of probe available for binding to the kinase.

Despite the above-mentioned drawbacks these experiments indicate that we were able to develop a set of inhibitor-probes suitable for experiments in cells. To measure the interaction between an inhibitor probe and kinase by FRET we employed fixed MCF-7 cells transiently transfected with EGFR-YFP. Fixed cells were used to circumvent the problem arising from probe accumulation on endo-membranes by permitting the use of sufficiently high concentrations of probe to ensure a large enough soluble fraction. Additionally fixed cells can be used in combination with LRh-based probes that exhibit poor uptake in live cells.

In the following sections the binding of the acceptor labeled probes to donor labeled EGFR was characterized in fixed cells (Section 3.3.1) and live cells (Section 3.3.2).

Measurement of enzyme-inhibitor interactions using FRET-FLIM

3.3.1 Measurement of enzyme-inhibitor interactions post-fixation.

Having confirmed the suitability of the selected donor and acceptor fluorophores as FRET partners (Figure 3.1), we aimed to use the interaction between EGFR-YFP with PD168393-LRh as the model system for imaging inhibitor-kinase binding in fixed MCF-7 cells.

MCF-7 human breast carcinoma cells were transiently transfected with EGFR-EYFP. The low endogenous level of EGFR (deFazio et al., 2000) in this cell type reduces inhibitor binding to non-fluorescent endogenous receptor. Cells were starved, stimulated with EGF and then rendered permeable to the LRh labeled inhibitor by methanol fixation. Pre-incubation with unlabeled drug BIBW2992 was carried out prior to EGF stimulation and fixation. Fixed cells were stained with PD168393-LRh and binding was measured by a

decrease in the fluorescence lifetime of the EYFP after incubation with the labeled inhibitor. To resolve the degree of non-specific binding due to the hydrophobic nature of LRh, cells were stained with lissamine rhodamine modified with the linker used in the PD168393-LRh probe (Figure 3.8, row 2). Fluorescence lifetime measurements were obtained by time-domain FLIM (Section 2.10.2).

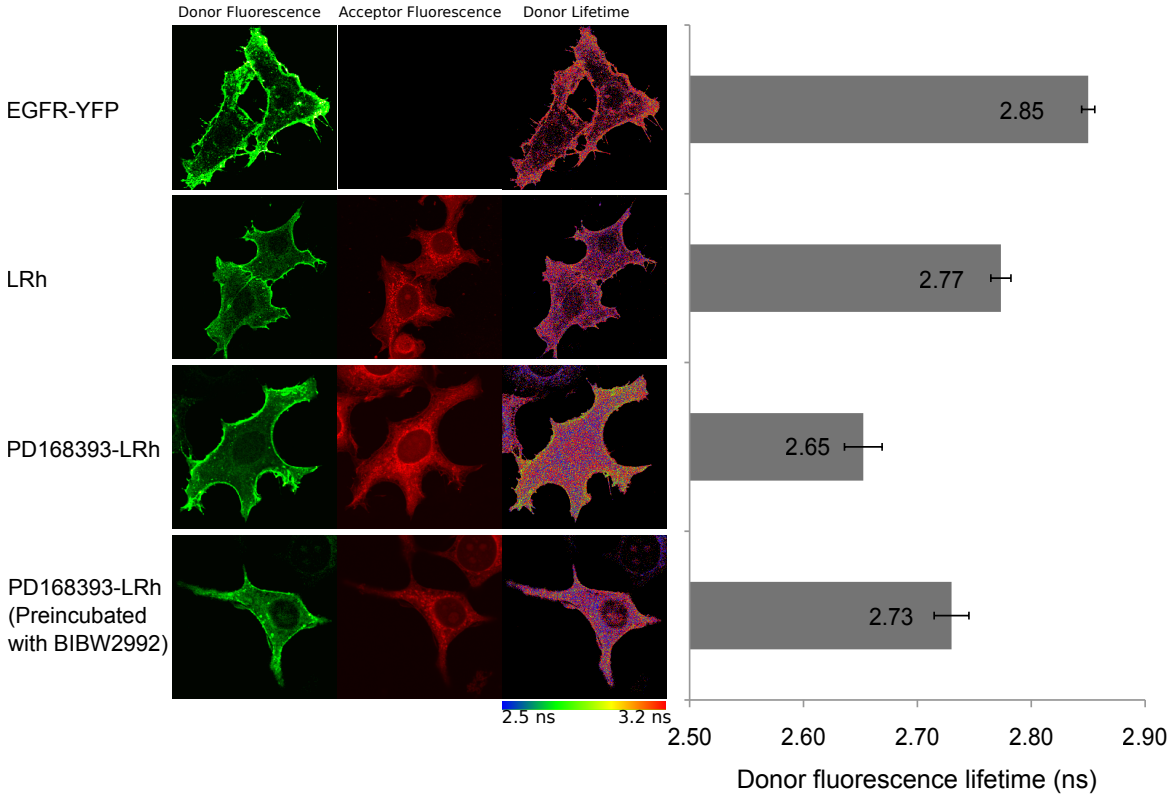

Figure 3.8 Binding of PD168393-LRh to EGFR-EYFP measured by FRET-FLIM

MCF-7 cells expressing EGFR-EYFP were starved (4 h, without FCS), stimulated with EGF (100 ng/ml, 5 min) and treated by methanol fixation. In the uppermost row, cells were left unstained; the second row shows cells treated with lissamine rhodamine; cells in the third and fourth rows were stained with PD168393-LRh (1 h incubation followed by washing with PBS). In the final row, cells were pre-incubated with inhibitor BIBW2992 (10 µM, 1 h, 37 °C, 5% CO_2) before stimulation, fixation and staining with PD168393-LRh. Staining was carried out by incubating the fixed cells with PD168393-LRh (1 µM, PBS, 0.5% pluronic) or LRh (1 µM, PBS, 0.5% pluronic) for 1 hour at RT. The graph (right) shows the average donor fluorescence lifetime for each of the conditions described: (EGFR-EYFP) indicates no acceptor present, (LRh) indicates the fluorescence lifetime of the donor in the presence of LRh, (BIBW2992 + probe PD168393-LRh) and (probe PD168393-LRh) indicates the fluorescence lifetime of the donor in the presence of probe PD168393-LRh in BIBW2992-treated and -untreated cells.

The fluorescence lifetime of EYFP showed a steeper decrease in the presence of PD168393-LRh (Figure 3.8, PD168393), as compared to cells stained with LRh (Figure

3.8, LRh). Preincubation of live cells with BIBW2992 followed by fixation and staining with PD168393-LRh showed a full recovery with respect to the LRh control (Figure 3.8, PD168393, pre-incubated with BIBW2992). Because BIBW2992 is an irreversible inhibitor that binds to the ATP binding pocket of EGFR this experiment shows that, the PD168393-LRh probe indeed binds to the ATP-binding site of EGFR and that the tertiary structure of EGFR remains intact after fixation.

Altered PD168393-LRh binding to modified ATP binding pocket in EGFR

Crystal structures of EGFR in complex with PD168393 reveal that the inhibitor is covalently bound to the active site. The β-carbon atom of the acrylamide Michael acceptor on the inhibitor binds to the γ-sulfur atom of Cys797. Additionally a hydrogen bond is formed by the quinazoline N1 to the main chain amide of Met793 along the hinge region. The C4 aniline resides in the hydrophobic pocket defined by the gatekeeper residue, Thr790 (Blair et al., 2007). By mutating the Cys797 to Ser and Thr790 to Met the covalent bond with the drug is disrupted and the nature of the hydrophobic pocket is altered. It is therefore expected that the interaction of PD168393-LRh with the mutant EGFR-T790M-C797S-YFP would be abrogated.

MCF7 human breast carcinoma cells were transiently transfected with EGFR-T790M-C797S-EYFP. Cells were starved, stimulated with EGF and methanol fixated. Fixed cells were stained with PD168393-LRh and binding was measured by a decrease in the fluorescence lifetime of the EYFP after incubation with the labeled inhibitor. The degree of non-specific binding due to the hydrophobic nature of LRh was resolved using lissamine rhodamine modified with the linker used in the conjugation to PD168393 (Figure 3.8, row 2).

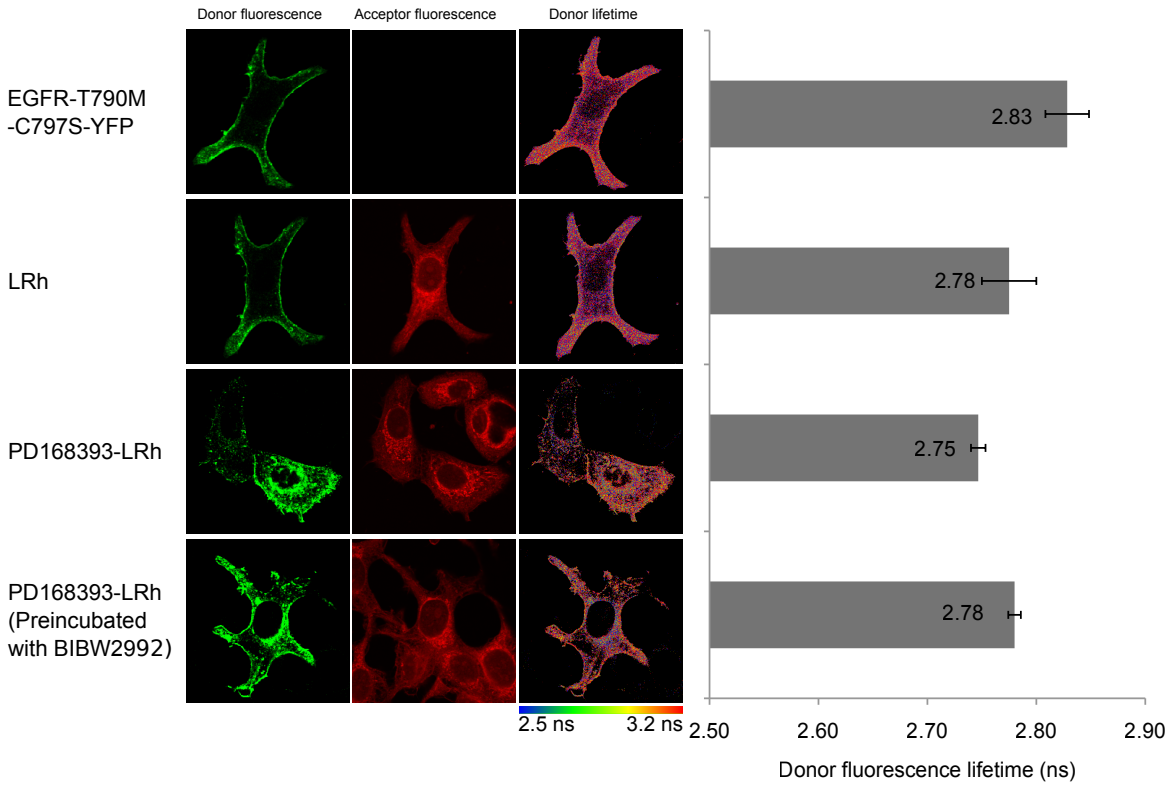

Figure 3.9 Binding of PD168393-LRh to EGFR-T790M-C797S-EYFP measured by FRET-FLIM

MCF-7 cells expressing EGFR-T790M-C797S-EYFP were starved, stimulated with EGF (100 ng/ml, 5min) followed by methanol fixation. In the uppermost frame cells were unstained; the second set of frames show cells stained with PD168393-LRh. Cells in the third frameset were treated with inhibitor BIBW2992 (10 µM, 1 h, 37 °C, 5% CO_2) before fixation and subsequently stained with PD168393-LRh. In the final frames cells were stained with lissamine rhodamine. The fixed cells were stained by incubation (1 h, RT) with PD168393-LRh (1 µM in PBS, 0.5% pluronic) or LRh (1 µM in PBS, 0.5% pluronic). The graph on the right shows the average donor fluorescence lifetime for each of the conditions described: (EGFR-T790M-C797S-EYFP) indicates no acceptor present, (LRh) indicates the fluorescence lifetime of the donor in the presence of LRh, (BIBW2992 + probe PD168393-LRh) and (probe PD168393-LRh) indicates the fluorescence lifetime of the donor in the presence of probe PD168393-LRh in BIBW2992-treated and -untreated cells.

Figure 3.9 shows that there is no significant binding of the probe to the mutant EGFR-T790M-C797S-EYFP, which confirms the high specificity of the probe for the ATP binding pocket of EGFR.

A comparison of PD168393-LRh binding to EGFR-YFP in native membrane sheets and fixed cells.

Methanol fixation works by denaturing and precipitating proteins, such denaturing effects could potentially reduce the efficacy of the method by reducing the accessibility of ATP binding pocket. Fluorescent proteins are known to consist of a tight barrel structure giving them a higher resistance to denaturation than the proteins that they are fused to. Therefore, the detection of fluorescence after fixation might not be an indication of the integrity of the fusion protein. Due to the limited uptake of PD168393-LRh in live cells a technique was required that would allow the receptor to access of similar concentrations of probe, as with fixation protocols, while maintaining the native tertiary structure of the receptor.

This was achieved by the use of native membrane sheet preparations. By adapting the protocol from Perez et al. (2006), cell membrane sheets were prepared by direct detachment from live cells using poly-L-lysine (PLL)-coated glass slides (Figure 3.10). This way, the resulting planar membranes retain the composition of the original plasma membrane including EGFR.

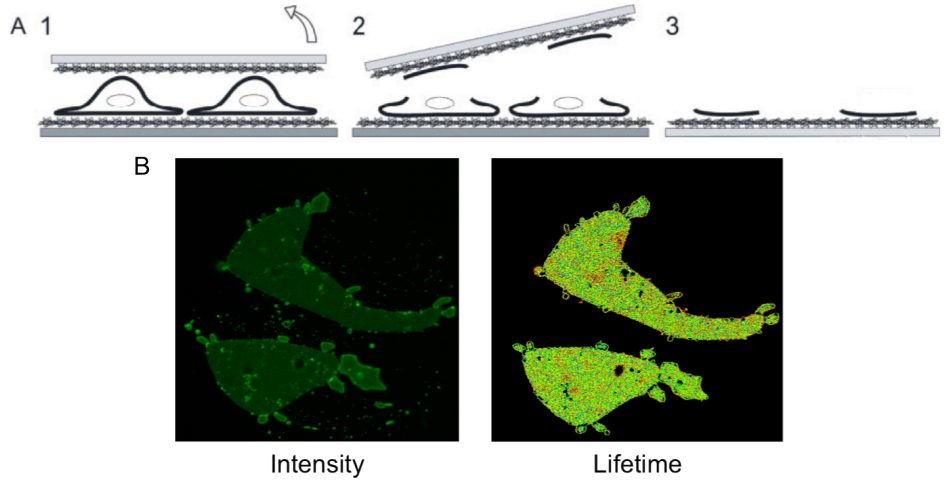

Figure 3.10 Preparation of native membrane sheet.

A) Preparation strategy: MCF-7 cells stably expressing EGFR-EYFP were grown in 35 mm Matek dishes pre-coated with PLL. A PLL-coated glass coverslip was pressed to the apical side of the cells. 2) After 3–4 min the coverslip was removed ripping off the apical membrane from the cells. 3) The cell membrane sheets remain attached to the PLL coated surface of the dish and can be imaged. B) Examples of intensity and fluorescence lifetime images of membrane sheets from MCF-7 cells expressing YFP fused to membrane anchor glycosylphosphatidylinositol. Part A) of figure is adapted from Perez et al. (2006).

During this procedure (Section 2.8) many cells are completely removed from the lateral surface and the yield of membrane sheets is relatively low. To ensure a higher probability of obtaining membrane sheets containing EGFR-EYFP, MCF-7 cell line stably expressing EGFR-EYFP were created (Section 2.3.4). The binding of PD168393-LRh to EGFR-YFP on native membrane sheets and fixed cells was compared to determine if the fixation procedure alters the tertiary structure of the kinase and thereby impacts probe binding.

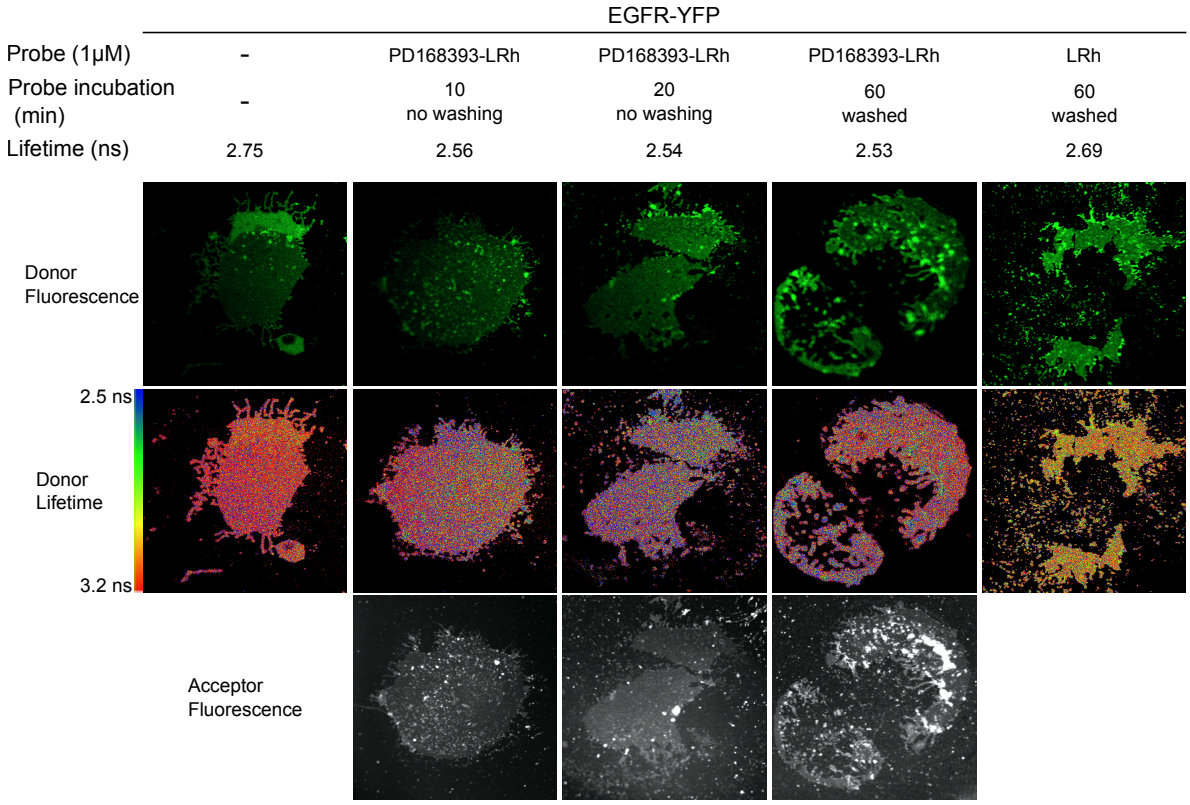

Figure 3.11 Binding of PD168393-LRh to EGFR-EYFP in native membrane sheets.

MCF-7 cells stably expressing EGFR-EYFP were used to prepare native membrane sheets. PD168393-LRh (1 µM) was added and the fluorescence lifetimes of membrane sheets were imaged at 10 min and 20 min without washing and after 60 min with washing. LRh (1 µM) was incubated for 1 h, washed, and fluorescence lifetimes were imaged.

The donor fluorescence lifetimes on membrane sheets were measured by time-domain FLIM and found to be in the expected range for EYFP. PD168393-LRh was added and the fluorescence lifetimes of EGFR-EYFP on membrane sheets were imaged at the indicated time points (Figure 3.11). These were compared to native membranes that were incubated with LRh.

Table 2.3: A comparison of fluorescence lifetime changes in fixed cells and native membrane sheets

	Fixed cells ($\Delta\tau_{average}$)	**Native membrane sheets ($\Delta\tau_{average}$)**
LRh	0.08 ns ± 0.03 ns	0.06 ns ± 0.03 ns
PD168393-LRh	0.20 ns ± 0.04 ns	0.20 ns ± 0.05 ns

The average reduction in fluorescence lifetimes of fixed cells (Figure 3.8) is of the same magnitude as in native membrane sheets indicating that methanol fixation does not affect the tertiary structure of the EGFR fusion protein.

In Section 3.3.1, enzyme–inhibitor binding in a fixed cell system was characterized. Binding was shown to occur specifically at the ATP-binding pocket of EGFR, firstly by blocking the ATP-binding of EGFR with a covalent inhibitor and secondly by disruption of the ATP-binding pocket through two point mutations. The effect of fixation on binding was also explored using native membrane sheets and binding of the probe to EGFR was comparable in both systems.

3.3.2 The measurement of enzyme-inhibitor interactions in live cells.

Initially the combination of EGFR-EYFP and Lapatinib-Bodipy 576/589 was used to measure interactions in live cells. MCF-7 cells were transfected with the EGFR-EYFP and starved. After starvation cells were imaged either immediately to obtain the fluorescence lifetime of EYFP or after staining with Lapatinib-BDP 576/589. Thereafter the cells stained with Lapatinib-BDP 576/589 were washed and fluorescence lifetime images were acquired using frequency-domain FLIM.

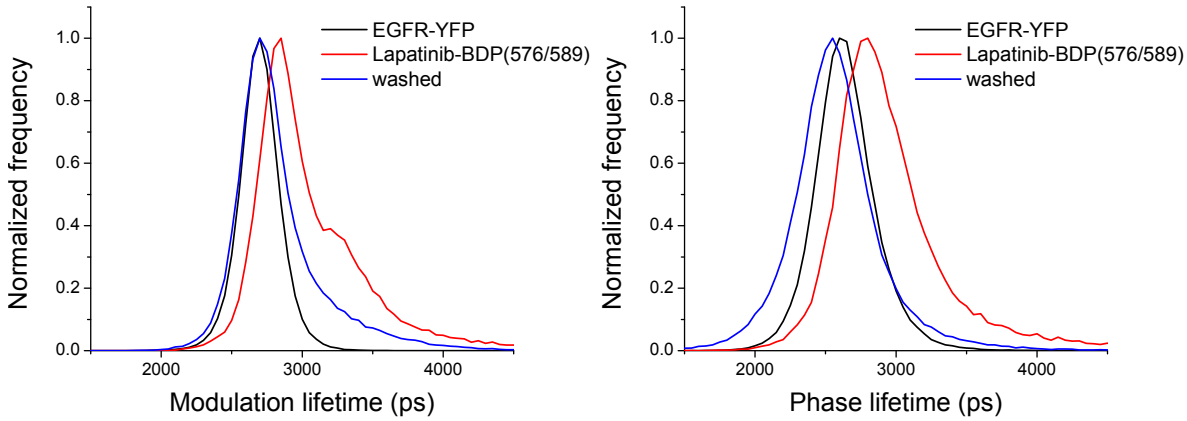

Figure 3.12 Fluorescence lifetime distribution of EGFR-EYFP in the presence of Lapatinib-Bodipy (576/589).

MCF-7 cells were transfected with the EGFR-EYFP plasmid 24 h after plating and the protein was expressed for 18–24 h. Cells were starved (4 h, DMEM without FCS) and thereafter imaged immediately or stained with Lapatinib-Bodipy (1 µM, 1 h, in serum free medium). Shown are the distributions of modulation (left) and phase (right) donor fluorescence lifetimes, measured using frequency domain FLIM. The fluorescence lifetime of EYFP in MCF-7 cells expressing EGFR-EYFP was measured (black line). Upon addition of Lapatinib-Bodipy 576/589 the distribution shifted to higher fluorescence lifetimes (red line). After washing (3× serum free medium), the fluorescence lifetime distribution shifted back to the range observed for the sample containing only the donor fluorophore (blue line).

An increase in donor fluorescence lifetime upon adding Lapatinib-Bodipy 576/589 was observed (Figure 3.12, red line). After washing out the probe (Figure 3.12, blue dashed line) the fluorescence lifetime reduced to a value close to that of the control sample containing only the donor fluorophore (Figure 3.12, black line). The reversible nature of the lapatinib/EGFR interaction was confirmed by the shift in fluorescence lifetime distributions, to that of EYFP alone, after washing out the probe. The shift in distribution of fluorescence lifetimes, upon addition of probe, to values higher than that of EYFP was counterintuitive.

To find the source of the higher fluorescence lifetime populations, detected upon addition of the probe, the spectra of the Bodipy 576/589 dye was re-visited. The manufacturer's spectra for Bodipy 576/589 were obtained in ethanol (EtOH) (Figure 3.2). The emission spectra of Bodipy 576/589 in EtOH and in PBS were measured using a 470 nm excitation source (Section 2.9).

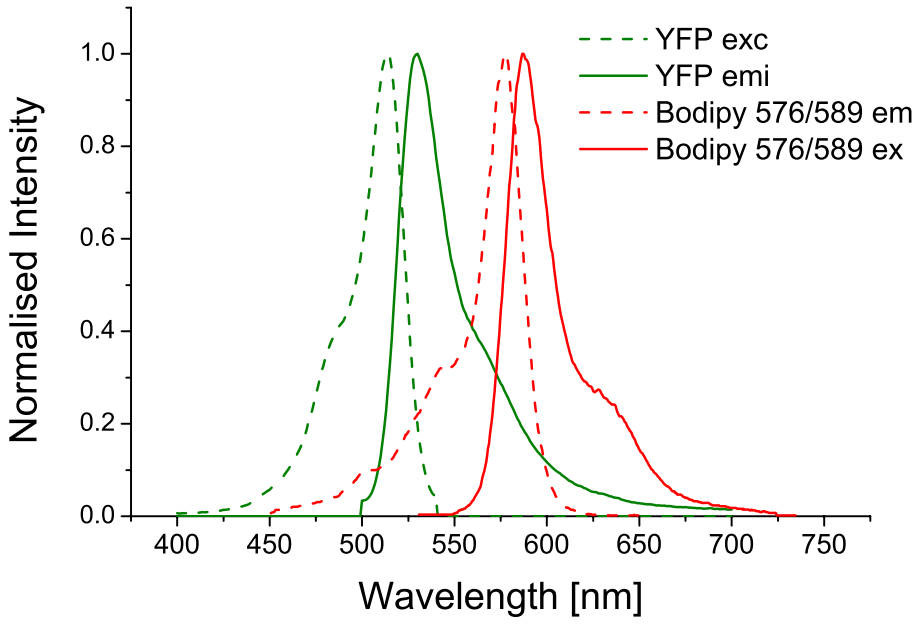

Figure 3.13 Excitation and emission spectra of YFP together with the emission spectra of Bodipy 576/589 in EtOH and PBS (measured).

The emission spectra of Bodipy 576/589 were measured in EtOH (maroon line) and PBS (red line) using an excitation of 470 nm. When compared to the emission spectrum of YFP (green line) there was an overlap in both FP and dye emission spectra that results in bleed through of the acceptor emission in the donor channel. YFP spectrum was re-plotted using data from (http://www.fluorophores.tugraz.at/substance/745).

The emission spectra of Bodipy 576/589 in EtOH was found to have a small emission in the green area of the spectrum, which we use to detect the donor signal. In PBS, however, there was a dramatic shift in the emission spectrum of Bodipy 576/589 (Figure 3.13, red line) showing a large emission peak in the EYFP emission range. This spectral shift due to the environmental sensitivity of Bodipy 576/589 makes it unsuitable for our current application.

With the option of a red acceptor for live cell imaging being unsuccessful, the green-shifted Bodipy-FL probe was explored. Bodipy-FL was found to be a suitable FRET acceptor for mTurquoise (Figure 3.3). MCF-7 cells were transfected with the EGFR-mTurquoise. To detect binding of this previously uncharacterized FRET pair, cells were starved and left unstimulated. Indicated cells were pre-treated with the drug BIBW2992. After starvation cells were stained with RL10-BodipyFL, washed with serum-free medium and imaged using time-domain FLIM.

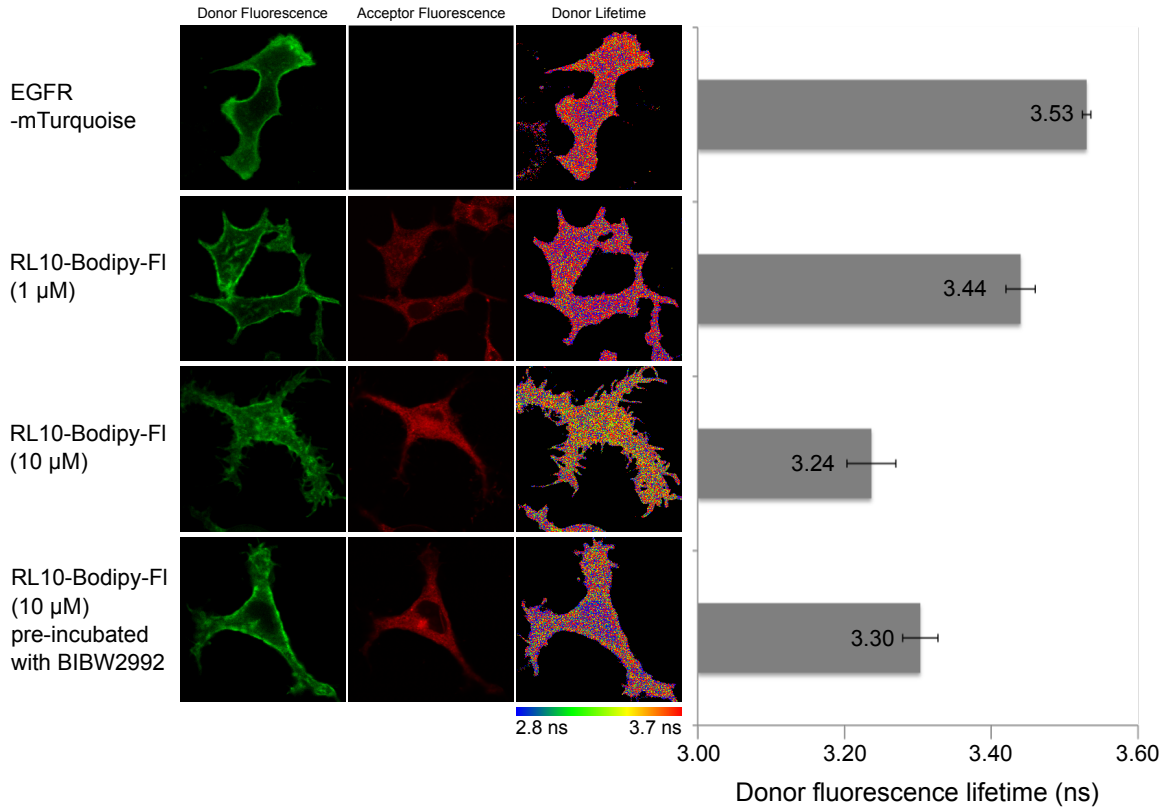

Figure 3.14 Probe-binding in live cells.

MCF-7 cells transfected with EGFR-mTurquoise were starved and imaged in serum-free imaging medium. Upper frame: cells were unstained; second frame: cells were stained with RL10-Bodipy-FL (1 µM, 1 h); in the lower frames cells were stained with RL10-Bodipy-FL (10 µM, 1 h). Cells in the lowest frame were pre-treated with BIBW2992 (10 µM, 1 h) before probe staining. On the right is a summary of the fluorescence lifetimes measured for the indicated conditions.

The donor fluorescence lifetime obtained for EGFR-mTurquoise in the absence of acceptor was 3.53 ns (Figure 3.14, EGFR-mTurquoise), which is slightly lower than the reported fluorescence lifetime of mTurquoise (3.7 ns) (Goedhart et al., 2010) and could be the result of the protein fusion. A greater change in the fluorescence lifetime occurred at the higher concentration of probe (Figure 3.14, RL10-Bodipy-Fl (10 µM)) again membrane affinity of the probe could reduce the fraction of probe available to interact with the kinase. In cells that were pre-incubated with BIBW2992 a partial recovery in the fluorescence lifetime was noted (Figure 3.14, RL10-Bodipy-Fl (10 µM) pre-incubated with BIBW2992). The reason for the partial blocking effect observed upon addition of BIBW2992 is not known. One speculation is that only a very small fraction of the drug bound to the EGFR. Incubation times and concentration of BIBW2992 used in Figure 3.14 are identical to those used in

Figure 3.8. In Figure 3.8 cells were stimulated with EGF, fixed and stained with PD168393-LRh and a blocking effect was noted. The first variable in the live cell versus fixed cell experiments is the EGF stimulation, a high concentration of BIBW2992 was used to overcome possible differential affinities for different conformations of the EGFR, but perhaps this was not sufficient. The second difference is the fixation process. The third variation between the live and fixed cell experiments is the reactive group of the probe although both PD168393 and RL10 have nanomolar affinities for EGFR (Sos et al., 2010). Lastly a 10 fold higher concentration of RL10-Bodipy-FL is used in comparison to fixed cell experiments.

3.3. Using labeled inhibitors to probe protein conformation

Ligand-dependent EGFR dimerization results in the trans-phosphorylation of tyrosine residues on the C-terminal tail. These phoshorylated residues serve as docking sites for signaling molecules containing SH2 or PTB domains. However, unlike most kinases, trans-phosphorylation of EGFR is not critical to its activation but rather the formation of an asymmetric dimer is the key feature of EGFR activation (Zhang et al., 2006). Crystal structures of EGFR kinase domains reveal that the active asymmetric conformation involves contacts between the C-terminal lobe of one kinase with the N-terminal lobe of the other (Zhang et al., 2006). Although dependent on the former only the latter is active within the dimer (Figure 3.15). This dimer interface is also known to be the target of protein inhibitors of EGFR activity such as Mig6 (Zhang et al., 2007).

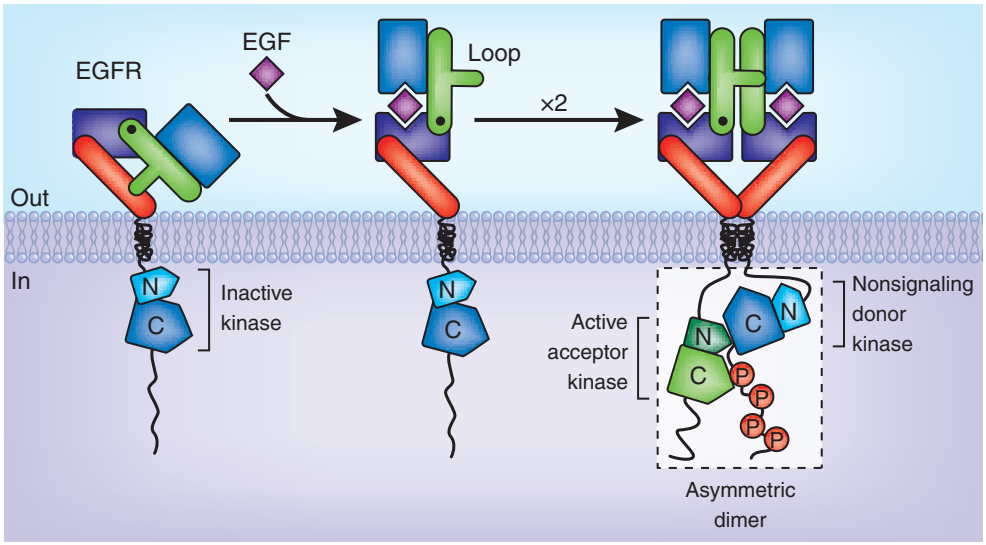

Figure 3.15 Schematic model of EGFR activation

In the absence of ligand, EGFR adopts a compact conformation in which a loop on domain II (green) is buried (left). Ligand binding promotes a domain rearrangement in which domains I and II (blue rectangle and green) rotate and expose the domain II loop (middle). The exposed domain II loop mediates dimerization of the extracellular regions, which leads to formation of an asymmetric dimer of the kinase regions, activation of the 'acceptor' kinase (green) by a 'donor' kinase (blue) and trans-phosphorylation of the C-terminal tail region (right). The cell membrane is indicated by the blue bilayer. (Figure and legend from Leahy (2007)).

By determination of the combined structure of extracellular and cytoplasmic domains of EGFR using negative-stain EM, the formation of the asymmetric dimers upon ligand binding was confirmed (Mi et. al., 2011). Inhibitors that bind to the active site can stabilize inactive and active conformations of the kinase domain. PD168393 has been shown to stabilize the active conformation (Blair et al., 2007). However, the question remains: does the drug bind to the already active conformation and then stabilize it or is it capable of binding to all conformations of the EGFR and drive them to an active conformation?

Prior to ligand binding the EGFR kinase domain is in an auto-inhibited state. However, Zhang et al. showed that the purified wild-type kinase domain could increase catalytic activity in a concentration-dependent manner on vesicle surfaces (Zhang et al., 2006). The increased activity stems from intermolecular interactions other than auto-phoshorylation activation (Zhang et al., 2006).

To assess the effect of EGFR conformation on probe binding we measured the interaction between PD168393-LRh and EGFR-EYFP in EGF-stimulated cells that would contain a high fraction of EGFR in the active conformation as compared to unstimulated cells.

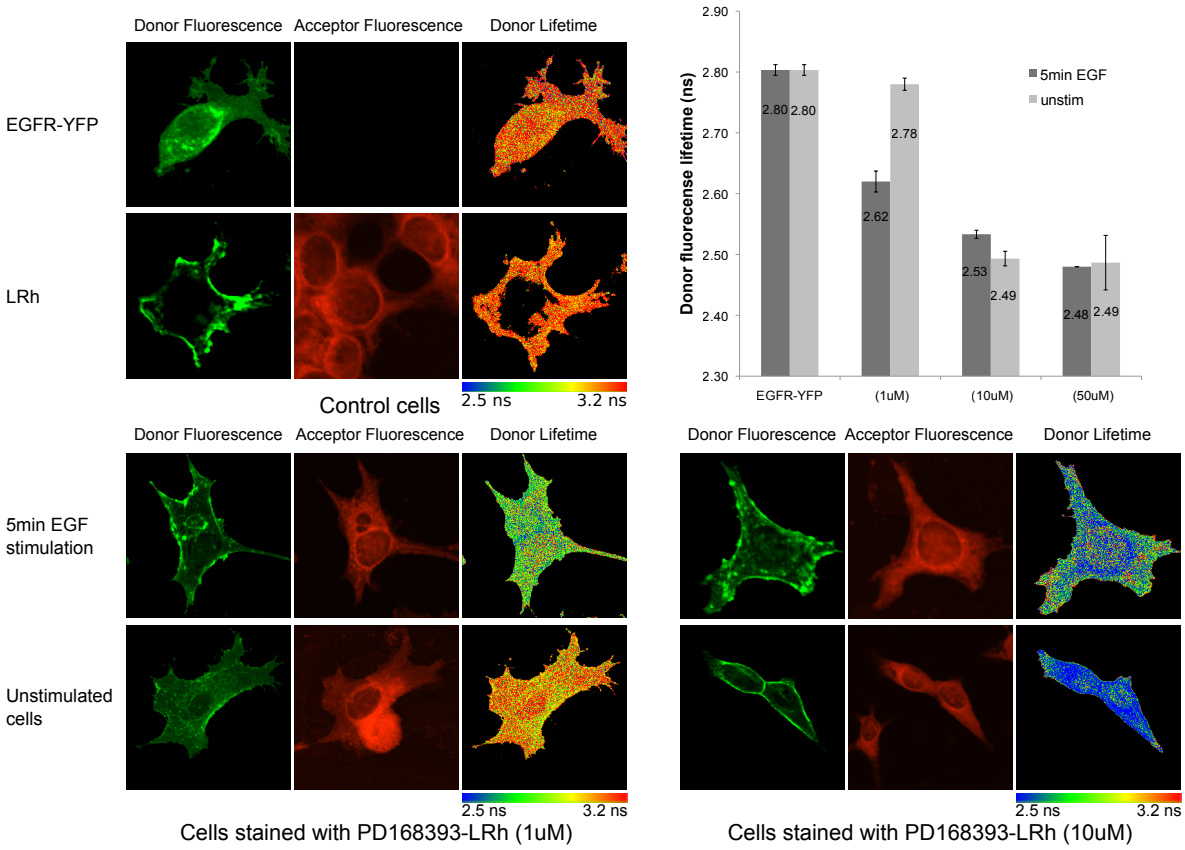

Figure 3.16 Binding of PD168393-LRh to EGFR-EYFP measured by FRET-FLIM in cells unstimulated and stimulated with EGF.

MCF-7 cells expressing EGFR-EYFP were starved (4 h, DMEM without FCS), stimulated with EGF for (100 ng/ml, 5 min, where indicated) followed by methanol fixation. In the uppermost frame cells were unstained; the second set of frames show cells stained with LRh. Cells in the lower framesets were stained with indicated concentrations of PD168393-LRh. Staining was carried out by incubating the fixed cells with 1 μM or 10 μM or 50 μM of PD168393-LRh for 1 h at RT. The graph (right) shows the average donor fluorescence lifetime for each of the conditions described. EGFR-EYFP indicates no acceptor present; 1 μM, 10 μM and, 50 μM indicate the concentration of PD168393-LRh.

At 1 μM PD168393-LRh differential binding in stimulated and unstimulated cells is observed (Figure 3.16), but at higher concentrations there is no distinction. The lack of differential binding at higher concentrations could imply the introduction of non-specific binding due to high acceptor concentrations of this probe or that the probe has differential affinities for the different conformational populations. At 1 μM the probe PD168393-LRh retains a preference for binding to the activated form of the receptor, but at higher concentrations it is capable of binding to all conformations.

The activation of EGFR has severe consequences for cellular signaling. Inappropriate EGFR activation is synonymous with multiple cancers. One such example is the L858R mutant of EGFR with is constitutively in the asymmetric dimer conformation (Zhang et al., 2006). The use of conformational probes could prove a rapid way of determining the activation state of disease-related mutants for which dimeric crystal structures are not available.

3.4. Probe profiling

To determine the selectivity of the labeled inhibitors EGFR, EGFR-T790M, PDGFRb, Src and Csk were included in the study. Fixed cells expressing these kinases were stained with LRh labeled versions of PD168393, BIBW2992, lapatinib and sorafenib.

The lifetime of the donor fluorescence was determined in the presence and absence of acceptor labeled probe, using frequency-domain FLIM. Frequency-domain FLIM is a faster mode of acquiring FLIM images than time-domain FLIM and was preferred because of the larger number of measurements undertaken. MCF-7 cells were, starved, stimulated as indicated in the figure legends and fixed. Prior to imaging cells were stained with the indicated probe. Acquired FLIM images were analyzed using the approach described in Section 2.11. From the phase and modulation lifetime images for each field of view, a histogram was plotted using 50 ps bins, 50 ps is the upper limit of the empirically determined instrumental error for the setup used. The averaged histogram of donor fluorescence lifetimes for each combination of donor and acceptor fluorophores was plotted together with the averaged histogram of the corresponding donor fluorescence lifetimes without acceptor fluorophore. LRh modified with the linker was used as the negative control and these measurements were pooled with the donor fluorescence lifetime distributions without acceptor fluorophore.

A two-sample Kolmogorov-Smirnov test was used to compare the distributions of values in the paired histograms (control and sample). The null hypothesis is that the control and sample are from the same continuous distribution. P-values less than 0.05 indicate that the null hypothesis is rejected. The P-values for each pair of histograms is summarized on Table 3.3 and 3.4.

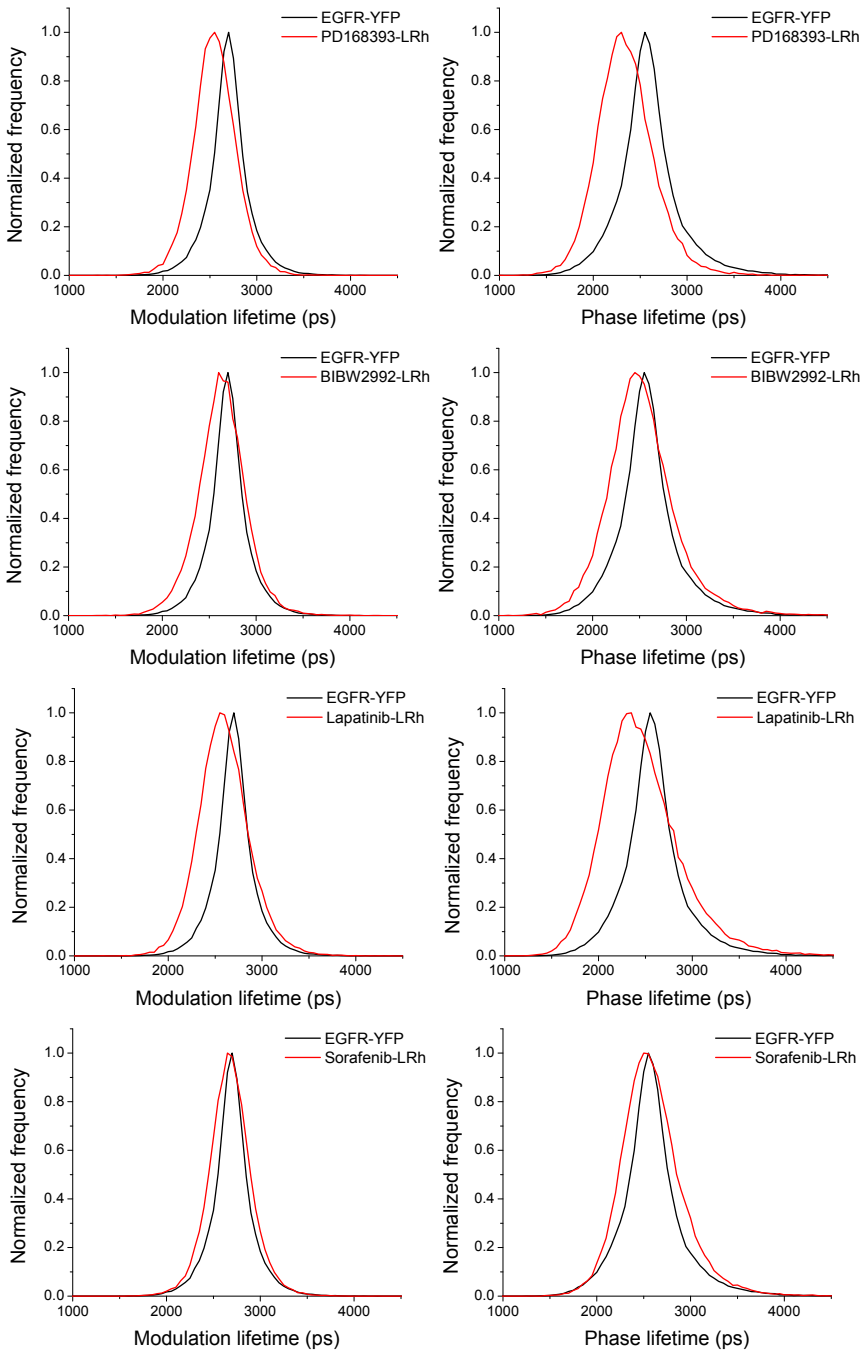

Figure 3.17 Modulation and phase lifetime distributions of probe binding to EGFR-EYFP.

MCF-7 cells expressing EGFR-EYFP were starved, stimulated with 100 ng/ml EGF for 5 min and fixed with methanol. The indicated probe was added to fixed cells at a concentration of 1 µM in PBS and incubated for 1 h at RT. Cells were washed with PBS (3×) and imaged in PBS. Plotted is the normalized frequency of fluorescence lifetimes in 50 ps bins. Repeated measurements of each condition were averaged and plotted alongside the averaged distribution of the control containing only donor fluorophores.

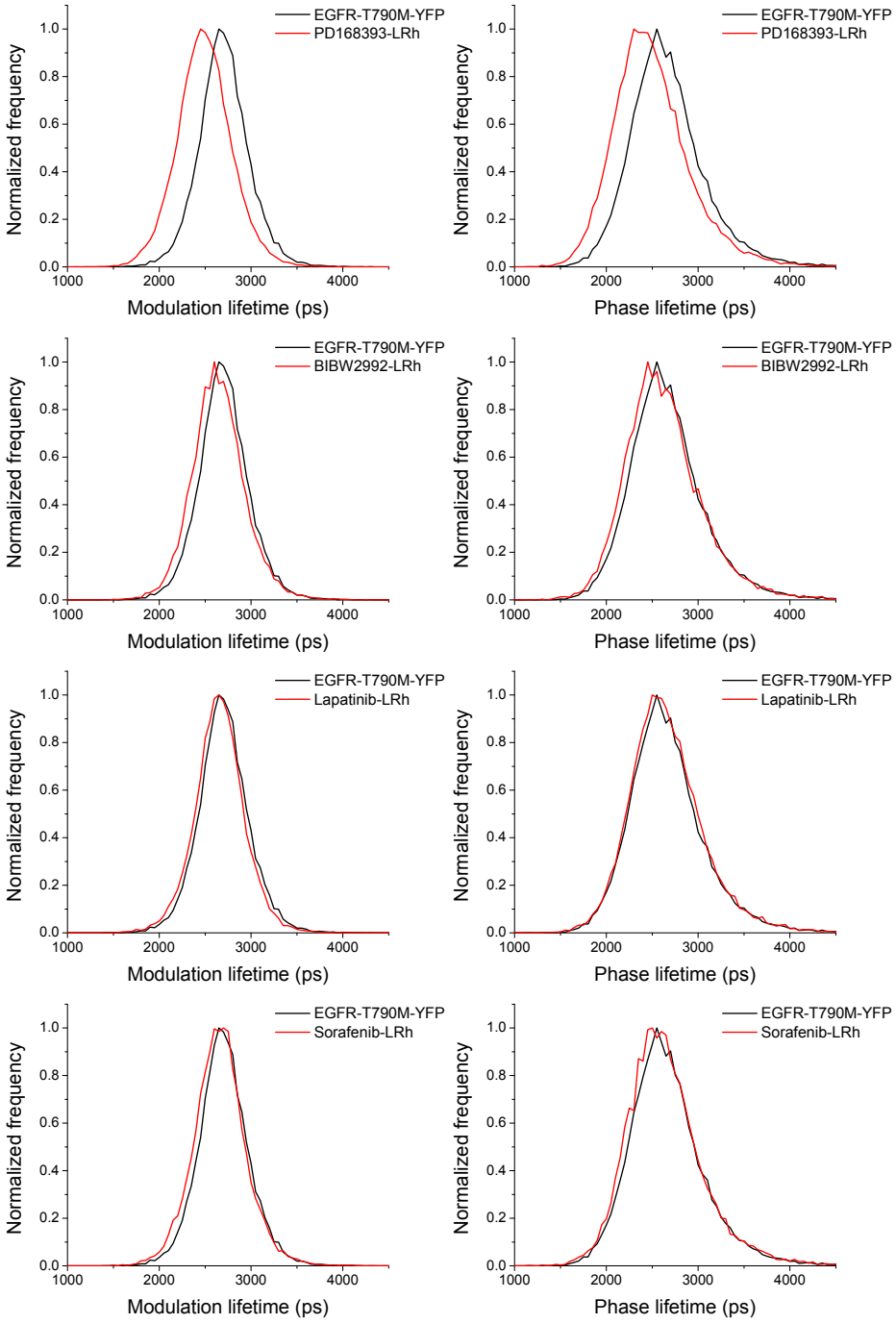

Figure 3.18 Modulation and phase lifetime distributions of probe binding to EGFR-T790M-EYFP.

MCF-7 cells expressing EGFR-T790M-EYFP were starved, stimulated with 100 ng/ml EGF for 5 min and fixed with methanol. The indicated probe was added to fixed cells at a concentration of 1 µM in PBS and incubated for 1 h at RT. Cells were washed with PBS (3×) and imaged in PBS. Plotted is the normalized frequency of fluorescence lifetimes in 50 ps bins. Repeated measurements of each condition were averaged and plotted alongside the averaged distribution of the control containing only donor fluorophores.

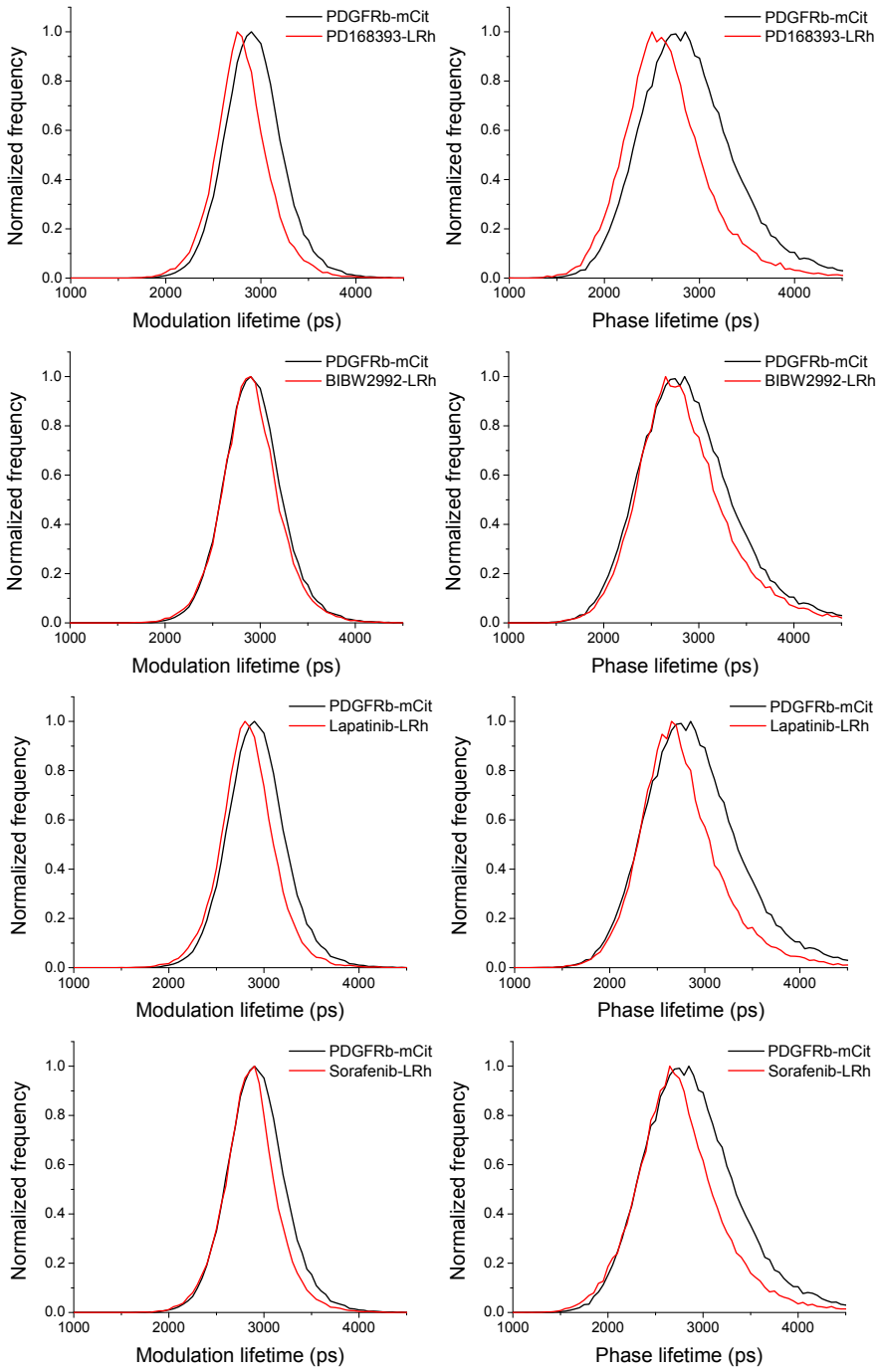

Figure 3.19 Modulation and phase lifetime distributions of probe binding to PDGFRb-mCit

MCF-7 cells expressing PDGFRb-mCit were starved, stimulated with 100 ng/ml PDGF-B for 10 min and fixed with methanol. The indicated probe was added to fixed cells at a concentration of 1 µM in PBS and incubated for 1 h at RT. Cells were washed with PBS (3×) and imaged in PBS. Plotted is the normalized frequency of fluorescence lifetimes in 50 ps bins. Repeated measurements of each condition were averaged and plotted alongside the averaged distribution of the control containing only donor fluorophores.

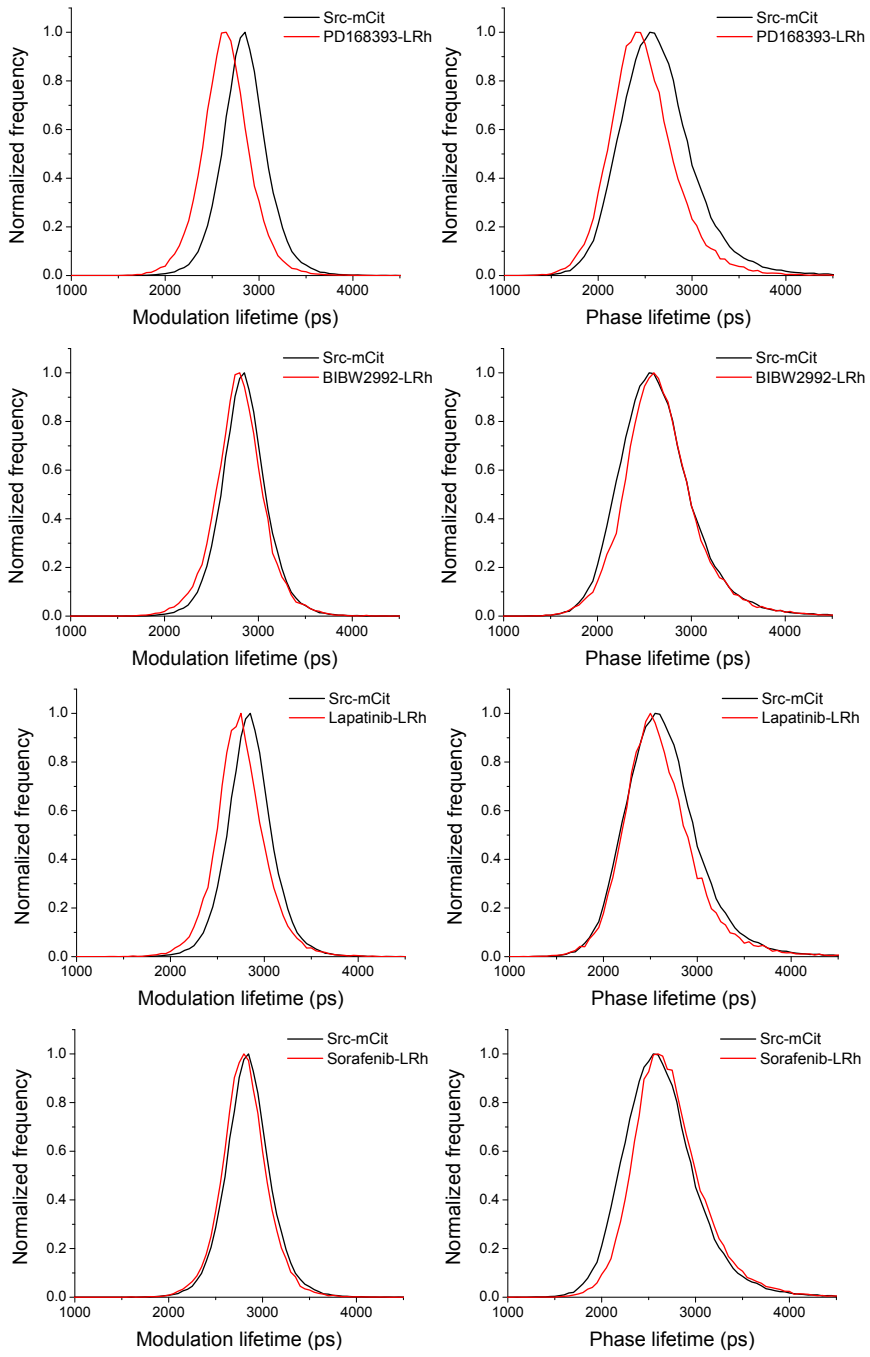

Figure 3.20 Modulation and phase lifetime distributions of probe binding to Src-mCit

MCF-7 cells expressing Src-mCit were starved, stimulated with 10 nM PMA for 20 min and fixed with methanol. The indicated probe was added to fixed cells at a concentration of 1 μM in PBS and incubated for 1 h at RT. Cells were washed with PBS (3×) and imaged in PBS. Plotted is the normalized frequency of fluorescence lifetimes in 50 ps bins. Repeated measurements of each condition were averaged and plotted alongside the averaged distribution of the control containing only donor fluorophores.

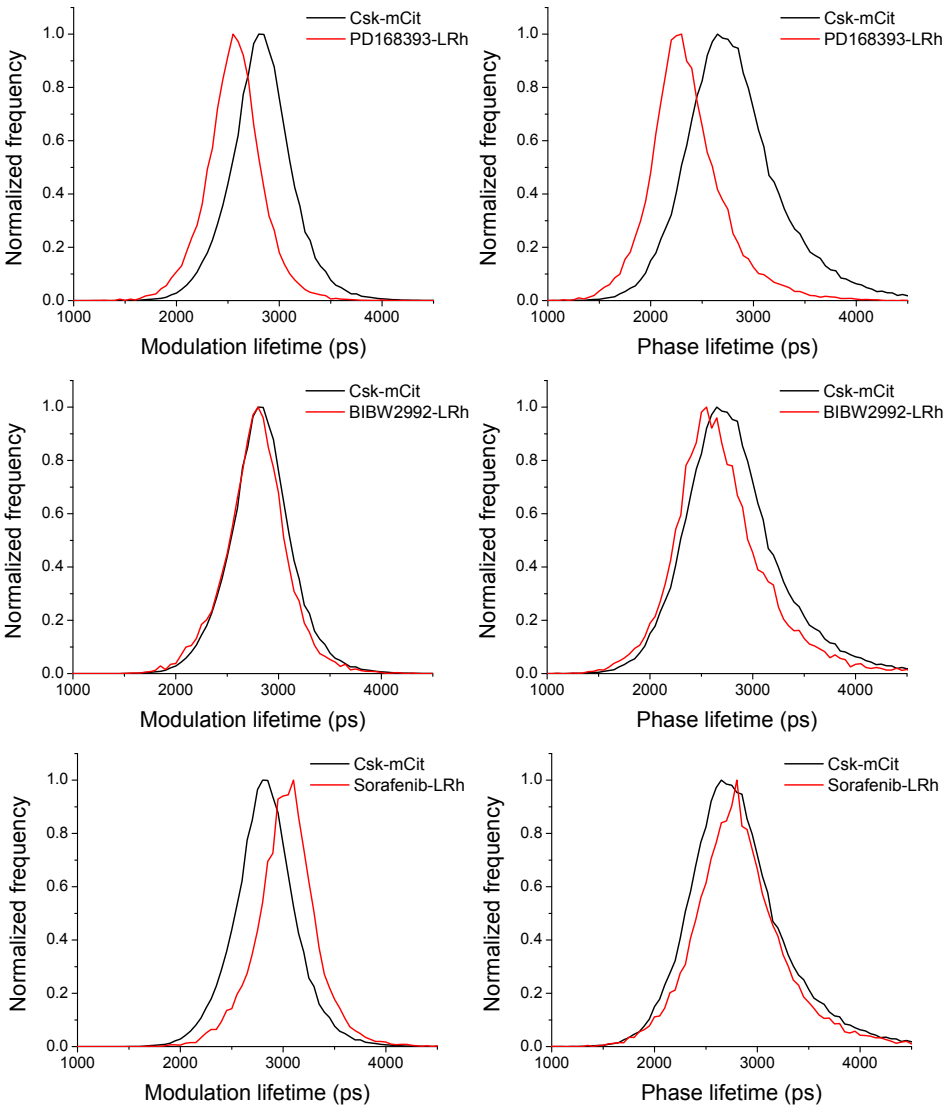

Figure 3.21 Modulation and phase lifetime distributions of probe binding to Csk-mCit

MCF-7 cells expressing Csk-mCit were starved, stimulated with 10 nM PMA for 20 min and fixed with methanol. The indicated probe was added to fixed cells at a concentration of 1 µM in PBS and incubated for 1 h at RT. Cells were washed with PBS (3×) and imaged in PBS. Plotted is the normalized frequency of fluorescence lifetimes in 50 ps bins. Repeated measurements of each condition were averaged and plotted alongside the averaged distribution of the control containing only donor fluorophores.

Table 3.3: P-values for shift in modulation lifetime distributions as determined by the Two-sample Kolmogov-Smirnov test

	'Donor' median (10000)	PD168393	BIBW2992	Lapatinib	Sorafenib
EGFR	0.9479	4.56E-04	0.4628	0.0302	0.9777
PDGFRb	0.7364	6.48E-02	1	0.3616	0.8582
Src	0.9951	2.65E-06	0.813	0.0323	0.8839
Csk	1	3.83E-13	0.0488		0.0125
EGFR-T790M	1	3.17E-05	0.7496	0.9983	0.9967

For p-values less than 0.05 (red), there is a 95% probability that the sample and the control distributions are significantly different.

Table 3.4: P-values for shift in phase lifetime distributions as determined by the Two-sample Kolmogov-Smirnov test

	'Donor' median (10000)	PD168393	BIBW2992	Lapatinib	Sorafenib
EGFR	0.5757	1.55E-04	0.9535	0.1193	0.962
PDGFRb	0.2846	2.23E-02	1	0.4253	0.5487
Src	0.6123	1.51E-02	1	0.8526	0.7751
Csk	0.9884	2.77E-13	0.1027		1
EGFR-T790M	0.8715	5.05E-02	1	1	1

For p-values less than 0.05 (red), there is a 95% probability that the sample and the control distributions are significantly different.

In order to calculate the p-value for the 'donor' sample (Figures 3.17–3.21, black line), two random subsamples were drawn from the datasets containing donor fluorescence lifetime distributions without the acceptor present. This process was repeated 10000 times and the median was calculated (Tables 3.3 and 3.4). The median P-value for each experimental condition indicates that the individual samples used to create the averaged histogram of donor fluorescence lifetime distributions in absence of acceptor are not significantly different. The variation of the 'donor' median p-value from a value of one provides an indication of the variance in the experimental setup (Tables 3.3 and 3.4).

The greatest shift towards lower fluorescence lifetimes across the board of profiled kinases came from the interaction with PD168393-LRh (Figures 3.17–3.21, row 1). The drug PD168393 is a known covalent inhibitor of EGFR hence probe interactions with EGFR and the EGFR-T790M mutant were expected. The T790M mutant of EGFR confers resistance to EGFR inhibitors such as gefitinib but not PD168393 (Sos et al., 2008). It is not clear from literature whether Csk is a target of PD168393 however binding is observed. PD168393 has an IC_{50} > 27 μM against Src (Blair et al., 2007) and IC_{50} > 50 μM PDGFRb (Fry et al., 1998) indicating a lower binding preference for these kinases, however, PD168393-LRh probe binding is observed therefore, means of validating these interactions should be explored. As Src lacks the relevant Cys in the active site the interaction is reversible (Blair et al., 2007). By introducing a S345C mutation in the active pocket of Src covalent binding of an inhibitor would be possible, which would then serve to hinder probe binding to the ATP binding pocket. Alternatively competitive binding using varying drug and probe concentrations could provide information on the site of PD168393-LRh binding to Src, PDGFRb and Csk.

Lapatinib-LRh shows a shift towards lower fluorescence lifetimes when incubated with EGFR-EYFP (Figure 3.17, row 3). Lapatinib targets the inactive conformation of EGFR and despite activation, by stimulation of cells with EGF, binding of Lapatinib-LRh to EGFR-EYFP was detected (Figure 3.17, row 3). Binding of both Lapatinib-LRh (targets inactive conformation) and PD168393-LRh (targets active conformation) in EGF stimulated cells indicates a mixed population of receptor conformations (Figure 3.17, row1 and row 3). Crystal structures of the T790M mutant indicate that despite this mutation some reversible and irreversible inhibitors can still be accommodated in the ATP binding pocket of the kinase (Yun et al., 2008). Additionally Yun et al. predict that this mutation enhances the stability of the active conformation relative to the inactive conformation (Yun et al., 2008). By stimulating the cells expressing the EGFR-T790M mutant with EGF it was assumed that there was higher population of receptors in that active conformation as compared to stimulated cells expressing the EGFR. When stained with PD168393-LRh (targets active conformation) a shift to lower fluorescence lifetimes was observed indicating a bound fraction to the EGFR-T790M (Figure 3.18, row 1). However, when stained with Lapatinib-LRh (Figure 3.18, row 1) no binding was detected indicating that the

EGFR-T790M does indeed have a preference for the active conformation. In Figure 3.16 we show that PD168393-LRh may be used to probe the active conformation of EGFR. Lapatinib-LRh may prove to be a complementary probe for the inactive conformation of EGFR. In the case of PDGFRb and Src (Figure 3.19 and 3.20 row 3) it is difficult to conclude if there is any binding to Lapatinib-LRh; the drug binds weakly to both kinases (K_d > 10 μM, (Karaman et al., 2008)).

BIBW2992-LRh showed no significant binding to EGFR-EYFP despite the drug BIBW2992 being a potent irreversible inhibitor of EGFR and the EGFR T790M mutant (IC_{50}: WT: 0.5 nM, L858R/T790M: 10 nM). No clear binding of this probe was observed to PDGFRb, Src or Csk. (Figures 3.17–3.21, row 2).

Sorafenib is a small molecule inhibitor of PDGFR. Profiling of this drug carried out by Karaman et al., (2008) shows a K_d of 37 nM for PDGFRb and K_d > 10 μM for EGFR, Src and Csk. (Karaman et al., 2008) The binding of Sorafenib-LRh to PDGFRb is difficult to conclude from the current data. As a probe Sorafenib-LRh showed a high degree of precipitation in PBS. The PDGFRb-mCit fluorescence lifetime distributions in the absence of probe have a comparatively wider distribution as compared to the donor fluorophore lifetime distributions of for example EGFR-EYFP (Figure 3.17, Figure 3.19, black lines). This broadening of lifetime distribution can be attributed to variance in the system (instrumental or experimental). No binding was observed to EGFR, EGFR-T790M, Src, or Csk. We are unable to distinguish if this lack of binding is due to the selectivity of the reactive group or the insolubility of the probe (Figures 3.17–3.21, row 4). The design of the Sorafenib-LRh probe needs to be re-evaluated to create water-soluble probe.

Chapter 4

General discussion, conclusions and outlook

4.1. Active site occupancy probes

The concept of activity-based probes (ABP) has been around since the early 1990s. An ABP unit generally consists of a reactive group and a detection tag. By using inhibitors to create ABPs we have a well-characterized, potent reactive group. APBs with inhibitors as the reactive group have been developed for several cancer-related proteins including proteases (Fonović and Bogyo, 2008), lipid kinases (Yee et al., 2005) and protein kinases (Blair et al., 2007). Presented in this thesis is a technique that uses a fluorescently tagged reactive group to visualize drug-target interactions in cells.

Inhibitor-based fluorescence probes capable of detecting active site occupancy have been developed. These probes provide tools for obtaining quantitative information on the degree of drug binding in live cells. By treating live cells expressing the kinase of interest labeled with an FP with drugs at different doses, different incubation times and then staining with the labeled active site occupancy probe, the fraction of inhibited kinase per cell can be obtained. The fraction of inhibited kinase in the cell can also be correlated with a biological read-out of activity in the same cell.

An essential aspect of reverse engineering of signaling networks is quantification of the reaction states of each of the nodes in the network in response to a perturbation. Perturbations provide the causal interference necessary for deducing directionality between components. Small molecule inhibitors rapidly alter protein activity thereby producing acute perturbations (Zamir and Bastiaens, 2008). The combined approach of detecting kinase-drug binding and activity in single cells with spatial information proposed in this thesis provides a powerful approach to gain insight into causal relationships between the targeted kinase and its downstream substrates.

4.2. Kinase conformation probe

Tyrosine phosphorylation of a kinase or a downstream substrate provides a readout of tyrosine kinase activity. However, the activation state of the tyrosine kinase is strongly dictated by its conformation, as described in Section 3.3. Kinase inhibitors are known to target various conformational states of the kinases. PD168393, for example, targets the active conformation of EGFR whereas lapatinib targets the inactive conformation. When used as the reactive group of an inhibitor probe these conformation-specific properties appear to remain intact. In Figure 3.16 it was shown that the PD168393-LRh probe showed preferential binding to EGFR in cells that had been stimulated by EGF as opposed to unstimulated cells. Additionally in Figure 3.17 Lapatinib-LRh showed binding to EGFR in cells that were stimulated. This indicates that upon EGF stimulation in cells expressing WT-EGFR there is a heterogeneous population of active and inactive forms of the receptor. The EGFR-T790M mutant is in the constitutively active conformation, PD168393-LRh showed binding (Figure 3.18) whereas Lapatinib-LRh showed no binding to this mutant (Figure 3.18), providing evidence for conformational selectivity of the probes. The detection of mixed populations of receptors in cells expressing WT-EGFR upon EGF stimulation raises an interesting question about activity versus activation. The concentration of EGF used in stimulation experiments was at saturation in terms of the phosphorylation response. Does this imply that only a subpopulation of receptors needs to be active to bring about complete phosphorylation? One experiment to address this question would be to measure the relative populations of active and inactive receptor over a range of EGF concentrations while simultaneously observing phosphorylation of the receptor in the same cell.

Further characterization of the conformational aspects of EGFR can be explored by monitoring the shift in active/inactive state populations in response to disease-relevant mutations, different stimulation ligands, and different drugs (in particular allosteric inhibitors). This approach could also prove to be a valuable assay for screening allosteric inhibitors, as the protein target will be intact and in its native environment.

4.3. Target validation probe

The ATP binding pocket of protein kinases is highly conserved, which leads to the promiscuous behaviour of inhibitors targeting this pocket. The current study was originally conceived in the hopes of designing a method to address this issue in the cellular context. This aim can be achieved using the strategies outlined in Section 4.1. Before proceeding with using the probes to characterize drug binding to multiple kinases it was necessary to grasp the response of the probes themselves with different kinases. This was done by profiling a small number of tyrosines kinase, against a small number of probes (Section 3.4). In comparison to *in vitro* systems that use homogenous populations of purified proteins, the cell-based assay is subject to variance due to cell-cell variance and heterogeneity in protein populations within the cell. A variety of control experiment can be incorporated to verify observed trends. Mutational disruption in the ATP binding site of the kinase should abrogate probe binding as shown in Section 3.3.1, Figure 3.9. Because of the conserved nature of the ATP binding pocket similar mutations can be applied to different kinases as discussed in Section 3.4.

In Section 3.2 it was noted that the inhibitor probes show a strong affinity for membranes. This results in heterogeneous distribution of the acceptor fluorophores, which could lead to non-specific FRET signals. One approach to characterizing possible non-specific effects due to concentration variations and aggregation of probes would be to compare the fluorescence lifetime versus acceptor intensity in each pixel for a defined non-specific interaction with that of the sample. In the case of the non-specific interaction the decrease in fluorescence lifetime would be linearly proportional to increasing acceptor intensities. For a sample with specific interactions the decrease in fluorescence lifetime in the lower acceptor intensity region should be steeper than that of the non-specific sample and comparable at higher intensities when non-specific effects would start to appear. In this way it should be possible to find a threshold of acceptor intensities at which non-specific effects appear. One example of a defined non-specific effect would be the interaction of the probes with a GPI-anchored EYFP. The fluorophore would be positioned very close to the outer plasma membrane of the cell. The interaction would be non-specific because GPI-EYFP contains no ATP binding site or other pockets and because it is positioned on the

outside of the cell, it cannot interact with acceptor fluorophores of probes bound to trans-membrane kinases.

To examine the binding of multiple probes to the tyrosine kinase family of enzymes the current assay needs to be adapted to a high throughput automated FLIM format. An automated FLIM microscope has been developed in house and in combination with cell arrays was used to analyze tyrosine phosphorylation networks (Grecco et al., 2010). In the case of the cell array approach all the donors saw the same acceptor, a labeled generic anti-phosphotyrosine antibody. The current application will have several different inhibitors probes so it is more feasible to use a 96 well format in combination with automated FLIM imaging.

4.4. A comparison of live cell and fixed cell approaches

For the most part work covered in this thesis focuses on characterizing fixed cell systems. We investigated the effects of the fixation process on the PD168393-LRh and EGFR-EYFP binding by comparing the fluorescence lifetime change in fixed cells and native membrane sheets (Section 3.3.1). The change in fluorescence lifetime was comparable indicating that fixed receptor and native receptor showed the same degree of binding to the probe. Fixed cells were then used to investigate probe binding to membrane-bound (EGFR and PDGFRb), membrane-anchored (Src) and cytoplasmic (Csk) tyrosine kinases (Section 3.4).

The fixed cell system is preferred for a number of the previously described applications of this method. In Section 4.1 we describe a binding site blocking assay where live cells are treated with a drug and the fraction of drug binding to kinase is detected by the loss of binding of the probe. By fixing cells the drug-target reaction can be stopped at a defined time point making the drug treatment in the all the cells comparable at the point of measurement. Fixation does not appear to disrupt the binding of irreversible inhibitors; these effects need to be investigated for the binding of reversible inhibitors. The application outlined in Section 4.2, probing kinase conformational changes in response to stimuli, be it the natural activating ligand or chemical modulator, can be acutely monitored by fixing the cells. By stopping the stimulation reaction at defined time points detection is improved

because the relative population of each conformation in all cells in the sample would be identical. Additionally ‘snap shots’ of changes i.e. active versus inactive conformations in response to stimuli can be taken over time by fixing samples at different time points through the stimulation process.

Fixed cells are also preferred for automated FLIM screening approaches described in Section 4.3. The automated setup enables the measurement of a large number of samples and, depending on how many samples are in an experiment, the measurement time from the first to the last sample can be in the range of several hours. Live cells can be sustained during these time spans with the incorporation of an environmental control chamber in the microscope setup. However, live cells would undergo many processes during the measurement timeline making it difficult to directly compare conditions in the first sample with those in the last sample.

To detect probe binding, much higher concentrations of the probe were required as compared to the concentration of complimentary drug required to elicit a physiological response. One reason for this discrepancy was the high affinity of the probe for endo-membranes. Sequestration of the probe to endo-membranes could reduce the local concentration of probe available for binding to kinases. Cells fixed prior to probe addition are more tolerant to the non-physiological concentrations of probe used. Biological responses elicited by the probe itself are also eliminated.

The fixed cell approach is preferred for characterizing each new probe or kinase interaction. The live cell environment is continually in motion and changing. Trying to capture an event such as a drug-probe interaction in this continuum without comprehensive knowledge of its mechanisms could prove quite challenging. Once an assay is established in fixed cells moving it to the live cell approach would be beneficial. Visualizing enzyme regulation within a cell in real time provides information on how the protein functions amongst a complex composition of molecules and reactions. Live cell approaches provide the real time dynamics of drug binding and kinase conformational changes as opposed to the ‘snapshots’ obtained in fixed cells.

4.5. Quantification of molecular interactions in cells

The variance reflected on an average fluorescence lifetime value comprises of experimental noise and biological variance. Contained in the biological variance is information pertaining to the molecular mechanisms of probe binding.

To disentangle the experimental noise from biological variance we used histograms to show changes in the distribution of fluorescence lifetimes in samples with and without acceptor (3.16–3.20). By assessing the shape and broadness of the samples containing only the donor fluorophore (Figures 3.17–3.21, black line) the experimental noise can be inferred.

For the interaction between EGFR-YFP and PD168393-LRh (Figure 3.17, row 1) the distribution of fluorescence lifetimes in the presence of the probe (red line) shows a shift in the maximum frequency of fluorescence lifetimes to a lower value, this shift in the maxima represents the change in average fluorescence lifetime. However, in addition to the shift in maxima there is a broadening in the distribution of fluorescence lifetimes in the presence of the probe. This broadening of the distribution of fluorescence lifetimes in the FRET sample, as compared to the control represents the biological variance. The shape of the broadened distribution provides additional information on the biological variance. A skewed or asymmetric broadening towards lower fluorescence lifetimes gives a clearer indication of the presence of different populations of binding and non-binding species. When the distribution of fluorescence lifetimes of the FRET sample is symmetrically shaped, broadening is more likely due to experimental noise and it is less likely that such a distribution is significantly different to that of the donor alone sample (Figure 3.17, row 4).

It is not possible to disentangle the experimental noise from the biological variance from the mean fluorescence lifetime value and its standard deviation.

4.6. Conclusion

The aim of this study was to develop a method for visualizing tyrosine kinase-inhibitor interactions in cells. This aim has been achieved by the development of FRET-acceptor-based fluorescence inhibitor probes, and using FLIM to measure their interactions with

FRET-donor-labeled kinases. In addition this method can be used to probe occupancy of the kinase active site, providing a competitive approach to determining the binding of drugs to the active site of the kinase. The conformational selectivity of the probes provides a method to study kinase conformational dynamics in single cells.

The major areas of this method that need to be further developed are: (i) the adaptation of this approach to an automated FLIM system to allow profiling of a large number of kinases and drugs/inhibitor-probes; (ii) the effect of variance in fluorescence lifetime distributions, of FRET samples, due to biological effects should be better characterized; (iii) the spatial aspect of probe-binding has not been covered in the current work but it should be taken into consideration in future applications of this method.

The technology presented in this thesis has the potential to be integrated into drug screening and development programs to facilitate target validation prior to introduction in animal models.

References

Adrian, F.J., Ding, Q., Sim, T., Velentza, A., Sloan, C., Liu, Y., Zhang, G., Hur, W., Ding, S., Manley, P., et al. (2006). Allosteric inhibitors of Bcr-abl-dependent cell proliferation. Nat. Chem. Biol. *2*, 95–102.

Albertson, D.G. (2006). Gene amplification in cancer. Trends Genet. *22*, 447–455.

Amanchy, R., Periaswamy, B., Mathivanan, S., Reddy, R., Tattikota, S.G., and Pandey, A. (2007). A curated compendium of phosphorylation motifs. Nat. Biotech. *25*, 285–286.

Amit, I., Wides, R., and Yarden, Y. (2007). Evolvable signaling networks of receptor tyrosine kinases: relevance of robustness to malignancy and to cancer therapy. Mol. Syst. Biol. *3*,.

Ashworth, A., Lord, C.J., and Reis-Filho, J.S. (2011). Genetic Interactions in Cancer Progression and Treatment. Cell *145*, 30–38.

Åqvist, J., Kolmodin, K., Florian, J., and Warshel, A. (1999). Mechanistic alternatives in phosphate monoester hydrolysis: What conclusions can be drawn from available experimental data? Chem. Biol. *6*, R71–R80.

Babiychuk, E.B., Monastyrskaya, K., Potez, S., and Draeger, A. (2009). Intracellular Ca2+ operates a switch between repair and lysis of streptolysin O-perforated cells. Cell Death Differ. *16*, 1126–1134.

Baruch, A., Jeffery, D.A., and Bogyo, M. (2004). Enzyme activity – it's all about image. Trends Cell Biol. *14*, 29–35.

Bastiaens, P.I., Majoul, I.V., Verveer, P.J., Söling, H.D., and Jovin, T.M. (1996). Imaging the intracellular trafficking and state of the AB5 quaternary structure of cholera toxin. EMBO J. *15*, 4246–4253.

Bastiaens, P.I.H., and Pepperkok, R. (2000). Observing proteins in their natural habitat: the living cell. TIBS *25*, 631–637.

Bastiaens, P.I.H., and Squire, A. (1999). Fluorescence lifetime imaging microscopy: spatial resolution of biochemical processes in the cell. Trends Cell Biol. *9*, 48–52.

Bean, J., Riely, G.J., Balak, M., Marks, J.L., Ladanyi, M., Miller, V.A., and Pao, W. (2008). Acquired Resistance to Epidermal Growth Factor Receptor Kinase Inhibitors Associated with a Novel T854A Mutation in a Patient with EGFR-Mutant Lung Adenocarcinoma. Clin. Cancer Res. *14*, 7519–7525.

Blair, J.A., Rauh, D., Kung, C., Yun, C.H., Fan, Q.W., Rode, H., Zhang, C., Eck, M.J., Weiss, W.A., and Shokat, K.M. (2007). Structure-guided development of affinity probes for tyrosine kinases using chemical genetics. Nat. Chem. Biol. *3*, 229–238.

Citri, A., and Yarden, Y. (2006). EGF–ERBB signalling: towards the systems level. Nat. Rev. Mol. Cell Biol. *7*, 505–516.

Clegg, R.M. (1995). Fluorescence resonance energy transfer. Curr. Opin. Biotechnol. *6*, 103–110.

Cohen, M.S., Zhang, C., Shokat, K.M., and Taunton, J. (2005). Structural Bioinformatics-Based Design of Selective, Irreversible Kinase Inhibitors. Science *308*, 1318–1321.

Cole, P.A., Burn, P., Takacs, B., and Walsh, C.T. (1994). Evaluation of the catalytic mechanism of recombinant human Csk (C-terminal Src kinase) using nucleotide analogs and viscosity effects. J. Biol. Chem. *269*, 30880–30887.

Cordes, T., Vogelsang, J., and Tinnefeld, P. (2009). On the Mechanism of Trolox as Antiblinking and Antibleaching Reagent. J. Am. Chem. Soc. *131*, 5018–5019.

Dawson, J.P., Berger, M.B., Lin, C.C., Schlessinger, J., Lemmon, M.A., and Ferguson, K.M. (2005). Epidermal Growth Factor Receptor Dimerization and Activation Require Ligand-Induced Conformational Changes in the Dimer Interface. Mol. Cell Biol. *25*, 7734–7742.

Desbois-Mouthon, C., Baron, A., Blivet-Van Eggelpoël, M.J., Fartoux, L., Venot, C., Bladt, F., Housset, C., and Rosmorduc, O. (2009). Insulin-Like Growth Factor-1 Receptor Inhibition Induces a Resistance Mechanism via the Epidermal Growth Factor Receptor/HER3/AKT Signaling Pathway: Rational Basis for Cotargeting Insulin-Like Growth Factor-1 Receptor and Epidermal Growth Factor Receptor in Hepatocellular Carcinoma. Clin. Cancer Res. *15*, 5445–5456.

deFazio, A., Chiew, Y.E., Sini, R.L., Janes, P.W., and Sutherland, R.L. (2000). Expression of c-erbB receptors, heregulin and oestrogen receptor in human breast cell lines. Int. J. Cancer *87*, 487–498.

Fonović, M., and Bogyo, M. (2008). Activity-based probes as a tool for functional proteomic analysis of proteases. Expert Rev. Proteomics *5*, 721–730.

Fry, D.W., Bridges, A.J., Denny, W.A., Doherty, A., Greis, K.D., Hicks, J.L., Hook, K.E., Keller, P.R., Leopold, W.R., Loo, J.A., et al. (1998). Specific, irreversible inactivation of the epidermal growth factor receptor and erbB2, by a new class of tyrosine kinase inhibitor. Proc. Natl. Acad. Sci. USA *95*, 12022–12027.

Giles, R.V., Spiller, D.G., Grzybowski, J., Clark, R.E., Nicklin, P., and Tidd, D.M. (1998). Selecting optimal oligonucleotide composition for maximal antisense effect following streptolysin O-mediated delivery into human leukaemia cells. Nucleic Acids Res. *26*, 1567–1575.

Gillet, J.P., and Gottesman, M.M. (2010). Mechanisms of multidrug resistance in cancer. Methods Mol. Biol. *596*, 47–76.

Goedhart, J., van Weeren, L., Hink, M.A., Vischer, N.O.E., Jalink, K., and Gadella, T.W.J. (2010). Bright cyan fluorescent protein variants identified by fluorescence lifetime screening. Nat. Methods *7*, 137–139.

Grecco, H.E., Roda-Navarro, P., Girod, A., Hou, J., Frahm, T., Truxius, D.C., Pepperkok, R., Squire, A., and Bastiaens, P.I.H. (2010). In situ analysis of tyrosine phosphorylation networks by FLIM on cell arrays. Nat. Methods *7*, 467–472.

Grimsby, J., Sarabu, R., Corbett, W.L., Haynes, N.E., Bizzarro, F.T., Coffey, J.W., Guertin, K.R., Hilliard, D.W., Kester, R.F., Mahaney, P.E., et al. (2003). Allosteric Activators of Glucokinase: Potential Role in Diabetes Therapy. Science *301*, 370–373.

Hah, J.M., Sharma, V., Li, H., and Lawrence, D.S. (2006). Acquisition of a "Group A"-Selective Src Kinase Inhibitor via a Global Targeting Strategy. J. Am. Chem. Soc. *128*, 5996–5997.

Hanks, S.K., and Hunter, T. (1995). Protein kinases 6. The eukaryotic protein kinase superfamily: kinase (catalytic) domain structure and classification. Faseb J. *9*, 576–596.

Hines, A.C., and Cole, P.A. (2004). Design, synthesis, and characterization of an ATP-peptide conjugate inhibitor of protein kinase A. Bioorg. Med. Chem. Lett. *14*, 2951–2954.

Ho, M., Bramson, H.N., Hansen, D.E., Knowles, J.R., and Kaiser, E.T. (1988). Stereochemical course of the phospho group transfer catalyzed by cAMP-dependent protein kinase. J. Am. Chem. Soc. *110*, 2680–2681.

Huisgen, R. (1984). In 1,3-Dipolar Cycloaddition Chemistry, Padwa, A., Ed., (Wiley: New York), Chapter 1, pp 1–176

Idone, V., Tam, C., Goss, J.W., Toomre, D., Pypaert, M., and Andrews, N.W. (2008). Repair of injured plasma membrane by rapid Ca^{2+}-dependent endocytosis. J. Cell. Biol. *180*, 905–914.

Karaman, M.W., Herrgard, S., Treiber, D.K., Gallant, P., Atteridge, C.E., Campbell, B.T., Chan, K.W., Ciceri, P., Davis, M.I., Edeen, P.T., et al. (2008). A quantitative analysis of kinase inhibitor selectivity. Nat. Biotech. *26*, 127–132.

Keyel, P.A., Loultcheva, L., Roth, R., Salter, R.D., Watkins, S.C., Yokoyama, W.M., and Heuser, J.E. (2011). Streptolysin O clearance through sequestration into blebs that bud passively from the plasma membrane. J. of Cell. Sci. *124*, 2414–2423.

Kim, K., and Cole, P.A. (1998). Kinetic Analysis of a Protein Tyrosine Kinase Reaction Transition State in the Forward and Reverse Directions. J. Am. Chem. Soc. *120*, 6851–6858.

Knighton, D., Zheng, J., Ten Eyck, L., Xuong, N., Taylor, S., and Sowadski, J. (1991). Structure of a peptide inhibitor bound to the catalytic subunit of cyclic adenosine monophosphate-dependent protein kinase. Science *253*, 414–420.

Lakowicz, J.R. (2006). Principles of Fluorescence Spectroscopy (Springer: US).

Lavogina, D., Enkvist, E., and Uri, A. (2010). Bisubstrate Inhibitors of Protein Kinases: from Principle to Practical Applications. ChemMedChem *5*, 23–34.

Lawrie, A.M., Noble, M.E.M., Tunnah, P., Brown, N.R., Johnson, L.N., and Endicott, J.A. (1997). Protein kinase inhibition by staurosporine revealed in details of the molecular interaction with CDK2. Nat. Struct. Mol. Biol. *4*, 796–801.

Leahy, D.J. (2007). A monkey wrench in the kinase machine. Nat. Struct. Mol. Biol. *14*, 1120–1121.

Lee, J.H., Kumar, S., and Lawrence, D.S. (2008). Stepwise Combinatorial Evolution of Akt Bisubstrate Inhibitors. ChemBioChem *9*, 507–509.

Lee, J.H., Nandy, S.K., and Lawrence, D.S. (2004). A Highly Potent and Selective PKCα Inhibitor Generated via Combinatorial Modification of a Peptide Scaffold. J. Am. Chem. Soc. *126*, 3394–3395.

Lim, W.A., and Pawson, T. (2010). Phosphotyrosine Signaling: Evolving a New Cellular Communication System. Cell *142*, 661–667.

Liu, Y., and Gray, N.S. (2006). Rational design of inhibitors that bind to inactive kinase conformations. Nat. Chem. Biol. *2*, 358–364.

Manning, G., Young, S.L., Miller, W.T., and Zhai, Y. (2008). The protist, Monosiga brevicollis, has a tyrosine kinase signaling network more elaborate and diverse than found in any known metazoan. Proc. Natl. Acad. Sci. USA *105*, 9674–9679.

Massey, F.J. (1951). The Kolmogorov-Smirnov Test for Goodness of Fit. J. Am. Stat. Assoc. *46*, 68–78.

McNeil, P.L., and Steinhardt, R.A. (2003). Plasma membrane disruption: Repair, Prevention, Adaptation. Annu. Rev. Cell. Dev. Biol. *19*, 697–731.

Miller, W.T. (2003). Determinants of Substrate Recognition in Nonreceptor Tyrosine Kinases. Acc. Chem. Res. *36*, 393–400.

Noble, M.E.M., Endicott, J.A., and Johnson, L.N. (2004). Protein Kinase Inhibitors: Insights into Drug Design from Structure. Science *303*, 1800–1805.

Otsu, N. (1979). A threshold selection method from gray-level histograms. IEEE Trans. Sys. Man. Cyber. *9*, 62–66.

Palmer, M., Harris, R., Freytag, C., Kehoe, M., Tranum-Jensen, J., and Bhakdi, S. (1998a). Assembly mechanism of the oligomeric streptolysin O pore: the early membrane lesion is lined by a free edge of the lipid membrane and is extended gradually during oligomerization. EMBO J. *17*, 1598–1605.
Palmer, M., Vulicevic, I., Saweljew, P., Valeva, A., Kehoe, M., and Bhakdi, S. (1998b). Streptolysin O: A Proposed Model of Allosteric Interaction between a Pore-Forming Protein and Its Target Lipid Bilayer. Biochemistry *37*, 2378–2383.

Parang, K., Till, J.H., Ablooglu, A.J., Kohanski, R.A., Hubbard, S.R., and Cole, P.A. (2001). Mechanism-based design of a protein kinase inhibitor. Nat. Struct. Mol. Biol. *8*, 37–41.

Parang, K., and Cole, P.A. (2002). Designing bisubstrate analog inhibitors for protein kinases. Pharmacol. Therapeut. *93*, 145–157.

Pawson, T. (1995). Protein modules and signalling networks. Nature *373*, 573–580.

Perez, J.-B., Martinez, K.L., Segura, J.-M., and Vogel, H. (2006). Supported Cell-Membrane Sheets for Functional Fluorescence Imaging of Membrane Proteins. Adv. Funct. Mater. *16*, 306–312.

Pincus, D., Letunic, I., Bork, P., and Lim, W.A. (2008). Evolution of the phospho-tyrosine signaling machinery in premetazoan lineages. Proc. Natl. Acad. Sci. USA *105*, 9680–9684.

Quintás-Cardama, A., and Cortes, J. (2008). Therapeutic Options Against BCR-ABL1 T315I-Positive Chronic Myelogenous Leukemia. Clin. Cancer Res. *14*, 4392–4399.

Rasnik, I., McKinney, S.A., and Ha, T. (2006). Nonblinking and long-lasting single-molecule fluorescence imaging. Nat. Methods *3*, 891–893.

Robinson, D.R., Wu, Y.M., and Lin, S.F. (2000). The protein tyrosine kinase family of the human genome. Oncogene *19*, 5548–5557.

Rostovtsev, V. V.; Green, L. G.; Fokin, V. V.; Sharpless, K. B. (2002). A stepwise Huisgen cycloaddition process: copper(I)-catalyzed regioselective ligation of azides and terminal alkynes. Angew.Chem., Int. Ed., 41, 2596–2599.

Saiki, R., Gelfand, D., Stoffel, S., Scharf, S., Higuchi, R., Horn, G., Mullis, K., and Erlich, H. (1988). Primer-directed enzymatic amplification of DNA with a thermostable DNA polymerase. Science *239*, 487–491.

Sanger, F., Nicklen, S., and Coulson, A.R. (1977). DNA sequencing with chain-terminating inhibitors. Proc. Natl, Acad, Sci, USA *74*, 5463–5467.

Shaner, N.C., Steinbach, P.A., and Tsien, R.Y. (2005). A guide to choosing fluorescent proteins. Nat Methods *2*, 905–909.

Shatursky, O., Heuck, A.P., Shepard, L.A., Rossjohn, J., Parker, M.W., Johnson, A.E., and Tweten, R.K. (1999). The Mechanism of Membrane Insertion for a Cholesterol-Dependent Cytolysin: A Novel Paradigm for Pore-Forming Toxins. Cell *99*, 293–299.

Shen, K., and Cole, P.A. (2003). Conversion of a Tyrosine Kinase Protein Substrate to a High Affinity Ligand by ATP Linkage. J. Am. Chem. Soc. *125*, 16172–16173.

Shreder, K.R., Wong, M.S., Nomanbhoy, T., Leventhal, P.S., and Fuller, S.R. (2004). Synthesis of AX7593, a Quinazoline-Derived Photoaffinity Probe for EGFR. Org. Lett. *6*, 3715–3718.

Simpson, J.C., Cetin, C., Erfle, H., Joggerst, B., Liebel, U., Ellenberg, J., and Pepperkok, R. (2007). An RNAi screening platform to identify secretion machinery in mammalian cells. J. Biotechnol. *129*, 352–365.

Smaill, J.B., Rewcastle, G.W., Loo, J.A., Greis, K.D., Chan, O.H., Reyner, E.L., Lipka, E., Showalter, H.D.H., Vincent, P.W., Elliott, W.L., et al. (2000). Tyrosine Kinase Inhibitors. 17. Irreversible Inhibitors of the Epidermal Growth Factor Receptor: 4-(Phenylamino)quinazoline- and 4-(Phenylamino)pyrido[3,2-d]pyrimidine-6-acrylamides Bearing Additional Solubilizing Functions. J. Med. Chem. *43*, 1380–1397.

Sos, M.L., Rode, H.B., Heynck, S., Peifer, M., Fischer, F., Klüter, S., Pawar, V.G., Reuter, C., Heuckmann, J.M., Weiss, J., et al. (2010). Chemogenomic Profiling Provides Insights into the Limited Activity of Irreversible EGFR Inhibitors in Tumor Cells Expressing the T790M EGFR Resistance Mutation. Cancer Res. *70*, 868–874.

Sos, M.L., Zander, T., Thomas, R.K., Staratschek-Jox, A., Claasen, J., and Wolf, J. (2008). Expression of Signaling Mediators Downstream of EGF-Receptor Predict Sensitivity to Small Molecule Inhibitors Directed Against the EGF-Receptor Pathway. J. Thorac. Oncol. *3*, 170–173.

Taylor, S.S., and Radzio-Andzelm, E. (1994). Three protein kinase structures define a common motif. Structure *2*, 345–355.

Traxler, P., and Furet, P. (1999). Strategies toward the Design of Novel and Selective Protein Tyrosine Kinase Inhibitors. Pharmacology & Therapeutics *82*, 195–206.

Verveer, P.J. and Bastiaens, P.I.H. (2003). Evaluation of global analysis algorithms for single frequency fluorescence lifetime imaging microscopy data. J. Microsc. *209*, 1–7.

Walev, I., Bhakdi, S.C., Hofmann, F., Djonder, N., Valeva, A., Aktories, K., and Bhakdi, S. (2001). Delivery of proteins into living cells by reversible membrane permeabilization with streptolysin-O. Proc. Natl. Acad. Sci. USA *98*, 3185–3190.

Weinstein, I.B., and Joe, A. (2008). Oncogene Addiction. Cancer Res. *68*, 3077–3080.

Wilhelm, S.M., Carter, C., Tang, L., Wilkie, D., McNabola, A., Rong, H., Chen, C., Zhang, X., Vincent, P., McHugh, M., et al. (2004). BAY 43-9006 Exhibits Broad Spectrum Oral Antitumor Activity and Targets the RAF/MEK/ERK Pathway and Receptor Tyrosine Kinases Involved in Tumor Progression and Angiogenesis. Cancer Res. *64*, 7099–7109.

Wood, E.R., Truesdale, A.T., McDonald, O.B., Yuan, D., Hassell, A., Dickerson, S.H., Ellis, B., Pennisi, C., Horne, E., Lackey, K., et al. (2004). A Unique Structure for Epidermal Growth Factor Receptor Bound to GW572016 (Lapatinib). Cancer Res. *64*, 6652–6659.

Xia, W., Bacus, S., Hegde, P., Husain, I., Strum, J., Liu, L., Paulazzo, G., Lyass, L., Trusk, P., Hill, J., et al. (2006). A model of acquired autoresistance to a potent ErbB2 tyrosine kinase inhibitor and a therapeutic strategy to prevent its onset in breast cancer. Proc. Natl. Acad. Sci. USA *103*, 7795–7800.

Yee, M.C, Fas, S.C., Stohlmeyer, M.M., Wandless, T.J., and Cimprich, K.A. (2005). A Cell-permeable, Activity-based Probe for Protein and Lipid Kinases. J. Biol. Chem. *280*, 29053–29059.

Yudushkin, I.A., Schleifenbaum, A., Kinkhabwala, A., Neel, B.G., Schultz, C., and Bastiaens, P.I.H. (2007). Live-Cell Imaging of Enzyme-Substrate Interaction Reveals Spatial Regulation of PTP1B. Science *315*, 115–119.

Yun, C.H., Mengwasser, K.E., Toms, A.V., Woo, M.S., Greulich, H., Wong, K.K., Meyerson, M., and Eck, M.J. (2008). The T790M mutation in EGFR kinase causes drug resistance by increasing the affinity for ATP. Proc. Natl. Acad. Sci. USA *105*, 2070–2075.

Zamir, E., and Bastiaens, P.I.H. (2008). Reverse engineering intracellular biochemical networks. Nat. Chem. Biol. *4*, 643–647.

Zhang, J., Yang, P.L., and Gray, N.S. (2009). Targeting cancer with small molecule kinase inhibitors. Nat. Rev. Cancer *9*, 28–39.

Zhang, X., Gureasko, J., Shen, K., Cole, P.A., and Kuriyan, J. (2006). An Allosteric Mechanism for Activation of the Kinase Domain of Epidermal Growth Factor Receptor. Cell *125*, 1137–1149.

Zhang, X., Pickin, K.A., Bose, R., Jura, N., Cole, P.A., and Kuriyan, J. (2007). Inhibition of the EGF receptor by binding of MIG6 to an activating kinase domain interface. Nature *450*, 741–744.

Zhou, W., Ercan, D., Chen, L., Yun, C.H., Li, D., Capelletti, M., Cortot, A.B., Chirieac, L., Iacob, R.E., Padera, R., et al. (2009). Novel mutant-selective EGFR kinase inhibitors against EGFR T790M. Nature *462*, 1070–1074.